BS EN 16253:2013

BSI Standards Publication

Air quality — Atmospheric measurements near ground with active Differential Optical Absorption Spectroscopy (DOAS) — Ambient air and diffuse emission measurements

bsi.

...making excellence a habit.™

National foreword

This British Standard is the UK implementation of EN 16253:2013.

The UK participation in its preparation was entrusted to Technical Committee EH/2/3, Ambient atmospheres.

A list of organizations represented on this committee can be obtained on request to its secretary.

This publication does not purport to include all the necessary provisions of a contract. Users are responsible for its correct application.

ISBN 978 0 580 74164 7

ICS 13.040.20

Compliance with a British Standard cannot confer immunity from legal obligations.

This British Standard was published under the authority of the Standards Policy and Strategy Committee on 31 July 2013.

Amendments issued since publication

Date	Text affected

EUROPEAN STANDARD

NORME EUROPÉENNE

EUROPÄISCHE NORM

EN 16253

July 2013

ICS 13.040.20

English Version

Air quality - Atmospheric measurements near ground with active Differential Optical Absorption Spectroscopy (DOAS) - Ambient air and diffuse emission measurements

Qualité de l'air - Mesurages atmosphériques à proximité du sol par Spectroscopie d'Absorption Optique Différentielle (DOAS) - Mesurages de l'air ambiant et des émissions diffuses

Luftqualität - Messungen in der bodennahen Atmosphäre mit der aktiven Differentiellen Optischen Absorptionsspektroskopie (DOAS) - Immissionsmessungen und Messungen von diffusen Emissionen

This European Standard was approved by CEN on 15 May 2013.

CEN members are bound to comply with the CEN/CENELEC Internal Regulations which stipulate the conditions for giving this European Standard the status of a national standard without any alteration. Up-to-date lists and bibliographical references concerning such national standards may be obtained on application to the CEN-CENELEC Management Centre or to any CEN member.

This European Standard exists in three official versions (English, French, German). A version in any other language made by translation under the responsibility of a CEN member into its own language and notified to the CEN-CENELEC Management Centre has the same status as the official versions.

CEN members are the national standards bodies of Austria, Belgium, Bulgaria, Croatia, Cyprus, Czech Republic, Denmark, Estonia, Finland, Former Yugoslav Republic of Macedonia, France, Germany, Greece, Hungary, Iceland, Ireland, Italy, Latvia, Lithuania, Luxembourg, Malta, Netherlands, Norway, Poland, Portugal, Romania, Slovakia, Slovenia, Spain, Sweden, Switzerland, Turkey and United Kingdom.

EUROPEAN COMMITTEE FOR STANDARDIZATION
COMITÉ EUROPÉEN DE NORMALISATION
EUROPÄISCHES KOMITEE FÜR NORMUNG

Management Centre: Avenue Marnix 17, B-1000 Brussels

Contents

Page

Foreword

This document (EN 16253:2013) has been prepared by Technical Committee CEN/TC 264 “Air quality”, the secretariat of which is held by DIN.

This European Standard shall be given the status of a national standard, either by publication of an identical text or by endorsement, at the latest by January 2014, and conflicting national standards shall be withdrawn at the latest by January 2014.

Attention is drawn to the possibility that some of the elements of this document may be the subject of patent rights. CEN [and/or CENELEC] shall not be held responsible for identifying any or all such patent rights.

According to the CEN-CENELEC Internal Regulations, the national standards organisations of the following countries are bound to implement this European Standard: Austria, Belgium, Bulgaria, Croatia, Cyprus, Czech Republic, Denmark, Estonia, Finland, Former Yugoslav Republic of Macedonia, France, Germany, Greece, Hungary, Iceland, Ireland, Italy, Latvia, Lithuania, Luxembourg, Malta, Netherlands, Norway, Poland, Portugal, Romania, Slovakia, Slovenia, Spain, Sweden, Switzerland, Turkey and the United Kingdom.

Introduction

Differential Optical Absorption Spectroscopy (DOAS) has been successfully progressed, starting in the late 1970s, from a laboratory based method to a versatile remote sensing technique for atmospheric trace gases. In the DOAS measuring process, the absorption of radiation in the ultraviolet, visible or infrared spectral range by gaseous constituents is measured along an open monitoring path between a radiation source and a spectrometer, and the integral concentration over the monitoring path is determined.

DOAS systems support direct multi-constituent measurements. They provide alternative measuring techniques in that they can handle a large number of measuring tasks which cannot be adequately addressed by in situ techniques based on point measurements. Examples of such tasks include the monitoring of diffuse emissions from area sources such as urban settlements [1], traffic routes, sewage treatment plants and industrially or agriculturally used surface areas; the minimisation of production losses through a detection of leaks in equipment zones or pipeline systems; or ambient air monitoring in any of the above-mentioned applications.

With an appropriate measuring set-up, the local air pollution can usually be assessed very quickly. Measurements can be taken effectively even in areas which are difficult or impossible to access, or where the direct presence of personnel or equipment would be hazardous. The measurement in the open atmosphere eliminates potential losses by sample handling. An overview on the DOAS measurement technique can be found in [2].

1 Scope

This European Standard describes the operation of *active* DOAS measuring systems with continuous radiation source, the calibration procedures and applications in determining gaseous constituents (e.g. NO_2, SO_2, O_3, BTX, Hg) in ambient air or in diffuse emissions.

2 Terms and definitions

For the purposes of this document, the following terms and definitions apply.

2.1
active DOAS
DOAS with artificial radiation source

2.2
background spectrum
spectrum taken by the DOAS system with the light beam blocked or the lamp switched off

Note 1 to entry: The background spectrum results mainly from scattered sunlight.

2.3
complete spectral modelling
process of using synthetic spectra to match with observed experimental spectra

2.4
dark spectrum
spectrum which identifies the thermal effects of the detector when no radiation is admitted to the detector

2.5
electronic offset spectrum
spectrum which identifies the electronic effects of the detector when no radiation is admitted to the detector

2.6
instrument line shape
ILS
mathematical function which describes the effect of the instrument's response on a monochromatic line

2.7
intensity
radiant power per unit solid angle (non-collimated beam) or per unit area (collimated beam)

2.8
lamp spectrum
spectrum which is achieved by admitting direct light from the lamp to the spectrometer

2.9
monitoring path
actual path in space over which the pollutant concentration is measured and averaged

2.10
open-path measurement
measurement which is performed in the open atmosphere

2.11
path length
distance that the radiation travels in the open atmosphere

2.12
reference spectrum
spectrum of the absorbance versus wavelength for a pure gaseous sample under defined measurement conditions and known and traceable concentrations

2.13
signal-to-noise ratio
ratio between the signal strength and its standard deviation

3 Symbols and abbreviations

3.1 Symbols

$a(\lambda)$ specific absorption coefficient at wavelength λ

$a_i(\lambda)$ specific absorption coefficient of constituent i at wavelength λ

$a_{0i}(\lambda)$ portion of the specific absorption coefficient which varies little with the wavelength

$a_i'(\lambda)$ portion of the specific absorption coefficient which varies strongly with the wavelength

a_{M} Mie scattering coefficient

a_{R} Rayleigh scattering coefficient

c mass concentration

c_{AE} aerosol mass concentration

c_i mass concentration of constituent i

c_{LM} density of air

d_j coefficient j of a polynomial

$D(\lambda)$ optical density

$D'(\lambda)$ differential optical density

i index number

$I(\lambda, l)$ intensity of received radiation of wavelength λ after a path-length l

$I_0(\lambda)$ intensity of emitted radiation of wavelength λ

$I_0^{'}(\lambda,l)$ differential initial intensity

$I_{\mathrm{mod}}(\lambda)$ modelled intensity

l length of the monitoring path

M_i molar mass of component i

p atmospheric pressure

R molar gas constant (= 8,3145 J/(mol·K))

$S(\lambda)$ intensity of scattered solar radiation of wavelength λ

T ambient temperature

x_i mixing ratio of component i

$\tau(\lambda)$ attenuation factor of the optical system

3.2 Abbreviations

DOAS Differential Optical Absorption Spectroscopy

IR Infrared

UV Ultraviolet

UV/VIS Ultraviolet/Visible

4 Principle

4.1 General

The DOAS measurement is based on the principle whereby the atmospheric concentration of gaseous constituents is quantified on the basis of their characteristic absorption of radiation. The radiation spectrum examined for this purpose ranges from near ultraviolet to near infrared (approximately 250 nm to 2 500 nm). Accordingly, the analysed absorption of radiation will be based on electronic transitions in molecules and, possibly, atoms and in the near infrared on molecular vibrational transitions.

The method shows high selectivity and sensitivity due to the following combination of features:

— The measurement of radiation intensities is conducted with a high spectral resolution (0,1 nm to 1 nm) over a broad spectral range comprising numerous vibrational and/or rotational bands of one or more electronic transition(s).

— Reference spectra are fitted to the measured spectra by the least squares method. Thus, the characteristic absorption structures of the target compounds are employed to identify the measured compounds. Superimposed absorption structures of other constituents may be separated.

— Since the structured spectral absorption is analysed, unusually low optical densities (in some cases below 10^{-3}) can be identified. This fact, in conjunction with the long monitoring paths (usually from ca. 100 m to several kilometres, depending on the compounds to be measured) in the open atmosphere, yields low limits of detection for the trace gases.

— Quasi-continuous absorptions resulting from absorption processes by particles and droplets (e.g. radiation attenuation due to aerosol dispersion or decreasing transmittance of the optical system) as well as moderate fluctuations of the radiation intensity will not affect the result over a wide measurement range because in this technique differential absorption is used rather than the absolute absorption.

4.2 Configuration of the measurement system

Open-path techniques measure the 'concentration × path-length' product of one or more species in the atmosphere within a defined, extended optical path. The concentration of the species is derived from this measurement value. Two of the basic configurations for an open-path monitoring system are given in Figure 1 and Figure 2.

In the bistatic system (Figure 1) the transmitter and the detector are separated at the two ends of the optical path. The monostatic system (Figure 2) operates by transmitting the optical beam into the atmosphere to a passive retroreflector which returns the beam to the detector.

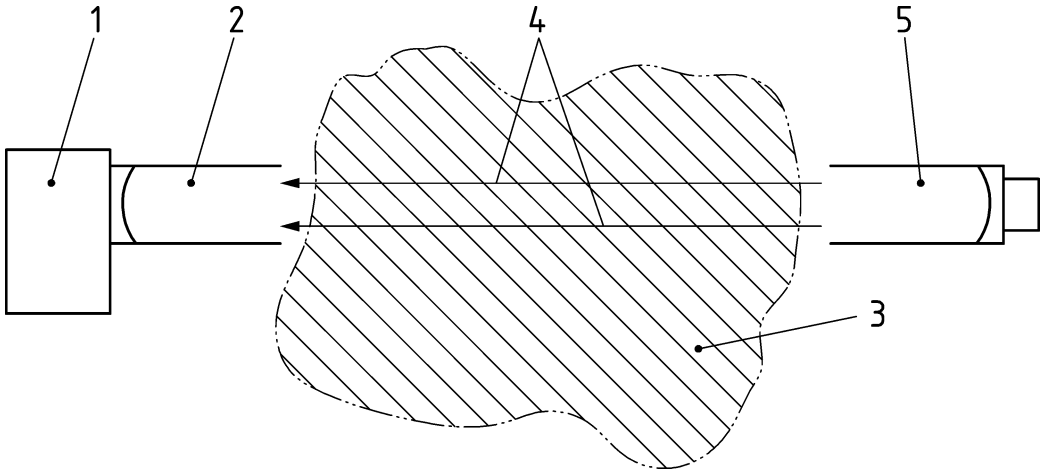

Key
1 DOAS spectrometer
2 Telescope for radiation collection
3 Ambient air
4 Monitoring path
5 Radiation source with collimating optics

Figure 1 — Bistatic arrangement for DOAS remote sensing

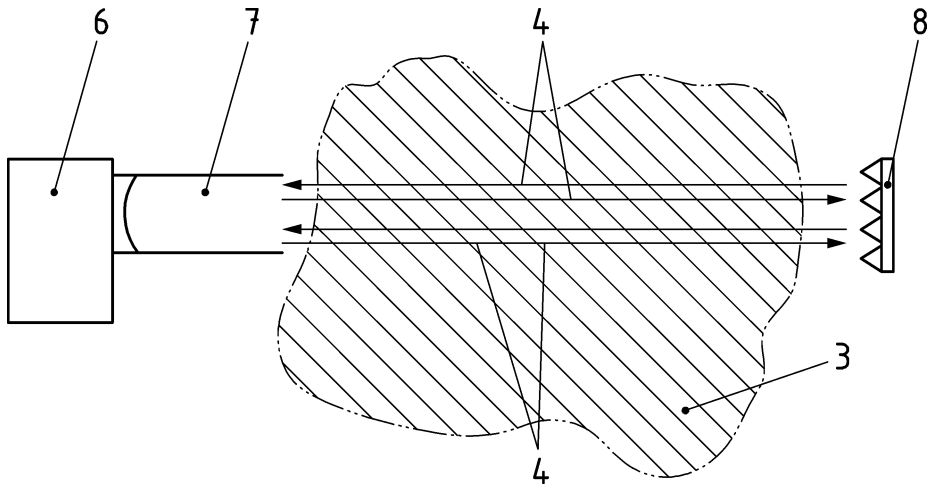

Key
3 Ambient air
4 Monitoring path
6 DOAS spectrometer including radiation source
7 Telescope for transmission and collection of radiation
8 Retro-reflector

Figure 2 — Monostatic arrangement for DOAS remote sensing

In the bistatic measurement set-up, the radiation source (5) and the DOAS spectrometer (1) are spatially separated. The two instrumental parts are oriented in such a way that the radiation emitted from the radiation source and collimated by a parabolic mirror is collected by the DOAS spectrometer telescope (2). The monitoring path length is the distance between collimating and receiving optics.

For a monostatic measurement set-up, transmitting and receiving optics are an integral part of the DOAS spectrometer (6), which also includes the radiation source and a beam splitter serving to separate the received and transmitted beams. By means of a retroreflector (8) the radiation beam passes twice through the measurement volume. The monitoring path length in this case is twice the distance between the transmitter/receiver and the retroreflector optics.

4.3 The Beer-Lambert law

When radiation passes through a medium, e.g. the atmosphere, it undergoes a change in intensity that can be expressed by means of the Beer-Lambert law:

$$I(\lambda, l) = I_0(\lambda) \cdot \exp\left(-a(\lambda) \cdot c \cdot l\right) \quad (1)$$

where

$I(\lambda, l)$ is the intensity of the radiation of wavelength λ incident on the receiver after passing the atmosphere along the monitoring path l;

$I_0(\lambda)$ is the intensity of the radiation of wavelength λ emitted by the radiation source;

$a(\lambda)$ is the specific absorption coefficient of the medium at wavelength λ in $(\mu g/m^3)^{-1} \cdot m^{-1}$;

c is the concentration of the measured constituent in $\mu g/m^3$;

l is the length of the monitoring path in m.

The radiation absorption produces changes in the energy state of the absorbing gaseous species. In the UV/VIS range considered here, this implies a change in the rotational and vibrational state of the gaseous species, in addition to the change in their electronic state. In general, the rotational bands are not resolved, so what is measured essentially is the vibrational structure of the electronic transitions [3].

By introducing the optical density $D(\lambda)$

$$D(\lambda) = \ln\left(\frac{I_0(\lambda)}{I(\lambda)}\right) \tag{2}$$

and from Formula (1), the concentration c of the absorbing gaseous species is:

$$c = \frac{D(\lambda)}{a(\lambda)\cdot l} \tag{3}$$

NOTE The term *extinction* is also widely used for $D(\lambda)$. The quotient $\frac{I(\lambda)}{I_0(\lambda)}$ is defined as the transmittance.

4.4 Extended Beer-Lambert law

In atmospheric measurements, radiation is attenuated not merely by molecular absorption effects. It also disappears from the monitoring path due to scattering by air molecules (Rayleigh scattering) and to absorption and scattering by aerosol particles (Mie scattering). Apart from these attenuation effects, Rayleigh scattering of solar radiation leads to an increase in the radiation intensity incident on the detector. This additional contribution shall be determined and taken into account, as appropriate (see Annex B). Considering all these effects the absorption law (1) takes the following form:

$$I(\lambda,l) = I_0(\lambda)\cdot exp\left(\left(-a_R(\lambda)\cdot c_{LM} - a_M(\lambda)\cdot c_{AE}\right)\cdot l + \sum_i -a_i(\lambda)\cdot c_i \cdot l\right) + S(\lambda) \tag{4}$$

where

$I(\lambda, l)$ is the intensity of the radiation of wavelength λ incident on the receiver after passing the atmosphere along the monitoring path l;

$I_0(\lambda)$ is the intensity of the radiation of wavelength λ emitted by the radiation source;

$a_R(\lambda)$ is the Rayleigh scattering coefficient in $(\mu g/m^3)^{-1}\cdot m^{-1}$;

c_{LM} is the density of the ambient air in $\mu g/m^3$;

$a_M(\lambda)$ is the Mie scattering coefficient in $(\mu g/m^3)^{-1}\cdot m^{-1}$;

c_{AE} is the aerosol concentration in $\mu g/m^3$;

l is the length of the monitoring path in m;

$a_i(\lambda)$ is the specific absorption coefficient of constituent i at wavelength λ in $(\mu g/m^3)^{-1}\cdot m^{-1}$;

c_i is the concentration of constituent i in $\mu g/m^3$;

$S(\lambda)$ is the intensity of scattered solar radiation.

NOTE The concentration of the constituent i in a mixed medium is expressed as a mass concentration ($c_i=m_i/V$). It can also be expressed as a mixing ratio $x_i= n_i/n_{tot}= N_i/N_{tot} = V_i/V_{tot}$ (n is the number of molecules, N is the number of moles, $N = n/N_L$, N_L being the Loschmidt constant) in µmol/mol or nmol/mol using the following conversion formula:

$$c_i = x_i \cdot \frac{p \cdot M_i}{T \cdot \mathrm{R}}$$

where

c_i is the mass concentration of constituent i in µg/m^3 (or mg/m^3);

x_i is the mixing ratio of constituent i in nmol/mol (or µmol/mol);

p is the atmospheric pressure in Pa;

T is the ambient temperature in K;

M_i is the molar mass of component i in kg/mol;

R is the molar gas constant (= 8,314 5 J/(mol·K)).

Reference conditions (pressure, temperature) for ambient air measurements are usually 1 013 hPa and 20 °C.

Formula (4) does not yet allow an analysable correlation between $I(\lambda, l)$ and $I_0(\lambda)$ to be established, i.e. determining a concentration averaged over the monitoring path. This is due to the difficulty of determining the intensity $I_0(\lambda)$ incident on the absorber and to the variability of light scattering effects in the atmosphere as expressed by $a_R(\lambda)$ and $a_M(\lambda)$.

4.5 Differential optical density

The DOAS method relies only on the high-frequency (narrowband) part of the absorption structure. For this purpose, the absorption coefficient $a_i(\lambda)$ is considered the sum of two components as shown in Figure 3:

$$a_i(\lambda) = a_{0i}(\lambda) + a'_i(\lambda) \tag{5}$$

where

$a_{0i}(\lambda)$ is the portion of the specific absorption coefficient which varies little with the wavelength;

$a'_i(\lambda)$ is the portion of the specific absorption coefficient which varies strongly with the wavelength.

The parameters $a_{0i}(\lambda)$ and $a'_i(\lambda)$ denote the low-frequency and high-frequency portion of the absorption coefficient of the gaseous component i (see Figure 3).

Formula (4) can then be modified as follows:

$$I(\lambda,l) = I_0(\lambda) \cdot \exp\left(\left(-a_R(\lambda) \cdot c_{LM} - a_M(\lambda) \cdot c_{AE}\right) \cdot l + \sum_i - a_{0i}(\lambda) \cdot c_i \cdot l \right) \cdot \exp\left(\sum_i - a'_i(\lambda) \cdot c_i \cdot l \right) + S(\lambda) \tag{6}$$

The differentiation with respect to the absorption coefficient $a_i(\lambda)$ permits definition of the differential initial intensity $I'_0(\lambda)$ which corresponds to the initial intensity $I_0(\lambda)$ after attenuation through Rayleigh and Mie scattering and through the continuous portion of the component-related absorption. Furthermore it is assumed that the intensity of the scattered solar radiation $S(\lambda)$ (see Formula (4)) will be determined and subtracted. Additionally, the attenuation factor $\tau(\lambda)$ is introduced which allows for the broad wavelength-dependent

transmission of the entire optical system (radiation source, telescopes, spectrometer (cf. Annex A)), including the spectral sensitivity of the detector. Thus, Formula (6) can be modified as follows:

$$I'_0(\lambda) = I_0(\lambda) \cdot exp\left(\left(-a_R(\lambda) \cdot c_{LM} - a_M(\lambda) \cdot c_{AE} \right) \cdot l + \sum_i -a_{0i}(\lambda) \cdot c_i \cdot l \right) \cdot \tau(\lambda) \quad (7)$$

where

$I'_0(\lambda)$ is the differential initial intensity;

$\tau(\lambda)$ is the attenuation factor of the optical system.

The optical density determined on the basis of the differential initial intensity $I'_0(\lambda)$ is referred to as the differential optical density $D'(\lambda)$:

$$D'(\lambda) = \ln \frac{I'_0(\lambda)}{I(\lambda)} = \sum a'_i(\lambda) \cdot c_i \cdot l \quad (8)$$

This procedure ensures that DOAS spectra can be properly analysed, as the optical density definition is expanded by taking into account the influence of the continuous absorption structures, i.e. those which do not vary much with the wavelength. By relying on the concept of differential initial intensity $I'_0(\lambda)$, DOAS solves the problem that the intensity of initial radiation $I_0(\lambda)$ emitted by a radiation source is impossible to determined from a measured spectrum due to absorption and scattering effects. Figure 3 illustrates the difference between the intensities $I(\lambda)$, $I_0(\lambda)$, $I'_0(\lambda)$.

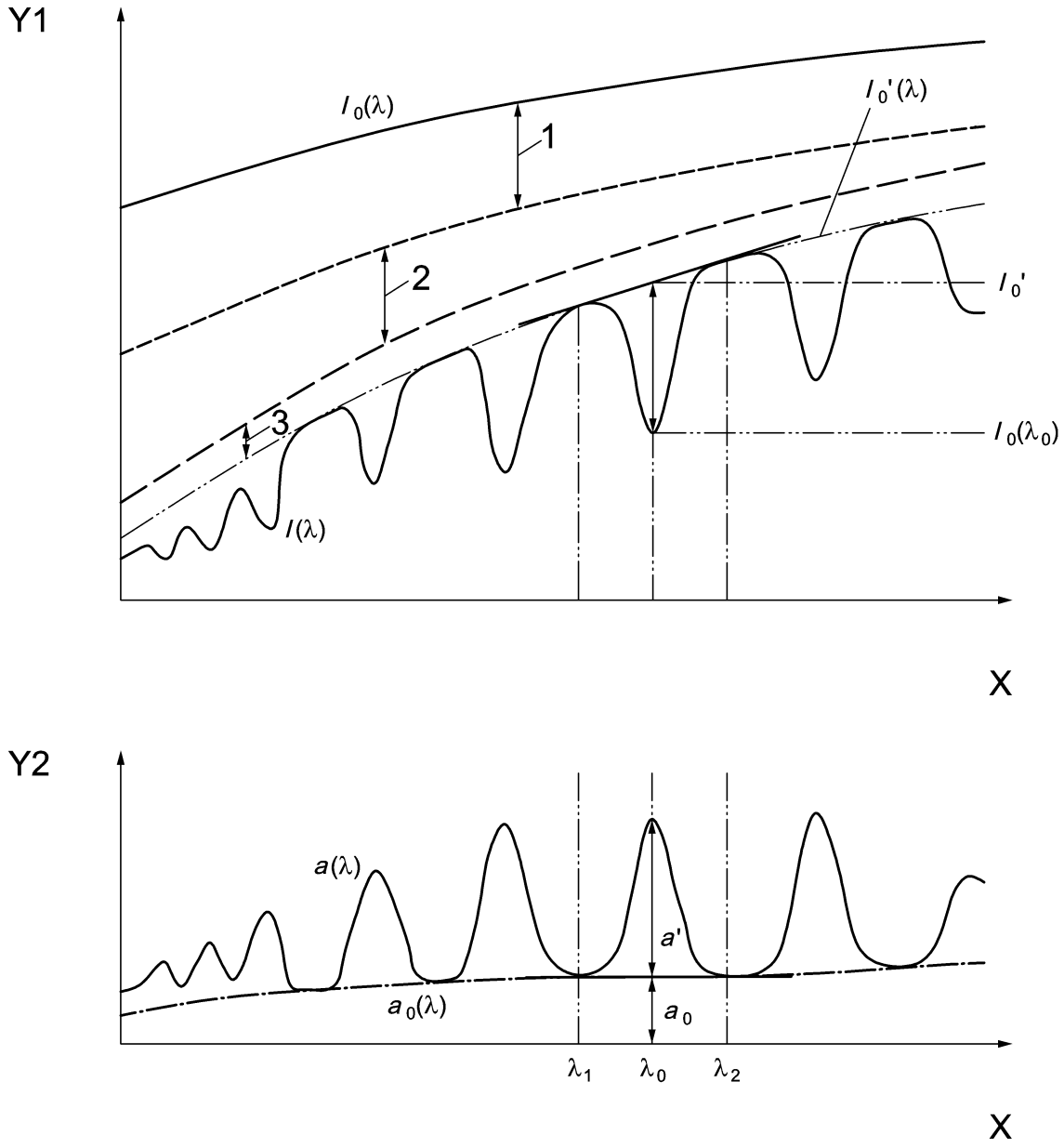

Key
1 Mie extinction
2 Rayleigh extinction
3 Continuous absorption component
X Wavelength
Y1 Intensity
Y2 Absorption coefficient

Figure 3 — Intensities $I(\lambda)$, $I_0(\lambda)$ and $I_0'(\lambda)$ in an absorption spectrum (upper panel) and associated absorption coefficients $a(\lambda)$, $a_0(\lambda)$ and $a'(\lambda)$ (lower panel)

$I_0'(\lambda)$ can be determined by interpolation between the shoulder values $I(\lambda_1)$ and $I(\lambda_2)$. $D'(\lambda)$ is then obtained from the quotient of the intensities $I_0'(\lambda)$ (centre of band) and $I(\lambda)$ according to Formula (9).

$$D'(\lambda) = \ln\frac{I_0'(\lambda)}{I(\lambda)} = \ln\left(I(\lambda_1) + \left(I(\lambda_2) - I(\lambda_1)\right)\cdot\frac{\lambda_0 - \lambda_1}{\lambda_2 - \lambda_1}\right) - \ln I(\lambda_0) \quad (9)$$

However, this method is used only in simple cases (one single strong, dominant absorber). Usually, the analysis is conducted by mathematical modelling of $I(\lambda)$ with the aim of minimising the deviation between $I(\lambda)$ and $I_{\mathrm{mod}}(\lambda)$, where $I_{\mathrm{mod}}(\lambda)$ is the modelled intensity as a function of wavelength (i.e. a modelled spectrum).

$$I_{\mathrm{mod}}(\lambda) = P(\lambda) \cdot \exp - \left(\sum_i a_i'(\lambda) \cdot c_i \cdot l \right) \tag{10}$$

$P(\lambda)$ describes the combined influences of all influencing variables which vary little with wavelength, such as $\tau(\lambda)$ or broadband absorbers (cf. Formula (7)), where it is not necessary to determine all coefficients. It suffices to approximate $P(\lambda)$ to the wavelength using a suitable smooth function, e.g. a higher-order polynomial:

$$P(\lambda) \approx \sum_{j=0}^{k} d_j \cdot \lambda^j \tag{11}$$

e.g. a 5$^{\mathrm{th}}$ order polynomial [3]) or a low-pass filtered spectrum of $I(\lambda)$ (e.g. with the aid of a Bessel filter [4]), see Figure 4 (SO_2 measurement).

The deviation between $I(\lambda)$ and $I_{\mathrm{mod}}(\lambda)$ is usually minimised by the least squares method:

$$\chi^2 = \left(I_{\mathrm{mod}}(\lambda) - I(\lambda)\right)^2 = \mathrm{minimal} \tag{12}$$

Thus the desired concentrations c_i of the absorbing constituents averaged over the monitoring path, the coefficients determining $P(\lambda)$ (e.g. the coefficients d_j of the polynomial), and such additional coefficients as may be involved (e.g. those describing wavelength shifts) are obtained.

NOTE The polynomial coefficients d_j (Formula (11)) can be useful for quality control purposes. Major variations of these coefficients during the measurement indicate pronounced changes in atmospheric or system conditions.

The advantage of this analytical procedure is that the differential optical densities of all bands of the given constituents will be taken into account in determining the average concentration across the spectral range selected for the analysis.

A selected spectral range may contain the absorption structures of several constituents. It is possible to distinguish between them and to determine their concentrations c_i independently. In addition, potential shifts in the wavelength scale can be corrected. A detailed description of this method is given in [5].

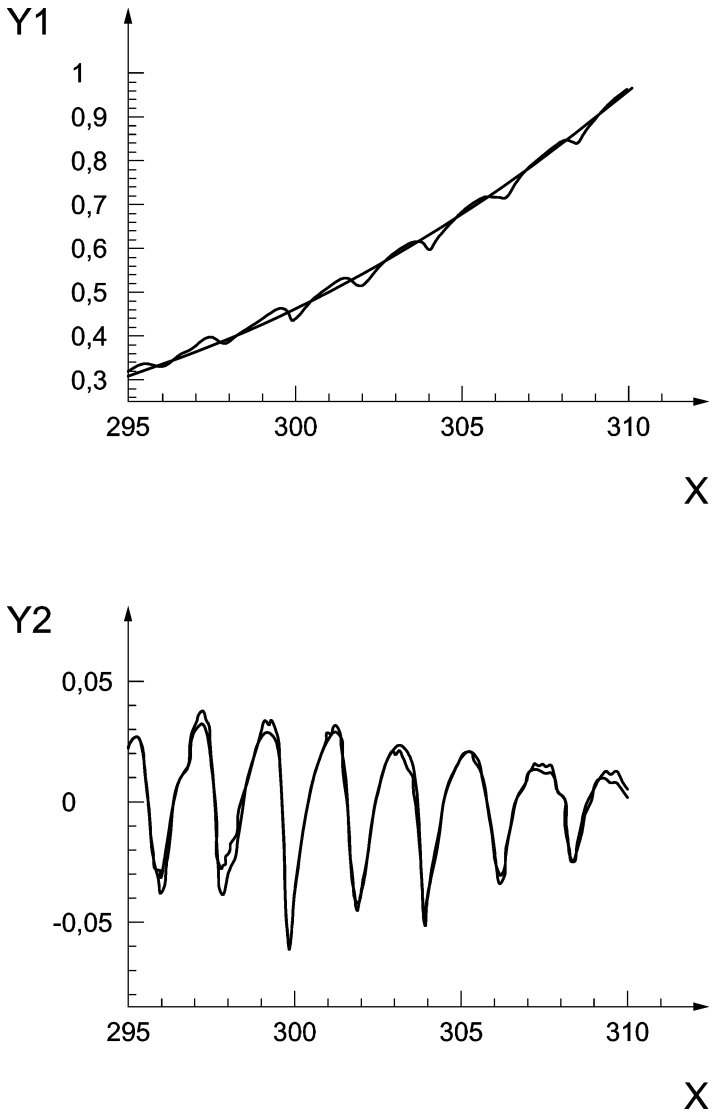

Key
X Wavelength λ in nm
Y1 Intensity I in relative units
Y2 log I_1/I_2

Figure 4 — Top: Measured raw spectrum and fitted fifth degree polynomial (smoothed line). Bottom: Quotient of raw spectrum and fitted polynomial produces the high-pass filtered spectrum, fitted SO_2 reference spectrum for comparison (smoother line)

5 Measurement procedure

5.1 General

DOAS measurements are based on the principle of recording and analysing absorption bands of the constituents of interest (see Clause 4). In addition, the following parameters shall be measured or recorded:

— monitoring path length, determined, e.g. using a geographical map, a range finder, GPS data or a tape measure (short distances);

— density (temperature and pressure) of the air column, if appropriate (depending on the measurement task), in order to express the results under standard conditions;

— instrument status data (e.g. received relative radiation intensity (e.g. in order to prevent saturation), detector temperature (relevant only for diode laser systems)).

DOAS measuring procedures depend on the instrument type. In addition to the atmospheric raw spectrum, the system shall measure at least the dark spectrum, electronic offset spectrum, lamp spectrum, and, in cases of measurements above 290 nm, the background spectrum due to scattered solar radiation [2]. In order to evaluate the spectra the reference compound spectra shall be known.

5.2 Principle

The general procedure for active long-path DOAS systems is outlined in Figure 5. Depending on the instrument technique not all of these steps and not all of the spectra are necessary.

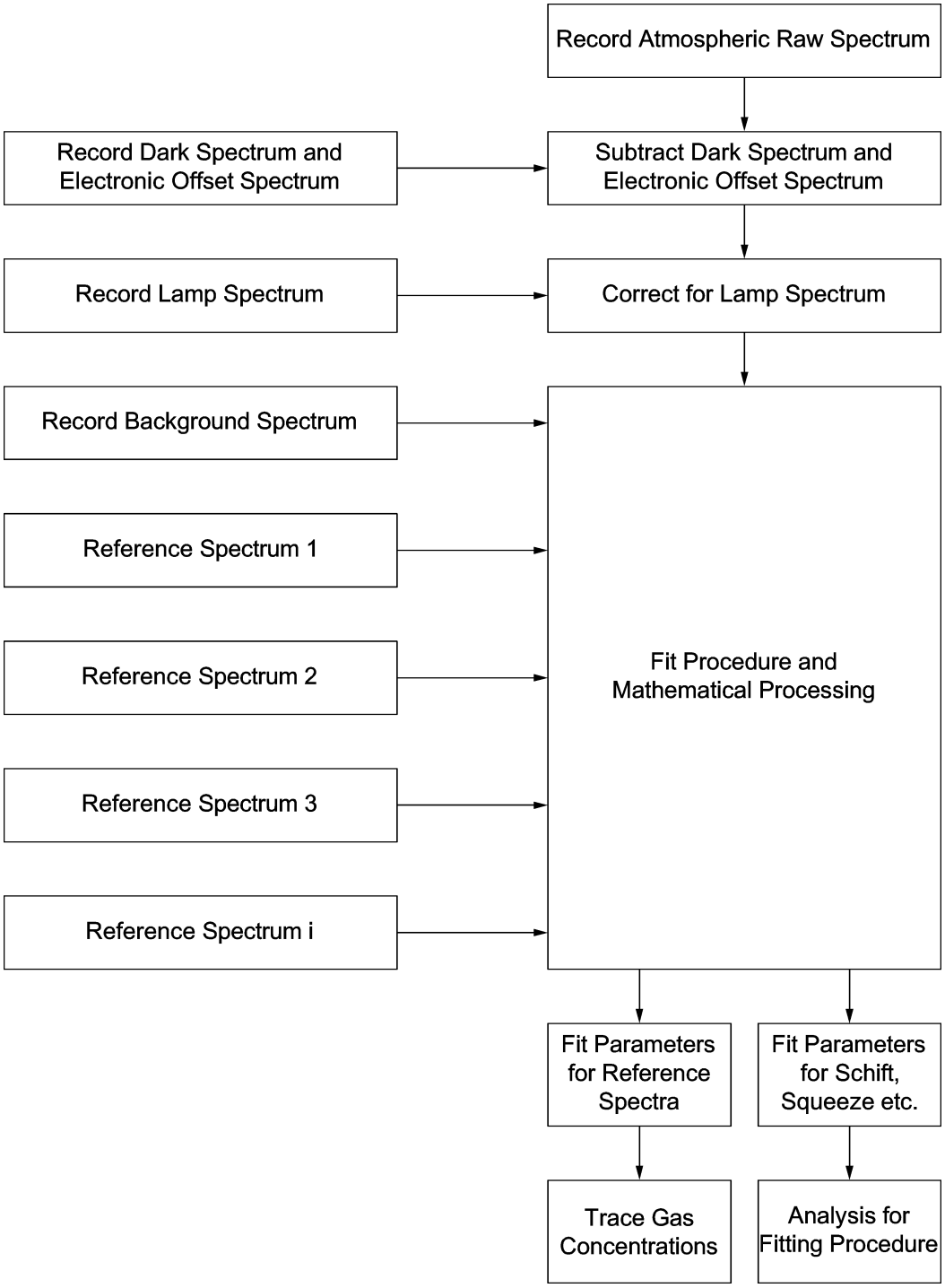

Figure 5 — Flow chart of a DOAS measurement and its evaluation

The true optical density $D'(k)$ is achieved by processing the following spectra:

— the atmospheric raw spectrum $I(k)$, i.e. the spectrum of the lamp with trace gas features and aerosol absorption plus solar scattered light. The standard procedure is to add several (N_M) individual spectra having the integration time (t_M) in each case;

NOTE k numbers the spectral interval covered by an individual detector pixel.

— the dark spectrum $I_D(k)$ (optional), in case of CCD or PDA as detector, with integration time t_D (including electronic offset), wherein the dark spectrum per time base $I_{D1}(k)$ is derived correcting for electronic offset (scan weighted) and integration time ($I_{D1}(k) = (I_D(k)-N_D*I_{Off1}(k)/t_D)$);

— the electronic offset spectrum $I_{Off}(k)$ (optional), in case of CCD or PDA as detector (with negligible dark spectrum due to shortest possible integration time), wherein the electronic offset I_{Off1} for one scan is obtained by dividing with the number of N_{Off} added spectra ($I_{Off1}(k) = I_{Off}(k) / N_{Off}$);

— the lamp spectrum $I_L(k)$, recorded by a direct scan of the lamp radiation excluding the atmosphere;

— the background spectrum $I_B(k)$, for wavelengths above 290 nm with an integration time t_B, since stray solar radiation may interfere with the measurement.

EXAMPLE In a specific DOAS technique the true optical density $D'(k)$ is calculated as follows:

$$D'(k) = -\ln \frac{\left[\left(I_M(k) - N_M \cdot I_{Off1}(k) - t_M \cdot I_{D1}(k)\right) - \frac{t_M}{t_B}\left(I_B(k) - N_B \cdot I_{Off1}(k) - t_B \cdot I_{D1}(k)\right)\right]}{\left(I_L(k) - N_L \cdot I_{Off1}(k) - t_L \cdot I_{D1}(k)\right)} \quad (13)$$

(N_B and N_L, respectively, indicate the number of background and lamp spectra added up).

As $I_{D1}(k)$ is an averaged dark spectrum, the factors N_M, N_B, N_L are introduced, in order to correlate the correct intensities within this algorithm for the raw atmospheric spectrum, the lamp spectrum, the dark spectrum and the background spectrum. For the same reason the ratio t_M/t_B is introduced, as I_M and I_B might have been recorded with different measurement times.

The true optical density $D'(k)$ can be processed as follows:

a) A *least-squares fit* is carried out with a series of reference spectra according to 4.5.

b) The resulting fit parameters indicating the optical densities of the respective trace gas are used to calculate the column density of this trace gas (as well as its standard deviation).

c) Dividing the column density by the length of the monitoring path gives the trace gas concentration, which can be converted into mixing ratios by using the pressure and temperature of the air column (see Note in 4.4).

d) In some cases it is necessary to fit additional parameters describing wavelength shift and/or stretch of the wavelength scale. These are not immediately necessary to calculate the trace gas concentration, but can be used to judge the quality of the spectrometer and provide an indication of error margins ([5], [6]). In this case also a non-linear fit procedure is necessary.

Background spectra need not be recorded in daytime when operating at wavelengths below 290 nm, due to the additionally recorded scattered solar radiation in $I_M(k)$ under these conditions. The lamp spectra shall be determined regularly since they may change due to ageing (i.e. over a span of several days/weeks) depending on instrument design. The use of current lamp spectra improves the data quality as the changes in lamp and also detector characteristics are compensated.

Reference spectra of the respective components can be recorded with the same spectrometer that is used for the atmospheric measurement. An alternative process is to convolute an available high-resolution spectrum (from the literature) with the instrument line shape function of the current spectrometer, which in turn can be obtained in high quality by recording an atomic line spectrum (usually a Hg vapour line spectrum).

Commercial implementations of the DOAS technique are presented in Annex C.

6 Measurement planning

6.1 Definition of the measurement task

In order to interpret and assess the measurement parameters it is necessary to clearly define the measurements to be carried out. This includes the species to be measured, experimental arrangement (field setup), likely interfering species, likely spatial distribution of the gases to be measured, required temporal information. Such limiting conditions shall be clearly defined in the scope of the measurements.

6.2 Selection of measurement parameters of the DOAS system

6.2.1 General

Before beginning the measurement it is necessary to define the relevant measurement parameters with respect to the objectives of measurement.

6.2.2 Monitoring path

The monitoring path (and specifically its length) is determined in accordance with the manufacturer's instructions for the constituents of interest, depending on the optical configuration (monostatic or bistatic). The minimum radiation level needed at the end of the monitoring path may differ, depending on the constituent to be measured. In this context, it is particularly important to take into account the light attenuation due to Mie scattering, as well as any optical filters employed for specific noxious constituents that might reduce the detection limit.

When the monitoring path is installed in public space, potential glare effects caused by the system's radiation source shall be avoided (e.g. accident hazard in the case of traffic-related measurements, health impairment of passers-by).

During installation of the monitoring path, care shall be taken to prevent direct incidence of strong scattered radiation (e.g. solar radiation) into the receiver's optical system.

6.2.3 Time resolution

Suitable averaging periods shall be selected for each constituent. They depend on the detection limits to be achieved, as well as on the spectral properties of the monitoring path. A high time resolution (e.g. short time intervals between the individual measurements) reduces the radiation dose available for each individual measurement and worsens the photo electron statistics. As a result, noise (or the minimum detectable optical density, respectively) will increase, in principle, in proportion to the square root of the radiation dose received. Thus, the detection limit and/or the measuring uncertainty of a DOAS measurement will vary with the square root of the measuring time in many cases (i.e. if photon statistics is applicable). Increasing the time resolution from 10 min (600 s) to 6 s would worsen the measuring error and the detection limit, respectively, by a factor of 10.

NOTE The maximum measurement accuracy for the specific constituent is mainly determined by the instrument characteristics and can be improved only to a certain limit by increasing the number of averaged measurements.

For usual applications, depending on the components to be determined, a time resolution of a few minutes (e.g. 0,5 min to 3 min) is chosen. This parameter may be varied for optimising particular applications.

7 Procedure in the field

7.1 Installation and start-up of the instrument

The following aspects shall be specifically observed during the mechanical installation of the optical components (including a separate analyser unit, where applicable), as well as when setting up and adjusting a monitoring path. The manufacturer's instructions shall be followed.

a) An adequate, uninterruptible power supply shall be used.

b) Depending on the measuring system employed, a torsion-resistant stand or sufficiently rugged attachment (wind load!) of the optical components shall be ensured. Particularly when using long measurement paths on systems devoid of automatic adjustment features, a sufficient long-term stability of the measured signal has to be guaranteed. In the case of pronounced ambient air temperature variations or changes in the solar radiation, the de-adjustment (change of alignment) caused by thermal effects needs to be taken into account.

c) Compliance with the operating conditions defined by the manufacturer (thermal requirements) for both the analyser unit and optical system components shall be ensured. On DOAS measuring systems combining the receiver and analyser unit in a single assembly, meeting these criteria may call for additional measures since the entire system is exposed to ambient conditions. If the optical components and the analyser unit are installed separately, appropriate steps shall be taken (e.g. air conditioning systems, heaters) to guarantee that the manufacturer-specified operating conditions (thermal requirements) will be met, particularly for the spectrometer unit. To optimise the system's availability, all optical components shall be protected against moisture effects (e.g. dew, precipitation).

d) The adjustment of a monitoring path is started by focussing the radiation source on the receiver's optical system (or, in the case of monostatic systems, on the retro-reflector or mirror element used). The size of the "focus point" shall be selected such that minor system de-adjustments (e.g. due to thermal effects) will not necessarily result in a total signal loss but can be tolerated (typically between 0,5 m to 2 m). These settings will be dependent on the selected monitoring path length and the size of the receiver's optical system; they shall be re-set during every new installation with a view to maximising the signal level.

e) For some systems adjustments shall preferably be carried out in the dark or in half-light (twilight) conditions since the visible spectral portion of the emitting light source is helpful when adjusting focus settings, optical transfer devices, etc.

NOTE New optical monostatic setups [7] do not require an adjustment at night. They are also simple to adjust at daylight. The adjustment of the light beam and focal point does not require the visibility of the emitting light.

f) Fibres for the deep UV range (solarisation stabilised) should be used, if working with light sources emitting below 280 nm, to avoid degradation of light transmittance.

g) If ozone-producing radiation sources are employed, suitable steps shall be taken (e.g. ventilation) to prevent any effects on the measurement and direct exposure to people.

h) Whenever the system is installed from scratch, its wavelength accuracy shall be re-checked. This can be done, for instance, with the aid of a mercury vapour spectral lamp.

i) A functional check of the DOAS measuring system shall be carried out before measurements are begun.

j) Beam alignment and blocking or optical path deflection systems may be necessary, especially for automatic operation. These systems shall be controlled as appropriate.

k) Once the monitoring path is set up and the optical adjustments have been made, all parameters of the DOAS measuring system which have been set or achieved for this specific monitoring path shall be duly documented so that any drift or de-adjustments can be identified. Where different monitoring paths are

used, all parameters shall be documented for each monitoring path used. These data will include the following:

1) overall system signal intensity achieved (a reduction in signal intensity due, e.g. to band pass filtering (to reduce stray light impact for individual constituents), shall be taken into account in this context);

2) monitoring path length(s);

3) averaging periods for the individual constituents;

4) calibration parameters for all constituents (e.g. span, offset, cross-sensitivity correction in the case of gas cell calibration; ILS function; reference spectra in the case of direct calibration);

5) pressure and temperature compensation settings.

7.2 Verification of optical properties

When checking the optical or spectral properties of the DOAS measuring system after its installation (but before the start of measurements), the following shall be noted:

— Optical windows and mirrors in the optical transfer devices employed shall be checked regularly for dirt or damage, and shall be cleaned according to the manufacturer’s instructions or replaced as appropriate.

— When using external calibration gas cells in conjunction with light guides, care shall be taken to ensure that the light guides are the same as those used in the real-life measurements so as to keep the spectral properties of the overall system constant. Any changes shall be documented.

— When conducting long-term measurements, the limited service life of the radiation sources shall be taken into account (see also A.2.1). When changing lamps or optical parts, observe the precautions defined by the manufacturer.

— All changes made in the course of the system's operation and adjustment of its optical components shall be documented.

7.3 Visibility

Under conditions of extremely poor visibility (e.g. fog or snow), all measurements shall be subjected to a special validation since the visibility has a direct influence on the signal intensity and hence, the measurements.

Particles increase the intensity of atmospheric scatter. Aerosols (mist, fog) or precipitation particles (e.g. rain, sleet, snow, “hydrometeors”) can interfere with DOAS measurements. This is attributable to two processes:

— attenuation of the useful radiation intensity, resulting in a deterioration of the signal-to-noise ratio;

— increase in the proportion of scattered solar radiation contributing to the measured signal (depending on time of day, weather, wavelength range).

The type and extent of measurement interferences due to elevated scatter will be evident from the analytical routines. Reduced signal intensities make for inferior photoelectron statistics, however, some compensation for these effects can be made through prolonged measuring times. In extreme cases (dense fog), measurements over a given path length may become altogether impossible. The effects of scattered solar radiation can be eliminated to a large extent with the methods described in Annex B.

8 Calibration methods

8.1 General

The calibration of the measurement system provides the relation between reference materials (reference gases or reference databases) and the measured values. The calibration procedure assures the accuracy of the measurement method.

Two different calibration approaches are applicable to DOAS systems:

— gas cell calibration with and without including the atmosphere using test gases (see 8.2);

— calibration with complete spectral modelling using reference spectra (see 8.3).

The basic calibration of a DOAS system is carried out by the manufacturer and is based on test gases, which shall be traceable to (inter)nationally accepted standards. If such test gases are not available (e.g. for reactive or non-stable compounds) the basic calibration may be based on reference spectra.

The periodic check of the calibration (typically once or twice a year) is carried out by the user according to the manufacturer's instructions and may be based either on test gases or reference spectra.

8.2 Gas cell calibration

8.2.1 Gas cell calibration with exclusion of the atmosphere

This laboratory-based calibration method using gas cells (possibly with different absorption lengths) is carried out under exclusion of the atmosphere. The radiation source should have the same emission characteristics as that which is used in the field measurements. For the calibration, the beam is passed through the gas cells so that any absorption by relevant ambient air constituents is ruled out. This can be achieved by transmitting the output of the radiation source directly through the gas cell using light guides or transfer optics. After transmitting the gas cells the measuring beam is passed directly to the spectrometer. Given the short absorption paths, very high radiation intensities may occur. These may have to be adapted to the level of the subsequent measurements by appropriate attenuation (e.g. de-adjustment, filtering).

One advantage of this calibration method is that it is not be affected by atmospheric absorption effects. In addition, it is possible to carry out a calibration under zero gas conditions. Cross-sensitivity surveys can also be made quite easily by using several gas cells arranged in series. Care shall be taken that the background intensity is negligible during the calibration experiment.

8.2.2 Gas cell calibration with inclusion of the atmosphere

This field-based method uses the full optical measurement path in the atmosphere and insertion of a gas cell. The differential optical density D' (see Formula (8)) is given by the gas concentration c in the atmosphere, the path length l, and the differential absorption coefficient a' as follows:

$$D' = a' \cdot c \cdot l \tag{14}$$

It follows that the optical density due to a low concentration over a long optical path is equivalent to the optical density due to a high concentration over a short path.

The insertion of a gas cell of length l_C which contains the measured gas in a concentration c_C into the optical path will raise the total differential optical density D'_{tot} by the contribution D'_C :

$$D'_C = a' \cdot c_C \cdot l_C \tag{15}$$

$$D'_{tot} = D' + D'_C \tag{16}$$

This permits an incremental calibration, i.e. it allows the calculation of an effective concentration change c_{eff}:

$$c_{\mathrm{eff}} = c_{\mathrm{C}} \cdot \frac{l_{\mathrm{C}}}{l} \tag{17}$$

As regard to the use of the gas cell method, the following limitations apply:

— Not all components which can be analysed by the DOAS method are stable in gas cells (especially under UV irradiation), e.g. NO_3 and other radicals.

NOTE Stable constituents such as SO_2 can be measured in sealed gas cells whereas for such compounds as NO, O_3 and some aromatic hydrocarbons dynamic flow through cells are used. In many cases flow-through gas cells have advantages for calibration purposes compared to sealed gas cells (wall effects).

— It is a necessary condition for the incremental measuring method that the atmospheric concentration of the gas remains constant throughout the measurement.

— In principle, the calibration gas cells shall extend over the entire diameter of the measuring beam. The cell (diameter typically 3 cm to 15 cm, length 3 cm to 10 cm) shall be positioned in the parallel part of the beam.

Gas cells can also be put at other locations in the light path where a parallel light beam is achieved (e.g. between light source and fibre). As the diameter of the light beam is typically much smaller (e.g. 3 cm) the application of cells is simpler and longer gas cells (e.g. up to 1 m) can easily be applied. This increases the calibration accuracy.

8.3 Calibration with complete spectral modelling

In this method an absolute calibration is performed by modelling the overall system and determining all model parameters in the laboratory. Knowledge of the following parameters is required:

— differential absorption coefficient $a'(\lambda)$ of the component for the wavelength used;

— instrument line shape function $H(\lambda)$ of the spectrometer employed;

— length of the monitoring path.

An additional parameter affecting the determination of the limit of detection is the lowest determinable optical density D_{min}. In addition, the calibration may be influenced by:

— stray light in the spectrum;

— non-linearity of the detector characteristic curve;

— apparent saturation of the absorption curve;

— dark current of the detector.

In this method these parameters have to be taken into account. The differential absorption coefficient and the ILS function can also be combined into a specific differential absorption coefficient $a_{\mathrm{H}}'(\lambda)$ for the apparatus at hand. The value of a'_{H} can be determined by the gas cell method according to 8.2.2 for the spectrometer used. However, it will usually be more favourable to determine it by convolution of the ILS function with a high-resolution absorption coefficient spectrum $a_{\mathrm{Ref}}(\lambda)$:

— Absorption coefficient spectra $a_{\mathrm{Ref}}(\lambda)$ established with a high resolution are an optical constant of the molecule considered and can be determined in the laboratory. Appropriate data are available for many constituents of interest (cf. HITRAN database [8]).

— The ILS function $H(\lambda)$ is defined as the spectrometer's response to a spectral distribution of the analysed radiation that is described by a Dirac's delta function or, in other words, as the spectrum produced by the spectrometer for monochromatic radiation. In practice, this intensity distribution can be approximated with high accuracy by means of atomic emission lines.

NOTE 1 The half-width of the mercury emission lines usually exploited is on the order of 10^{-3} nm, that of laser lines is often lower while the spectral resolution of DOAS spectrometers typically varies between 0,1 and 1 nm.

NOTE 2 The mercury lamp can be used for the calibration check.

Another possibility is to record high-resolution Fraunhofer structures of solar radiation (cf. WinDOAS [9]).

However, for use as a reference these spectra have to be convolved with the ILS H(λ) with the resolution of the spectrometer's detector unit. The reference spectrum $a_{\mathrm{H}}(\lambda)$ or $a'_{\mathrm{H}}(\lambda)$ thus obtained is used to determine the absolute trace substance concentration.

This method yields a reliable calibration of each DOAS system and an accurate determination of the limits of the measuring method [10] while requiring only elementary measurements on the instrument itself.

One potential disadvantage, on the other hand, is the complexity of the calibration procedure; this, however, resides in the necessary calculations rather than in the measurements to be carried out on the apparatus. Care shall therefore be taken while executing this procedure to avoid errors. A method which suggests itself for monitoring and validating the analytical calibration is to determine the line strength of the atmospheric O_4 (oxygen dimer) or, where appropriate, of H_2O or O_2 lines in the atmosphere. The O_4 lines are available within the entire spectral range used in the DOAS method, from near UV to near IR (cf. Figure 6) [11]. The strength of the lines depends only on the air density, which in turn varies only little or can be determined very accurate (via air pressure and temperature). In addition, the error probability can be minimised by automating the measurements (determination of the ILS function) and the analysis (e.g. by integrating the software).

The positions of the most pronounced absorption bands are listed in Table 1.

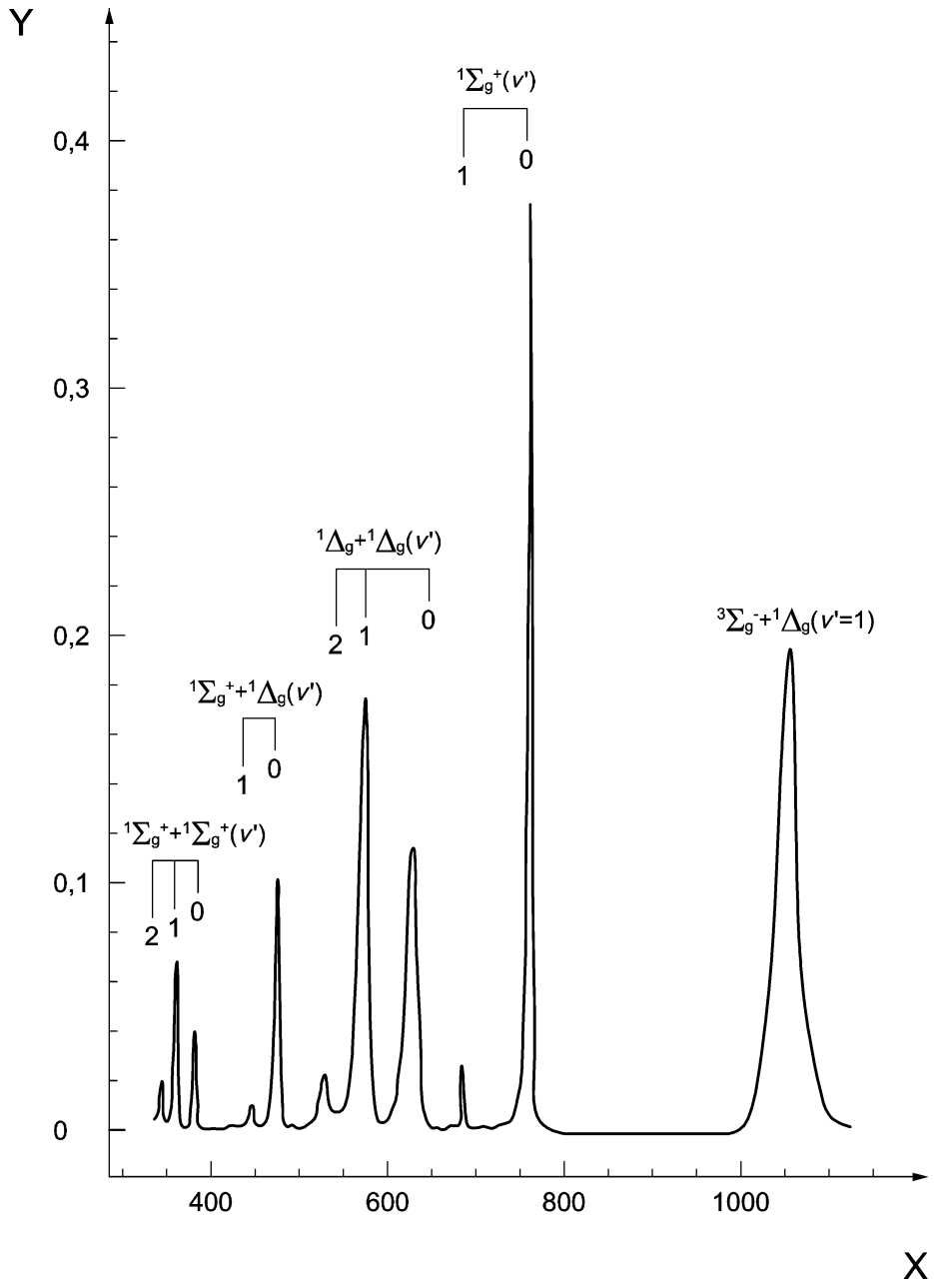

Key
X Wavelength
Y Absorption

Figure 6 — Spectra of O_4 and O_2

9 Quality assurance

9.1 Measurement procedure

9.1.1 General

As a general rule, a distinction can be made between quality-assurance steps performed before, during and after the measurements. The manufacturer's instructions shall be observed. All quality assurance measures and the changes made in response thereto shall be duly documented.

9.1.2 Steps carried out before the measurement

— Check of compliance with operating conditions (see Clause 8);

— wavelength calibration checks;

— selection of appropriate substance-specific averaging times, depending on intended performance characteristics;

— adjust the intensity level of the received radiation;

— steps designed to ensure that all system performance characteristics supplied additionally by the analytical algorithm will be stored in memory and/or documented along with the measurement so as to permit retroactive quality assurance steps (e.g. general and substance-specific signal intensities, signal-to-noise ratios, residuals).

9.1.3 Steps carried out during the measurements

— Verification of constituent-related signal intensities at suitable time intervals, depending on meteorological conditions (with readjustment if necessary);

— regular cleaning of optical components situated in the optical path;

— if the lamp spectrum is not recorded automatically, a possibility to manually check the light source stability and its spectrum should be provided.

9.1.4 Steps carried out after the measurements

— Plausibility checks of concentration measurements, e.g. via time series permitting a verification of influences such as zero drift, correlations between concentrations and signal intensities or meteorological parameters (e.g. air temperature, moisture, precipitation, radiation, visibility), or re-analysis of the raw spectral data by another DOAS evaluation algorithm (other software);

— examination of stored system performance parameters, or of the analytical algorithm, for unusual patterns (e.g. day curves of direct solar radiation incidence, drift of S/N-ratios or residuals).

9.2 Apparent saturation of absorption bands

Where unresolved spectral structures, usually atomic lines or molecular rotation lines, are present in low-resolution spectra, the instrument may measure an optical density that appears too low. The optical density of any such (unresolved) spectral structure does not increase in proportion with the density of the trace substance column; in extreme cases, the optical density reaches a saturation value.

According to the experience gathered to date, apparent saturation may occur with NO, H_2O and O_2 spectra.

In practice saturation may be mitigated by reducing the path length or selecting a different spectral interval for data evaluation.

This phenomenon can also be remedied by using a spectrometer with a higher resolution capacity or (if the saturation is weak) by mathematical correction. The latter option may be based on an empirically determined correction function or on a correction function calculated from high-resolution trace substance spectra which allocates a (lower) true column density to each measured apparent column density (concentration $\times$ path length) for a given absorber.

Annex A
(informative)

Components of the measurement system

A.1 General

Open-path DOAS measuring systems exist in various optical configurations which nevertheless operate on the same basic principle. Figure A.1 shows the schematic view of a DOAS instrument. Radiation from a suitable source undergoes absorption processes on its path through the atmosphere. In (a) an example of this radiation entering the spectrometer is given, where HCHO is assumed to be the sole absorber and the radiation source has smooth spectral characteristics. This absorption spectrum shows the vibrational - rotational structure of the absorption bands. (b) The same spectrum convoluted by the spectrometers ILS function reaches the detector. In the detector the wavelength is mapped to discrete pixels. This spectrum (c) is then amplitude-digitised and stored in the computer for numerical analysis.

In a bistatic set-up the transmitter and receiver are installed at either end of the absorption path, respectively. As a result, infrastructural resources such as a power supply shall be available at both ends. Alternatively, the optical path can be folded at one end of the absorption path by installing a retro-reflector. This monostatic version facilitates the operation of the instrument since major infrastructure equipment needs to be provided only at one end. The light passes the measurement volume twice and thus a better signal is achieved. This setup also allows regular lamp spectra measurements, which reduces measurement errors due to changes in the lamp spectrum and detector properties. On the other hand, the monostatic set-up exhibits additional losses of radiation intensity at the retroreflector.

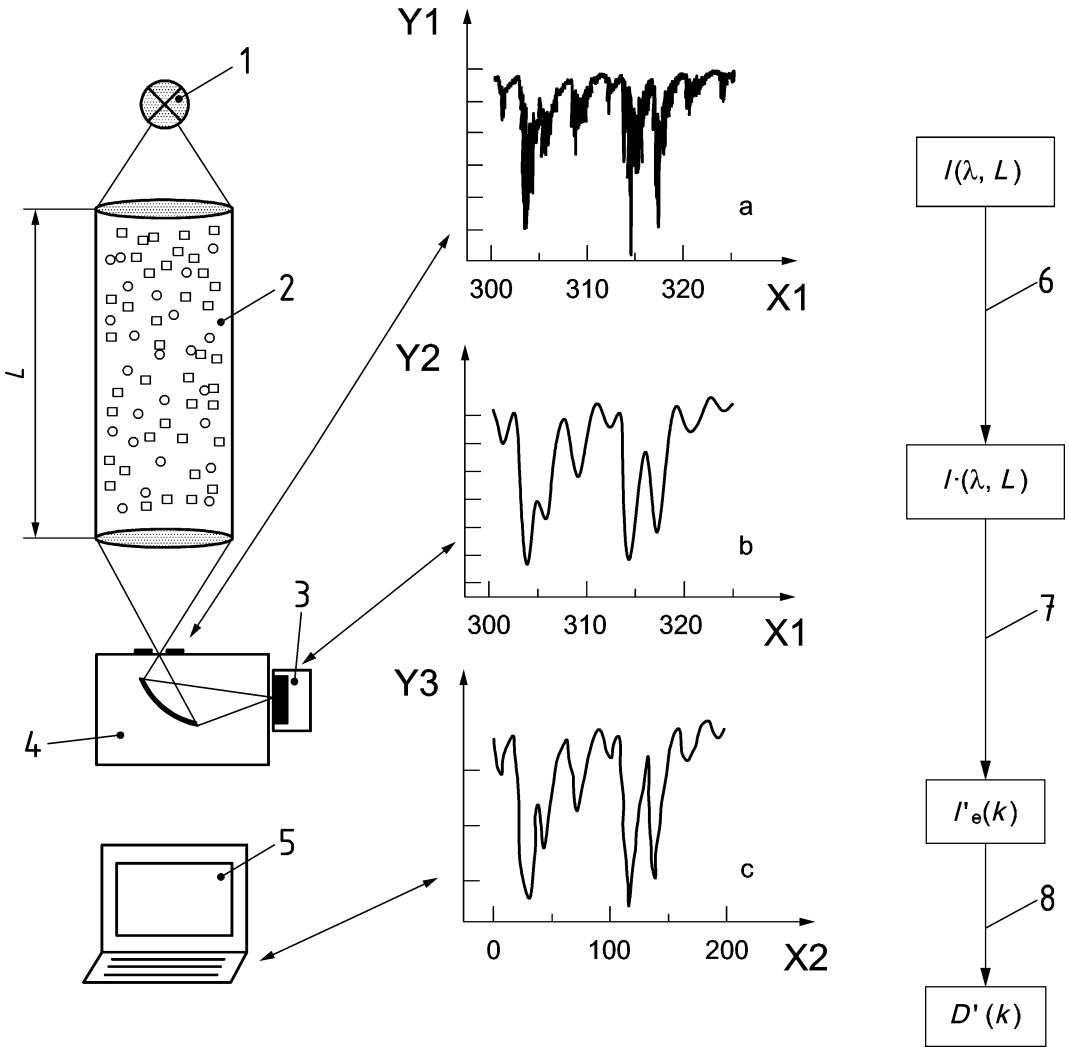

Key

1 Radiation source
2 Atmosphere
3 Detector
4 Spectrometer
5 Data processing
6 Convolution
7 Discretisation
8 Logarithm
X1 Wavelength
X2 Channel
Y1 $I(\lambda,l)$
Y2 $I(\lambda,l)\cdot H$
Y3 Binary units

Figure A.1 — Principle set-up of a DOAS system: the right part illustrates how the intensity of an absorption spectrum (here: formaldehyde) varies with the measurement and the analytical process

A.2 Main components

A.2.1 Radiation source and transmitter

High-pressure xenon short-arc lamps with an output between 75 W and 500 W are the most commonly employed radiation sources. These units have operating pressures between a few bars and 100 bars and are noted for their very small, powerful light spot (very little beam divergence). The colour temperature varies between 6 000 K and 10 000 K. The service life of the lamp ranges between 200 hours and six months, depending on the requirement profile. Xenon emission lines superimposed on the spectrum of the thermal radiator will coincide in part with the absorption lines of the gases to be measured. This needs to be duly taken into account in the spectral analysis. To increase the radiation yield, the lamp is usually fitted with optical projector equipment (e.g. a parabolic reflector).

In more straightforward applications (e.g. SO_2 emission measurements), commercially available halogen lamps may also be used. For some compounds (e.g. NO_2 and SO_2) LEDs are also available as radiation source.

The data treatment of a DOAS system is optimised for a certain lamp type. When the lamp is changed the manufacturer’s recommendations shall be followed.

A.2.2 Receiver

The purpose of the receiving unit is to feed the radiation into the spectrometer once it has passed the monitoring path. In the case of concentrated radiation sources (projector, mirror or retro-reflector) this means that the beam incident in quasi-parallel directions has to be focused on one small point, i.e. the entrance slit. Often the incoming radiation is first injected into an optical fibre, which terminates in the spectrometer's entrance slit.

The use of astronomic telescopes (see Figure A.2) is typical in this application. Commonly used reflector telescopes include the Newton telescope and the particularly compact Cassegrain type (with a defined focal distance). The most straightforward but also the longest type of optical receiver for a given focal length is a concentric parabolic reflector having the receiving end of an optical waveguide terminating in its focus.

Refracting, or lens-type, telescopes are used for smaller apertures and F-numbers (ratio of the focal length to the lens diameter) of more than 4. Designing a lens-type telescope with a small F-number for the DOAS application is a highly complex task, particularly because of the chromatic errors, if a broad spectral range is to be covered.

One particular technology involves the use of coaxial telescopes and retro-reflectors. Deflector mirrors are arranged so as to reserve coaxial rings on the main reflector for transmitted and received radiation, respectively. The emitted radiation is deflected by exactly 180°; it returns to the same telescope in a parallel direction with a yield of several percent, depending on the size and quality of the retro-reflectors and the absorption losses incurred on the monitoring path.

The retro-reflectors are passive and require no adjustment. However, they should be aimed at least roughly at the transmitter and should not be excessively dirty or frozen. If reflector prisms are used ensure that water condensation at the backside is avoided (e.g. by using a desiccant). Configured from triple prisms, they undergo no ageing but become dirty over time and should therefore be cleansed at regular intervals, e.g. annually. This characteristic makes this method very attractive for routine measurements. Coaxial telescopes can be built from any basic design. As a general rule, an outer ring is reserved for outgoing (transmitted) radiation while an inner ring is reserved for incoming (received) radiation.

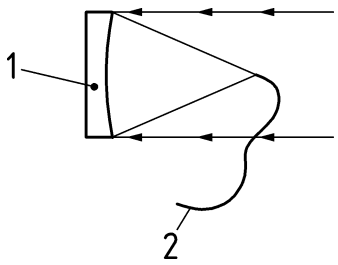

Key
1 Parabolic reflector
2 Fibre

a) Simple telescope

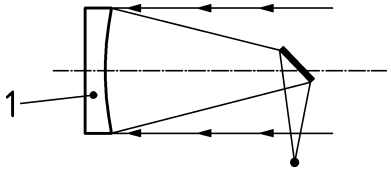

Key
1 Parabolic reflector

b) Newton telescope

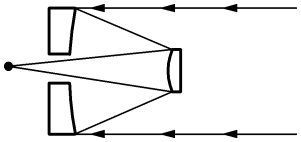

c) Cassegrain telescope

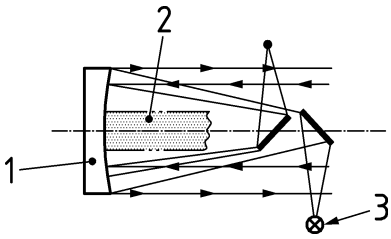

Key
1 Parabolic reflector
2 Blind zone
3 Lamp

d) Coaxial Newton telescope

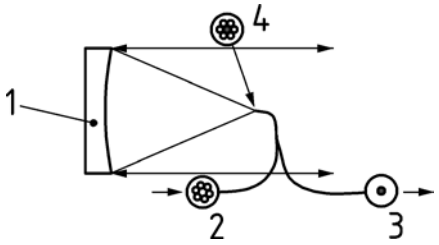

Key
1 Spherical/parabolic reflector
2 Emitting fibre (light source site)
3 Receiving fibre (spectrograph site)
4 Combined fibre

e) Telescope with combined emitting and receiving fibre

Figure A.2 — Examples of commonly used telescopes [7], [12], [13]

A.2.3 Spectrometer

A.2.3.1 General

Two types of spectrometer are currently in use, both generate a planar image of the entrance slit in the focal plane.

A.2.3.2 Czerny-Turner spectrometer

With this system, a plane grating is illuminated with measuring radiation which is incident in a parallel direction. Optical imaging devices (usually spherical reflectors) are mounted in front of the grating and behind it, so that a W-shaped beam path is obtained. The symmetrical design makes it possible to compensate for imaging aberrations. The grating for varying the wavelength interval is usually rotatable, but Czerny-Turner systems with a fixed wavelength range are also available. Some instruments have a grating stack containing several different gratings which are changed automatically during a measuring procedure.

A.2.3.3 Holographic grating with planar image field

This spectrometer usually consists of a single optical element, viz., a grating placed directly on an imaging mirror by a holographic technique. The beam geometry is strictly defined to obtain a flat image field. In general, a system of this type requires no moving parts. Sometimes such spectrometers are sealed shut after adjustment and will then remain maintenance-free for their entire service life.

The fact that the image is flat in its focal plane permits the use of diode arrays or matrix-type detectors providing an almost wavelength-independent spectral resolution.

A.2.4 Detector unit

A.2.4.1 General

The purpose of the detector is to convert the radiation intensity into an electrical signal. This conversion has to be made in a position-dependent manner so that the spectral information of the spectrum spread out in one plane will be preserved. Diverse varieties are available.

Detectors with movable parts (optomechanical detectors) may be more sensitive to abrupt movements than semiconductor detectors.

A.2.4.2 Optomechanical detectors

A.2.4.2.1 General

In an optomechanical detector, the spectrum is scanned through a moving slot. Due to the narrowness of this slot, only a small wavelength range reaches the sensor at any one time. This ensures that the spectrum is spatially scanned during the slot movement, and that the detector can convert the spectrum intensity into electrical signals consecutively over time. This principle supports the use of single-channel detectors (e.g. photomultipliers). It has the disadvantage that only a small portion of the radiation will be utilised at a given time.

A necessary condition for optomechanical detection is the use of sufficiently high scanning frequencies (typically > 100 Hz) so that the measurements will not be impaired by air turbulence on long optical paths. Usually, the influence of air turbulences is further reduced by averaging the measurement over several individual scans.

A.2.4.2.2 Optomechanical detectors with high-speed scanning function

A disk (Figure A.3) arranged in the spectrometer's focal plane has numerous (e.g. 50) radially extending exit slits. A suitable wavelength region (e.g. 50 nm) of the absorption spectrum is masked by a window, with radiation being admitted through no more than one exit slit at any given time. The radiation passing the exit slit is converted into an electric signal by a photomultiplier, then digitised (typically into a few hundred digital values per scan) and recorded by a computer. A scan takes about 10 ms to complete; the scans are repeated with a frequency of approx. 100 Hz, with an (infrared) light barrier signalling the start of a new scan (opto trigger). The number of scans superimposed for a typical measurement ranges from a few thousand to ten thousand.

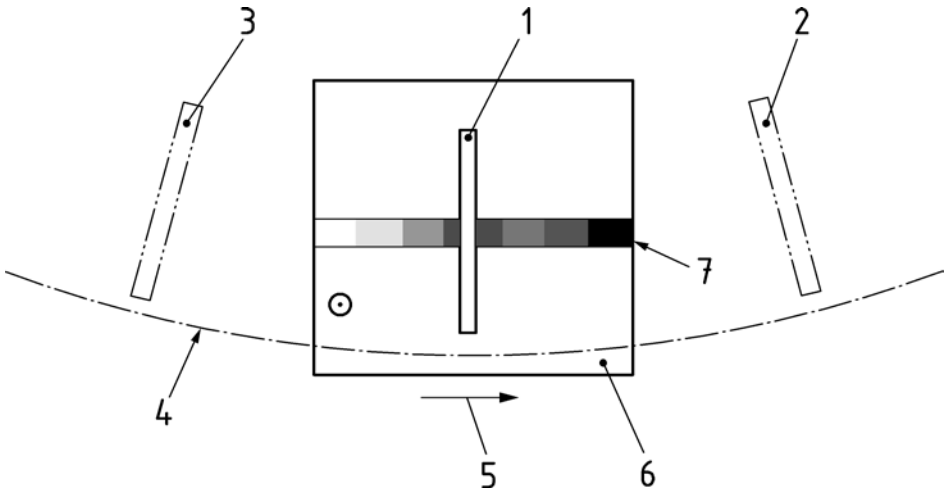

Key
1 Active slit
2 Preceding slit
3 Following slit
4 Opto trigger
5 Rotation direction
6 Window
7 Spectrum

Figure A.3 — Schematic representation of an optomechanical detector with rotating chopper

A.2.4.2.3 Optomechanical detector with horizontally oscillating slit

The output slit of the spectrometer is linked to a linear scanner which moves the slit in the dispersion direction and permits a servo-assisted, repeated scan of a 50 nm interval. The change in the wavelength is linear over

time. Since the output slit remains vertical to the dispersion direction at all times, the unit achieves a spectral resolution which is constant over the spectrum. A single scan will typically take 10 ms to complete. To achieve a high sensitivity, several thousand scans are co-added over an integration time of between 10 min and 15 min. Individual spectra are thus obtained at a frequency of approximately 100 Hz.

A.2.4.3 Semiconductor detectors

A feature common to all array detectors is that they combine several hundred to several thousand individual photosensors in a multi-line arrangement. Array detectors are normally implemented in the form of monolithic semiconductor circuits. They record all wavelengths of the selected spectral band simultaneously. Compared with optomechanical detectors, array detectors have the advantage of utilising the available radiation intensity much more efficiently, viz., by 2 to 3 orders of magnitude (multiplex advantage). In addition, they eliminate moving mechanical components. Basic problems involve pixel-related structures (*fixed pattern structure* or variation thereof as a function of illumination, age, temperature, etc.) and inter-pixel crosstalk.

There are currently three technical embodiments of semiconductor array detectors:

a) NMOS-PDA
This array type is characterised by a monolithic combination of individual photo diodes in N-Channel Metal Oxide Semiconductor (NMOS) technology. For scanning, the individual diodes are sequentially connected to scan lines via semiconductor switches (NMOS transistors) which transmit the photo charge to the amplifier. The main drawback is the fairly high scan noise of about 1 000 electrons.

b) CMOS-PDA
This type consists of a monolithic structure of individual photo diodes based on Complementary Metal Oxide Semiconductor technology (CMOS). Much as with NMPS-PDAs, the individual diodes are sequentially connected to scan lines via semiconductor switches and amplifiers, as appropriate. The scan lines transmit the photo charge or voltage to the amplifier. CMOS-type array detectors are gaining in importance since they can be combined with additional functionalities such as amplifiers, A/D converters and, potentially, processors. Scan noise can be greatly reduced via a built-in amplifier.

c) CCD array detectors (charge coupled devices)
These detectors normally contain no diode structures in the semiconductor itself; the photo charge is conveyed to the scanning amplifier via peristaltic electric fields in a direction parallel to the semiconductor surface. Issues include the charge transfer efficiency and the sensitivity reduction due to partial coverage of the sensitive semiconductor surface by the electrode structures generating the peristaltic field. The scan noise (typically 10 electrons) is normally dominated by electron shot noise on the order of 1 000 electrons.

Current instruments usually rely on silicon semiconductor elements in NMOS technology, typically with 512 or 1024 photodiodes, which are adapted to the geometry of the spectrometer. The influence of the dark current can be reduced by cooling the PDA and/or by separately determining its magnitude by masking and compensating for it arithmetically.

In addition, the inhomogeneous illumination of the pixels has to be taken into account with the aid of a transfer function (*fixed pattern noise*). The transfer function is individually determined for each detector and subsequently factored into the analysis. Nevertheless, the irregular illumination of the spectrometer (or rather, its detector) is a cause of residual structures with all instrument types based on PDA technology. These structures can be reduced by the application of optical fibre with mode mixers [14].

Annex B
(informative)

Influence of scattered solar radiation

Scattered solar radiation may enter the receiver system (telescope) and interfere with the analysis. The portion of scattered solar radiation depends on the following factors:

— Wavelength:
As a general rule, the amount of scatter increases markedly as the wavelength decreases. However, the radiation intensity at wavelengths below approximately 300 nm is extremely low due to the stratospheric ozone layer, so scattered solar radiation will not be a problem here.

— Time of day and meteorological conditions:
The amount of scattered radiation is greatly reduced, e.g. under cloud cover.

NOTE This factor does not affect the measurement itself.

— Aerosol content of the atmosphere:
Aerosol causes not only an attenuation of the beam radiation intensity but raises the incidence of scattered solar radiation above the level of Rayleigh scattering. In extreme cases (e.g. fog), only scattered solar radiation can be detected, thus making reliable measurements impossible.

— Length of the optical path and design of the optical system (spatial acceptance angle):
The useful radiation intensity is attenuated more strongly and the relative portion of scattered radiation increases with the length of the optical path.

— Background:
The amount of scattered sunlight strongly depends on the background of the transmitting telescope (bistatic setup) or retroreflector (monostatic setup). A sky background causes a high level of scattered solar radiation whereby a wall or mountain leads to a low level of scattered radiation.

Scattered solar radiation is a problem because it exhibits a pronounced Fraunhofer structure in the UV and visible spectral range. It may thus interfere with trace substance absorption structures; moreover, terrestrial trace substance absorption bands (e.g. ozone and NO_2 bands from the stratosphere) may be superimposed on the scattered solar radiation.

The influence of scattered solar radiation on DOAS measurements can be minimised or eliminated by a number of measures:

— Recording of scattered solar radiation spectra and subtracting them from the measured absorption spectrum.

  Scattered solar radiation spectra can be recorded, e.g. by switching off the radiation source (or blocking the light) or pointing the telescope besides the radiation source. The first method is more accurate, as background light may change very strongly even for small differences in viewing direction.

— Limitation of the receiver's spatial acceptance angle to the size of the radiation source.
Since scattered solar radiation will usually be incident from all over the spatial acceptance angle whereas useful radiation originates only from the radiation source, the ratio of useful radiation to scattered solar radiation can be improved in this manner.

— Inclusion of a scattered solar radiation spectrum into the above-described fitting process in the form of an additive portion $S(\lambda)$ (see Formula (4)).

This is possible, on the one hand, because the solar spectrum changes only little in time (mainly due to changes in terrestrial absorption and the Ring effect [15]), and on the other hand, because it exhibits highly characteristic spectral structures. Note that the effectiveness of this approach is limited because the Fraunhofer spectrum is modified by radiation transport in the atmosphere, which is difficult to be modelled.

Annex C
(informative)

Examples of implementations of the DOAS technique

C.1 The Opsis technique

C.1.1 General

The DOAS system AR500 (Opsis) has been type approved according to relevant European Standards (CEN) and VDI guidelines and according to the guide “Demonstration of equivalence of ambient air monitoring". The test results show that the DOAS system fulfils the requirements for ambient air monitoring instruments and is equivalent to the reference methods for O_3, NO_2 and SO_2.

C.1.2 Schematic presentation

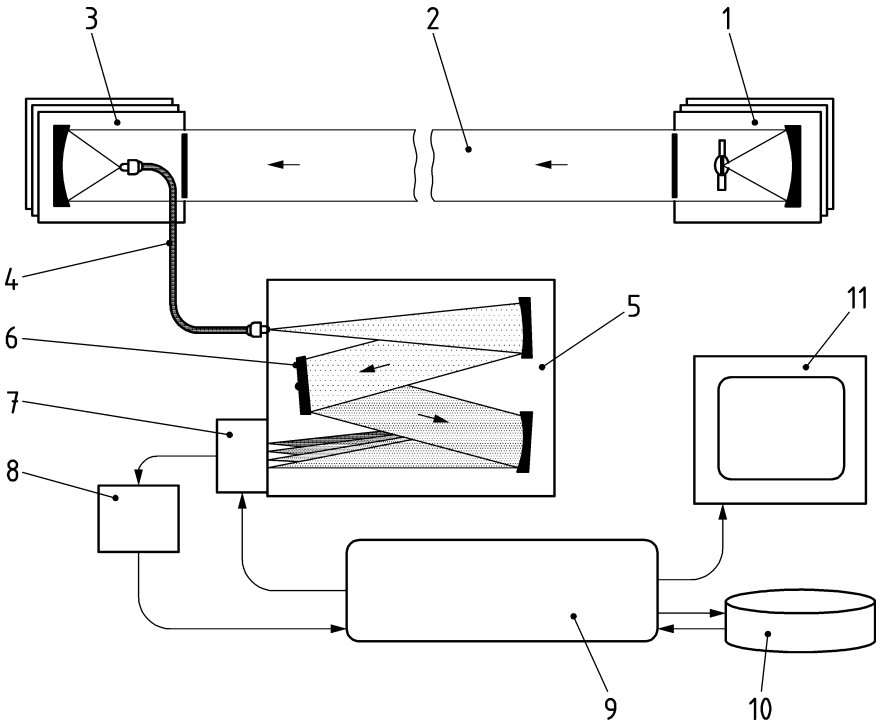

Key
1 Radiation source/emitter
2 Monitoring path
3 Receiver
4 Fibre optic cable
5 Spectrometer
6 Grating
7 Detector
8 A/D converter
9 Computer
10 Data storage
11 Screen

Figure C.1 — Schematic presentation of the Opsis monitoring technique

C.1.3 Procedure

Once the data has been collected, the atmospheric raw spectrum (Figure C.2) is stored in the computer's memory.

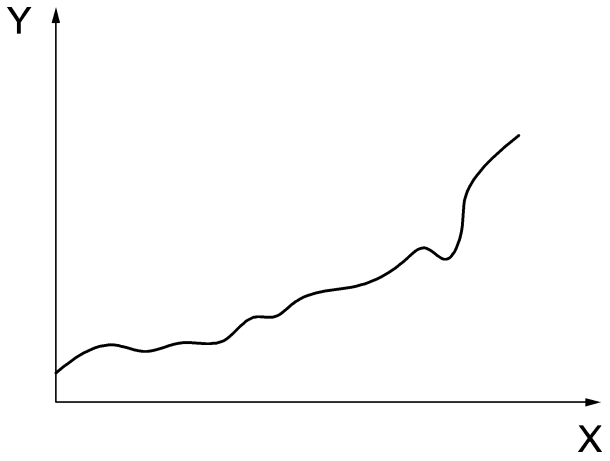

Key
X Wavelength λ
Y Intensity I

Figure C.2 — Atmospheric raw spectrum

First the atmospheric raw spectrum is compared with a lamp spectrum (zero gas spectrum). This has previously been registered with no absorption gases present and is used as a system reference (Figure C.3).

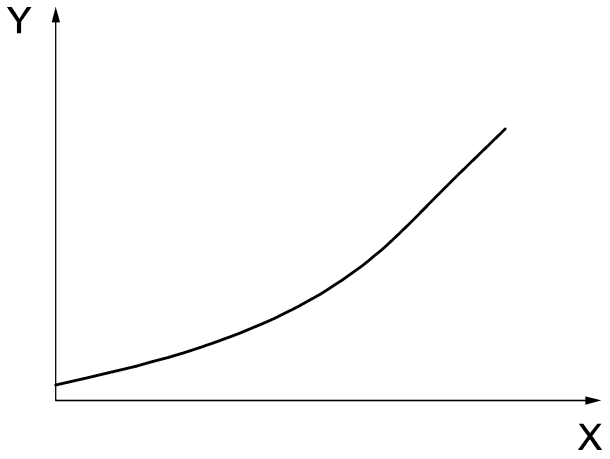

Key
X Wavelength λ
Y Intensity I

Figure C.3 — Lamp spectrum (zero gas spectrum)

After division by the lamp spectrum, the total radiation absorption between the transmitter and the receiver is obtained (Figure C.4). This result is caused not just by the gases that are present but also by, e.g. aerosol in the atmosphere or dirty optics.

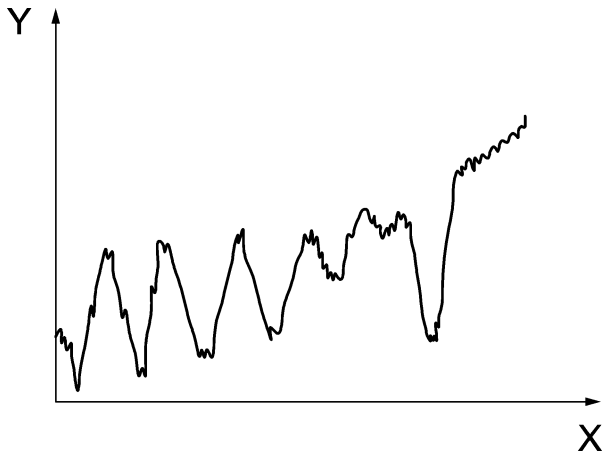

Key
X Wavelength λ
Y Optical density D

Figure C.4 — Absorption spectrum

The task now is to separate the radiation absorption of the gases from other influences. To do this, the system takes advantage of the fact that only gas molecules will cause rapid variations in the absorption spectrum (see Clause 5). The slow variations, which give rise to the gradient on the absorption curve, result from a large number of known and unknown factors. Their influence can be eliminated completely by mathematically matching a curve which follows the slow variations in the spectrum (curve fit), see Figure C.5.

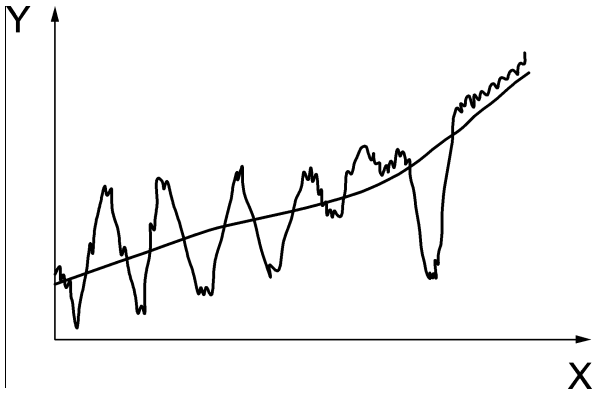

Key
X Wavelength λ
Y Optical density D

Figure C.5 — Curve fit

After dividing by the fitted polynomial, all that remains are the rapid variations. For the remaining calculations, the negative logarithm of the curve is taken, which turns the curve upside down (Figure C.6). A differential absorption spectrum has now been obtained. This spectrum is a combination of the various gases present between the transmitter and the receiver at the moment of detection. In the example this is called Z.

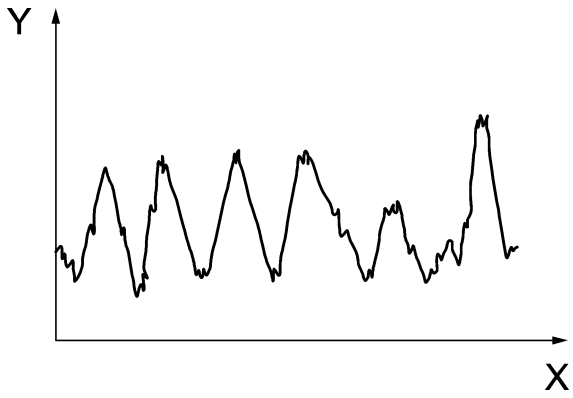

Key
X Wavelength λ
Y Differential optical density D'

Figure C.6 — Differential absorption spectrum (gas mixture Z, consisting of components X_1 and X_2)

The gases that absorb radiation in this wavelength range are already known, and a pre-recorded reference spectrum for each gas is stored in the computer's memory. In this example there are only two gases, called X_1 and X_2. The task is to determine their concentrations C_1 and C_2 that combine to give the best match for Z. The system achieves this by creating a new curve out of the sum of the two reference spectra (Figure C.7), varying values until the best correspondence is achieved with the lowest least squares residuum. The formula the computer uses can be expressed as $C_1 \times X_1 + C_2 \times X_2 = Z$.

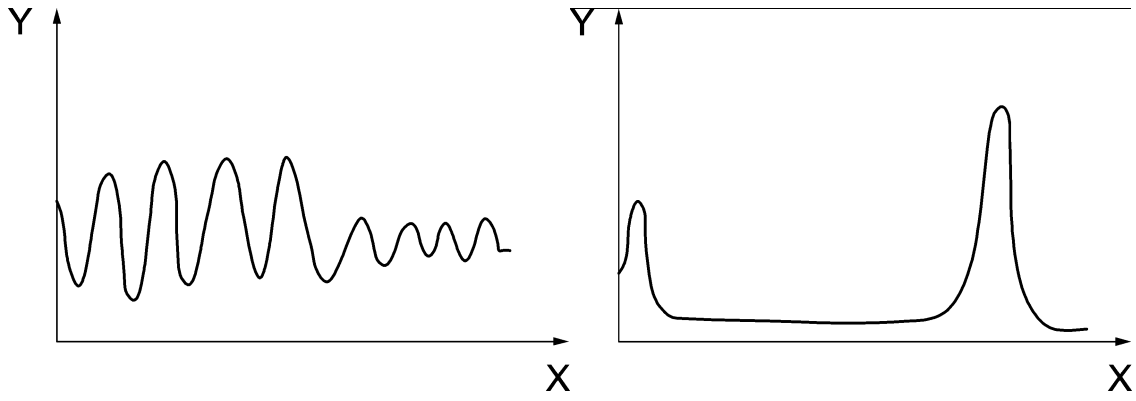

a) Component 1 (X_1) **b) Component 2 (X_2)**

Key
X Wavelength λ
Y Differential optical density D'

Figure C.7 — Components' reference spectra

Finally, the result is checked by determining the difference between the measured and the calculated curves by calculating the standard deviation representing the absolute deviation of the two curves for each point (Figure C.8). The shaded area shows the difference. The more reference curves stored in the computer's memory, the more accurate the result of the calculation will be. However, even if there should be some unexpected interference, i.e. when the measurements are affected by a gas whose reference spectrum is not stored in the computer's memory, the computer nevertheless evaluates the gases it is programmed for. The influence of the unknown gas is presented as an increase in the standard deviation in the measurement result.

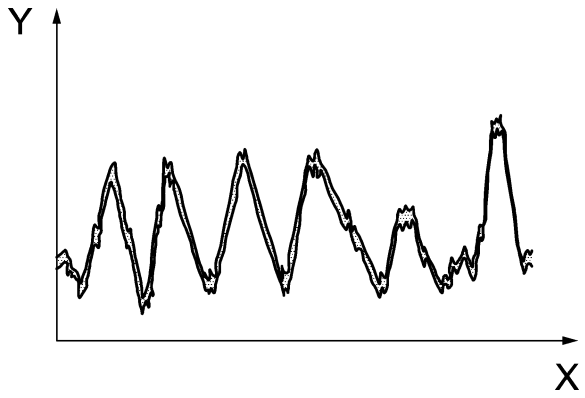

Key
X Wavelength λ
Y Differential optical density D'

Figure C.8 — Superposition of measured and calculated spectra; the shaded area shows the difference between both

C.2 The SANOA technique

C.2.1 Schematic presentation

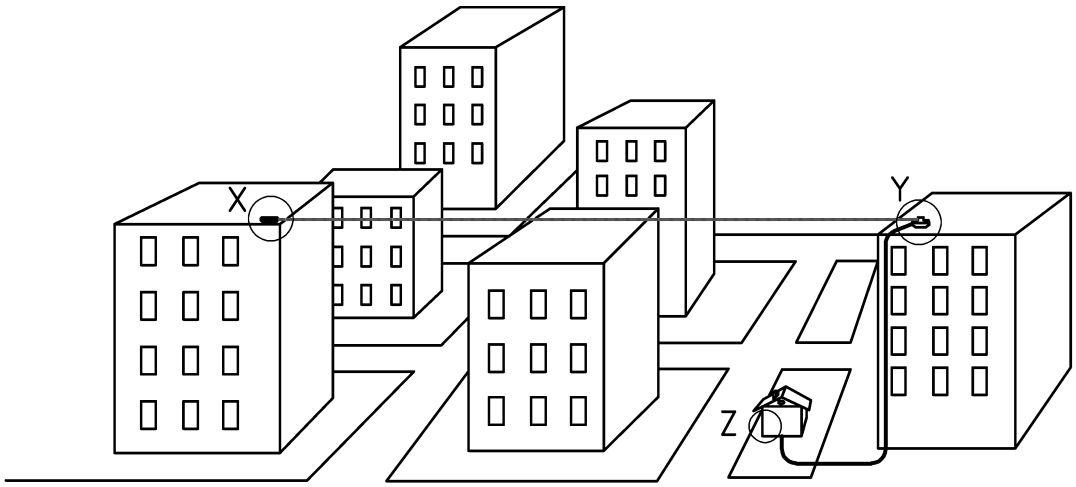

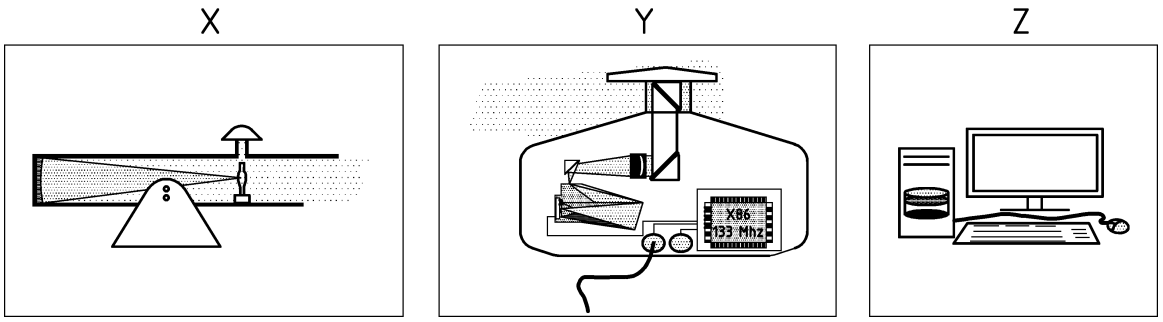

Figure C.9 — Schematic presentation of the SANOA monitoring technique

C.2.2 Procedure

C.2.2.1 Atmospheric raw spectra

The instrument's processor acquires atmospheric raw spectra (see Figure C.10) from the photodiode array at two different integration times in order to magnify the low signal in the deep UV range. The integration time is optimised according to the signal strength, then a 4 times longer integration time is used to magnify the deep UV range. For each acquired spectrum, an associated dark spectrum is collected using the same acquisition parameters such as integration time and averaging time. The spectra are then stored in the memory of the SANOA instrument and are ready to be transmitted to a VisionAIR platform.

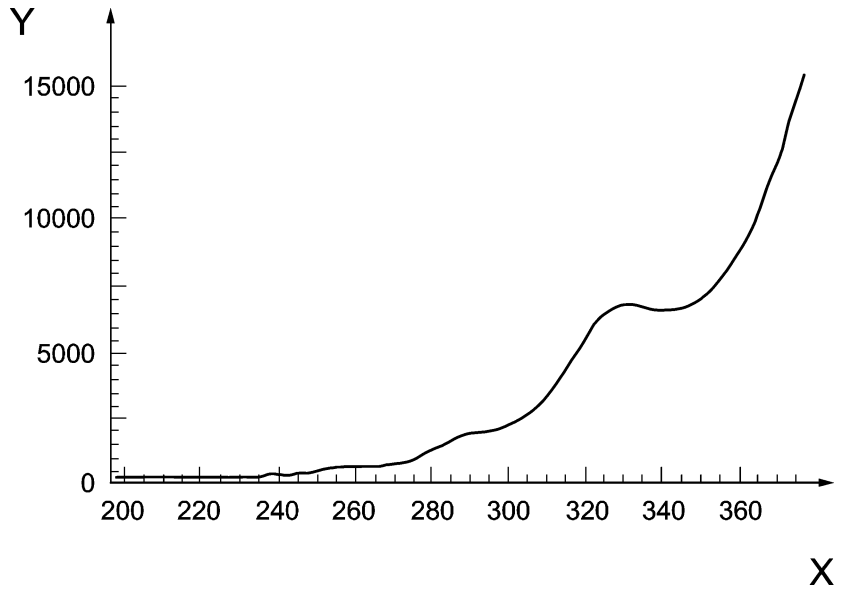

Key
X Wavelength λ
Y Intensity I

Figure C.10 — Atmospheric raw spectrum

C.2.2.2 Spectra quality check analysis

The instrument's processor sends the spectra to the VisionAIR platform for analysis via a communication line. This line is able to transmit the data to a distant location up to 1 600 m apart. For larger distances, the data transmission line can be extended by using telecommunication techniques such as satellite channels or fibre optic cables.

At first the spectra are analysed according to the intensity along the wavelength axis. The spectra may be rejected for insufficient intensity in the deep UV spectral range. Relevant wavelength intensity ratios are determined and shall fit with pre-established tolerances. These ratios show if the spectrum is well balanced within the wavelength range. For example, the intensity of a deep UV signal (i.e. for 220 nm) is compared to the 280 nm signal intensity and the ratio of intensities at 220 nm and 280 nm is formed. If the ratio is smaller than the tolerance value, the spectrum is rejected.

C.2.2.3 Baseline spectra analysis

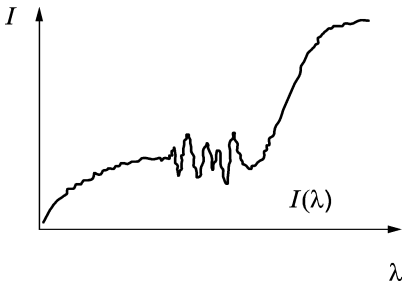

Figure C.11 — Atmospheric raw spectrum $I(\lambda)$

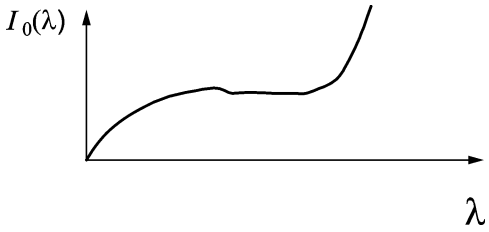

Figure C.12 — Baseline spectrum $I'_0(\lambda)$

The atmospheric raw spectrum (Figure C.11) is transformed into a transmittance signal by dividing the signal with the baseline spectrum I'_0 (Figure C.12). The baseline spectrum is determined by a dedicated Golay-Savitzky smoothing algorithm.

C.2.2.4 Differential spectra calculations

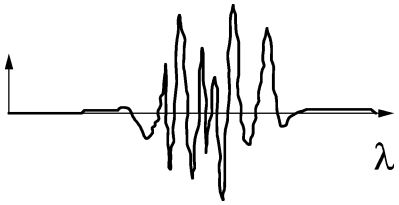

Figure C.13 — Differential atmospheric spectrum

According to the Beer-Lambert law, the quantity log (I'_0/I) is a linear function of path length and concentration. Slow variations are removed from this quantity using non-linear fit and normalisation processes. Only rapid variations of the spectral intensities are considered, while data processing eliminates the slow variations which are less relevant for the identification and quantification processes. According to the Beer-Lambert law the differential optical absorption spectrum (Figure C.13) is an algebraic linear combination of each signature of the species present in the optical path. It also includes a combination of lamp and solar signatures. Each spectrum signature reflects a component reference spectrum (Figure C.14).

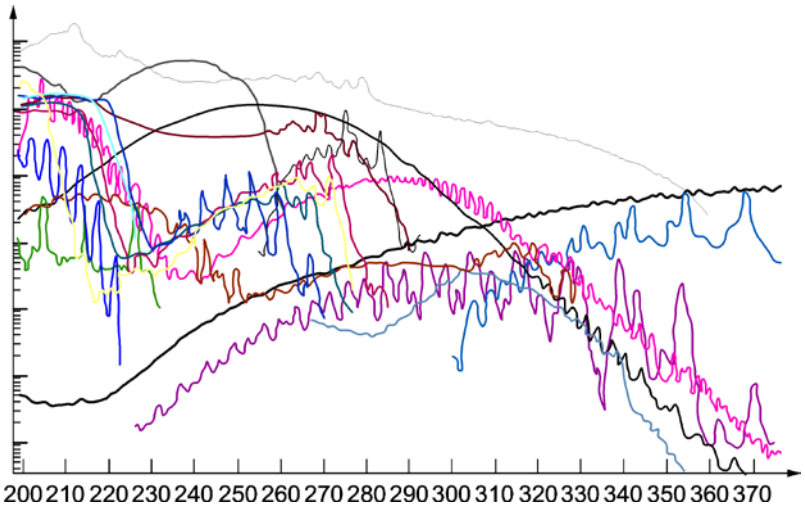

Figure C.14 — Examples of reference spectra (18 components)

C.2.2.5 Wavelength scale check

The differential optical absorption spectrum contains always the oxygen and the xenon signatures because oxygen is always present in the background at constant concentration and xenon is one of the major lamp component signatures. These signatures are used to calibrate the wavelength axis scale at each analysis of a single spectrum. Relevant absorption or emission lines are used to scale the wavelength axis. This scaling procedure ensures correct wavelength measurements and prevents any unwanted shifting effects in the spectrum due to mechanical movements within the optics of the spectrometer.

C.2.2.6 Residual spectra

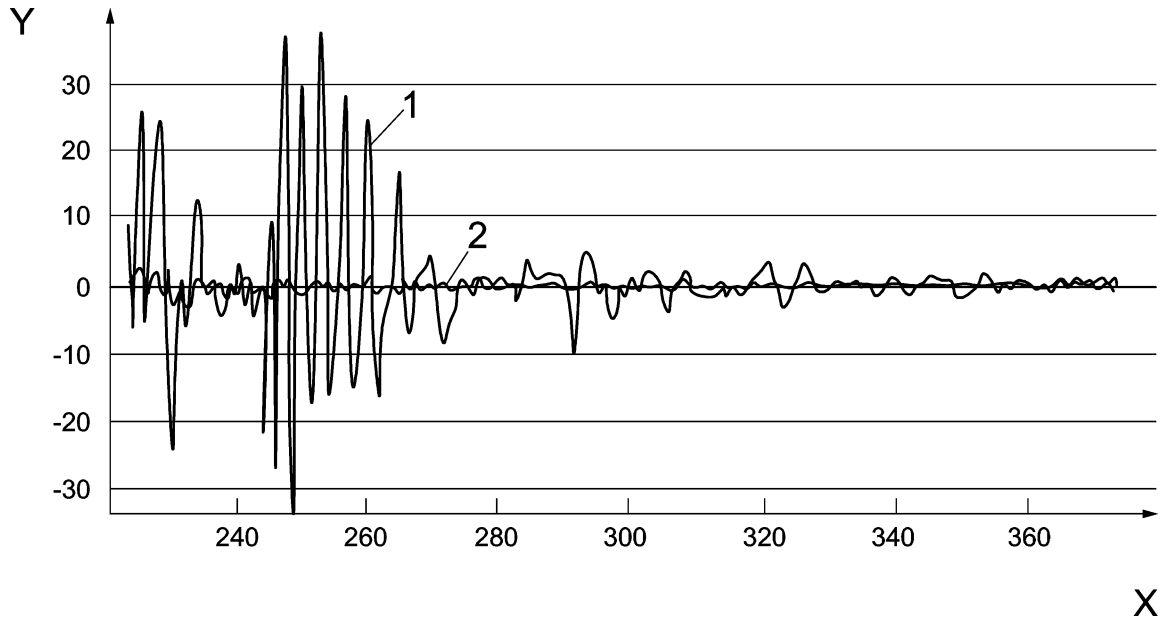

Key
1 Acquired DOAS
2 DOAS residual
X Wavelength λ
Y Differential optical density D'

Figure C.15 — Differential optical absorption spectrum and residual spectrum

Every component species has its own absorption spectrum. The slow variations are removed from the reference spectrum in the same way as applied to the atmospheric raw spectrum. Thus again, only the relevant information, originating from the rapid variations, is considered. This method makes it possible to compare the acquired differential optical absorption spectrum with the components reference spectra.

Each species signature is then removed from the differential optical absorption spectrum using a least squares method. A residual spectrum is then obtained by removing all identified reference signatures (Figure C.15). At the end of the process the residual spectrum should contain no features of species and should thus be as flat as possible. Any unwanted signature in this spectrum indicates that an unexpected signature has not been considered within the modelling stage. This unwanted signature can be attributed to a local environment signature and treated by the identification and quantification processes as applied to any reference component signature. This kind of iterative analysis may help to improve the model analysis used by the Vision AIR platform. The residual spectrum reflects the performance of the fitting procedure with the component spectra as part of the quantification process.

C.3 The Fibre LP-DOAS system

C.3.1 General

This method is described in detail in [2], [7], [14] and [16].

C.3.2 Schematic presentation

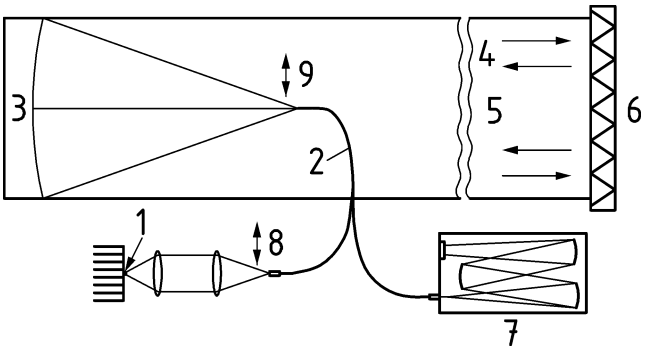

Key
1 Light source (LED or Xe arc)
2 Fibre bundle
3 Sending/ Receiving telescope
4 Light beam
5 Monitoring path
6 Retro reflector
7 Spectrometer (temperature stabilised) with detector
8 Shutter to block light source and perform background measurements
9 Lamp reference plate made of a diffusive material to reflect light back into the receiving fibre

Figure C.16 — Schematic presentation of the Fibre LP-DOAS System

C.3.3 Procedure

Prior to a start of a measurement, the detector offset (shortest integration time and approx 1 000 scans) and dark current (long integration time approx. 60 s, 1 scan) are measured. Dark current spectrum is corrected by the offset.

The system measures beside the atmospheric raw spectrum also regularly (at least every few minutes):

— an atmospheric background spectrum with a closed shutter at the light source;

— a lamp reference spectrum with the reference plate moved in front of the fibre bundle, this spectrum is used as system reference.

The atmospheric spectra are recorded at different wavelengths with different integration times to achieve similar intensities for the different wavelength regions. The integration time is optimised each time according to signal strength.

The data analysis first corrects all spectra by offset and dark current. Furthermore the atmospheric spectrum will be corrected using a recent background spectrum to remove any signal from scattered light. The spectral analysis compares the atmospheric spectrum with a recently recorded lamp reference spectrum, by dividing them and taking the logarithm multiplied by –1 according to Formula (8). The spectrum contains now narrowband (rapid variation) and broadband (slow variation) absorption as well as broad band losses, e.g. due to optical losses of the system. The different broadband absorptions cannot be separated. Only the narrowband structures contain characteristic trace gas information which is used in the DOAS analysis. To remove any broad band absorption and losses, the spectrum is high pass filtered. The spectrum is now the

differential absorption spectrum containing the narrow band absorption structures from the different trace gases. In the following step all relevant modelled spectral structures of trace gases are fitted to this spectrum by a linear-non linear Levenberg-Marquardt fit to derive their concentration. In the fitting procedure an additional polynomial is included to remove any remaining broad band structures. The final concentration is calculated by using the total absorption light path. For conversion to mixing ratios (e.g. nmol/mol) the simultaneously measured atmospheric pressure and temperature are used. An example for an NO_2 measurement with a LED system is shown in Figure C.17.

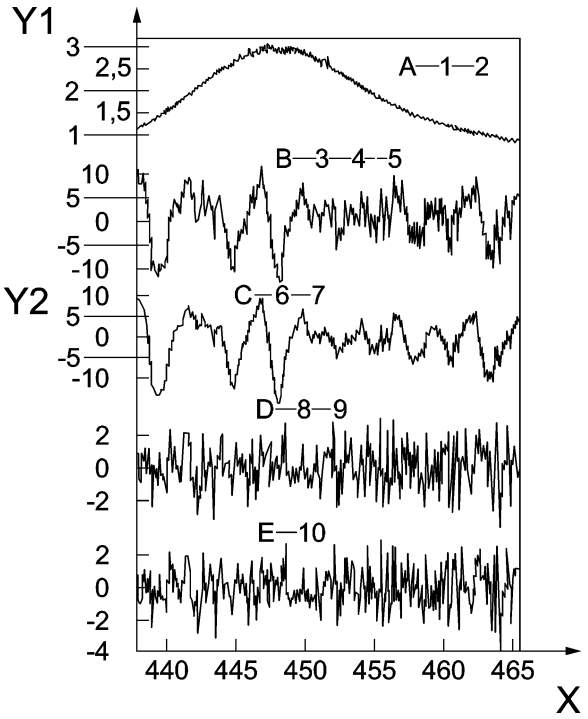

Key
X Wavelength λ
Y1 Intensity
Y2 Optical Density
A Measured spectra
1 Lamp spectrum (LED), zero gas
2 Absorption spectrum (NO_2 along a 556 m absorption path; absorption is weak and not directly visible)
B Corresponding differential optical density of the measured spectrum according to Eq. (8)
3 Sum of all fitted reference spectra
4 Measured optical density
5 Fitted polynomial of 3rd order
C Optical density of H_2O
6 Fitted H_2O optical density
7 Measured optical density
D Optical density of NO_2
8 Fitted NO_2 optical density
9 Measured optical density
E Remaining residuum which could not be attributed to any absorber

Figure C.17 – Example of a NO_2 measurement and analysis result (Note the different scales)

Annex D
(informative)

Performance characteristics

D.1 Detectable compounds and limits of detection

D.1.1 General

The limit of detection can be determined experimentally using the data of gas cell calibration [17] or by calculation based on reference spectra [5]. Detection limits are no fixed values but depend, e.g. on the spectral range, the measurement path and the specific conditions during the measurement.

D.1.2 Experimentally determined detection limits

The detection limit for the components ozone, benzene, nitrogen dioxide and sulphur dioxide was determined as element of the suitability test of the instrument OPSIS AR 500. To determine the detection limit according to [18] two instruments were supplied with zero gas alternating with five other test gas concentrations (15 times for 15 min in each case, the detection limits were calculated as three times the standard deviation of the measured values. No adjustments were made during the test period. The results are given in Table E.1.

Table D.1 — Experimentally determined detection limits

Compound	**Path length** in m	**Detection limit** in µg/m^3
Ozone	320	2,1
Benzene	300	0,4
Nitrogen dioxide	320	0,9
Sulphur dioxide	320	1,2

D.1.3 Calculated detection limits

The following table shows substances which are detectable by active DOAS. The detection limits were calculated for a minimum detectable optical density of 5×10^{-4}.

Table D.2 — Substances detectable by active DOAS and their calculated detection limits [2]

Species	**Wavelength interval** in nm	**Detection limit** [a] in pmol/mol
SO_2	200 – 230	62
	290 – 310	700
CS_2	320 – 340	10 000
NO	200 – 230	167
NO_2	330 – 500	1 600
NO_3	600 – 670	20
NH_3	200 – 230	22
HNO_2	330 – 380	780
O_3	300 – 330	40 000
H_2O	above 430	$1{,}33 \cdot 10^5$
CH_2O	300 – 360	8 300
ClO	260 – 300	110
OClO	300 – 440	35
BrO	300 – 360	40
OBrO	400 – 600	35
I_2	500 – 630	220
IO	400 – 470	20
OIO	480 – 600	36
Benzene	240 – 270	180
Toluene	250 – 280	310
Xylene (o/m/p)	250 – 280	2 000/650/210
Phenol	260 – 290	20
Cresol (o/m/p)	250 – 280	200/135/50
Benzaldehyde	280 – 290	90
Glyoxal	400 – 480	400

[a] Most of the values were calculated for an optical path length of 5000 m. For this table they were referred to an optical path length of 500 m using the conversion factor 10.

Spectral signatures for several compounds are illustrated in Figure D.1.

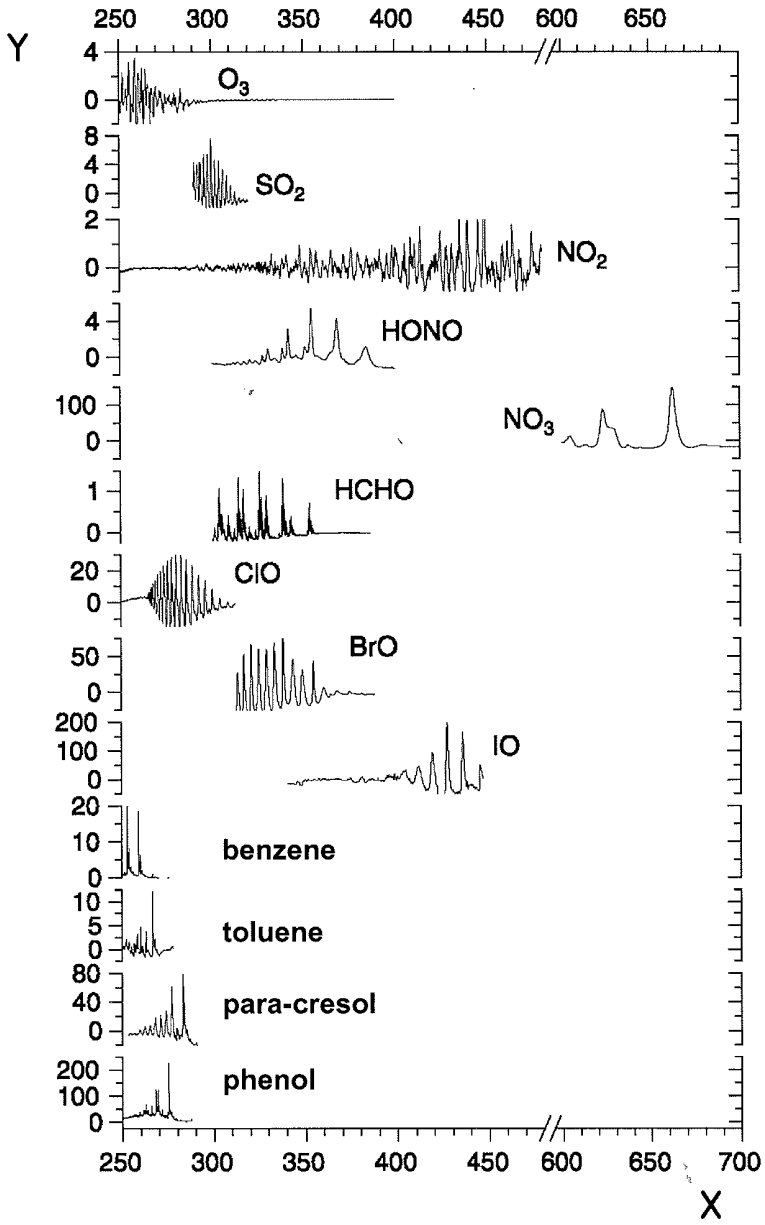

Key
X Wavelength in nm
Y Differential absorption cross-section in 10^{-19} cm^2

Figure D.1 — Examples of spectral signatures of several components

D.2 Expanded uncertainty

The expanded uncertainty is determined from the results of paired measurements with two identical measuring systems according to the following formula:

$$U_D = t_{n-1;0,95} \cdot s_D$$

where

U_D is the expanded uncertainty;

$t_{n\text{-}1;0,95}$ is the student factor for 95 % confidence and number of degrees of freedom n;

s_D is standard deviation for paired measurements.

The expanded uncertainty of DOAS measurements was determined in the context of type approval tests for NO_2, benzene and sulphur dioxide. To determine the expanded uncertainty of field measurements, two measuring systems of identical design were each installed on a 300 m monitoring path. The two monitoring paths lay about 10 m apart. The recorded measurements were integrated into half-hourly averages and then analysed. The field test measurements for NO_2 remained below 100 µg/m^3, whereas those for benzene varied mostly between 0 µg/m^3 and 2 µg/m^3. The expanded uncertainty for NO_2 was 1,55 µg/m^3 (related to the entire measuring range) and 0,17 µg/m^3 (related to the mean of all measurements taken, i.e. 42,4 µg/m^3), respectively. For benzene, the expanded uncertainty was 1,3 µg/m^3 in summer, 1,1 µg/m^3 in winter and 0,2 µg/m^3, related to the mean of all measurements taken.

The determination of the expanded uncertainty in the field for sulphur dioxide (300 m monitoring path) yielded values of 0,03 µg/m^3, 0,03 µg/m^3, 0,14 µg/m^3 and 0,09 µg/m^3 for the four concentration classes 15 µg/m^3, 30 µg/m^3, 70 µg/m^3 and > 100 µg/m^3, respectively.

D.3 Cross-sensitivities

The accuracy of DOAS measurements is also affected by interfering constituents (cross-sensitivities).

Before cross-sensitivities are determined, the maximum optical density of the potentially interfering constituent in the spectral range of the measured constituent should be compared to the optical density of the measured constituent at the detection limit or evaluation level (e.g. ambient air quality limit values). If this suggests interference, the cross-sensitivity can be determined either by using the experimental gas cell method or by mathematical modelling. Regulated components and components that frequently occur have to be checked with respect to cross-sensitivities if they absorb in the same spectral range.

In a mathematical way cross-sensitivities can be detected by modelling spectra according to Formula (6), where the parameters $a_i(\lambda)$ of the target compound and of the interfering species are included. Furthermore a realistic noise value is added. A series of evaluations with different optical densities of the potential interferents provides the optical densities and concentrations, at which the interferents affect the quantification of the target component. This procedure is carried out once, published and the results thus made known to the user. The results are specific for the interferents under consideration and the spectral range, but independent of the DOAS system used.

The cross-sensitivities for NO_2 measurements in the 0 µg/m^3 to 400 µg/m^3 range to various constituents (CO_2, CH_4, N_2O, ethane, H_2S, benzene, O_3, NO, CO, NH_3, acetone, formaldehyde, SO_2) are < 1 %.

D.4 Analysis of the residual spectrum

Removing all known trace substance structures from the differential optical absorption spectrum leaves a residual spectrum. The amplitude variation in this residual spectrum reflects the influence of systematic and accidental interference sources (e.g. noise). For details, refer to the literature (e.g. [15]).

The mean 1-σ-variation in the residual spectrum, for example, is a measure of the lowest determinable optical density (Formula (D.1)).

$$D_{\min} \approx \frac{\sigma_0}{I'} \qquad \text{(D.1)}$$

A more conservative measure is the optical density of the greatest structure in the residual spectrum, the spectral width of which is broader than the resolution of the spectrometer. Furthermore the analysis of the residual spectra of a series of measured spectra with respect to common features reveals systematic spectral

structures. These can be caused either by the measurement system itself or by not identified gaseous absorbing species in the atmosphere.

NOTE More accurate (and more sophisticated) methods of analysing residual spectra and of determining detection limits on the basis of such spectra are described in [5].

The following information can be obtained from the residual spectra:

— random structures (noise);

— possible systematic structures (either instrument-specific or unidentified substances);

— indications on cross-sensitivities which cause systematic errors in the determination of the target substances.

Annex E
(informative)

SI and common symbols and units in spectroscopy

Table E.1 — SI and common symbols and units in spectroscopy [20]

Parameter	Symbol	Definition	SI unit	Common unit
wavelength	λ		m	nm
speed of light in vacuum	c_0	$c_0 = 299792458$ m·s^{-1}	m·s^{-1}	
speed of light in medium	c	$c = c_0 / n$	m·s^{-1}	
wavenumber in vacuum	$\tilde{\nu}$	$\tilde{\nu} = \nu / c_0 = 1 / n \cdot \lambda$	m^{-1}	cm^{-1}
wavenumber in medium	σ	$\sigma = 1 / \lambda$	m^{-1}	cm^{-1}
frequency	ν	$\nu = c / \lambda$	s^{-1}	Hz
refractive index	n	$n = c_0 / c$		
radiant energy	Q, W		J	
radiant power, radiant energy per time	Φ, P	$\Phi = dQ / dt$	W	
radiant intensity	I	$I = d\Phi / d\Omega$	W·sr^{-1}	
radiant exitance (emitted radiant flux)	M	$M = d\Phi / dA_{source}$	W·m^{-2}	
radiance	L	$L = \frac{d^2\Phi}{d\Omega \cdot dA_{source}}$	W·sr^{-1}· m^{-2}	
intensity, irradiance, (radiant flux received)	I, E	$I = d\Phi / dA$	W·m^{-2}	
spectral intensity, spectral irradiance	$I(\lambda), E(\lambda)$	$I(\lambda) = dI / d\lambda$	W·m^{-1}	
emittance	ε	$\varepsilon = M / M_{bb}$		
étendue (throughput, light gathering power)	$E, (e)$	$E = A \cdot \Omega = \Phi / L$	m^2·sr	
resolution	δ, λ		m	
resolving power	R	$R = \lambda / \delta\lambda$		
transmittance, transmission factor	τ	$\tau = \Phi_{tr} / \Phi_0$		
reflectance, reflectance factor	ρ	$\rho = \Phi_{refl} / \Phi_0$		
(decadic) absorbance	A_{10} , A	$A_{10} = -\lg(1 - \alpha_i)$		
napierian absorbance (optical density)	A_e ,(D)	$A_e = -\ln(1 - \alpha_i)$		
absorption coefficient, (linear) decadic	a, K	$a = A_{10} / l$	m^{-1}	
absorption coefficient, (linear) napierian	α	$\alpha = A_e / l$	m^{-1}	
absorption coefficient, molar (decadic)	ε	$\varepsilon = a / c = A_{10} / c \cdot l$	m^2·mol^{-1}	l·mol^{-1}·cm^{-1}; cm^2·mol^{-1}
absorption coefficient, molar napierian	κ	$\kappa = \alpha / c = A_e\, c \cdot l$	m^2·mol^{-1}	
specific absorption coefficient	a	$A / l \cdot c$	m^2·kg^{-1}	m^2·g^{-1} or l·g^{-1}·cm^{-1}
specific absorption coefficient of constituent i at wavelength λ	$\alpha_i(\lambda)$	$A / l \cdot c_i$	m^2·kg^{-1}	(µg/m^3)$^{-1}$·m^{-1}

Annex F
(informative)

Application examples

F.1 Ozone measurement campaign

These measurements were conducted as part of an urban measurement campaign aimed at determining the secondary trace substances responsible for "summer smog". Figure F.1 also shows a comparison of the results obtained with an UV-DOAS system and with a conventional ozone analyser taking point measurements.

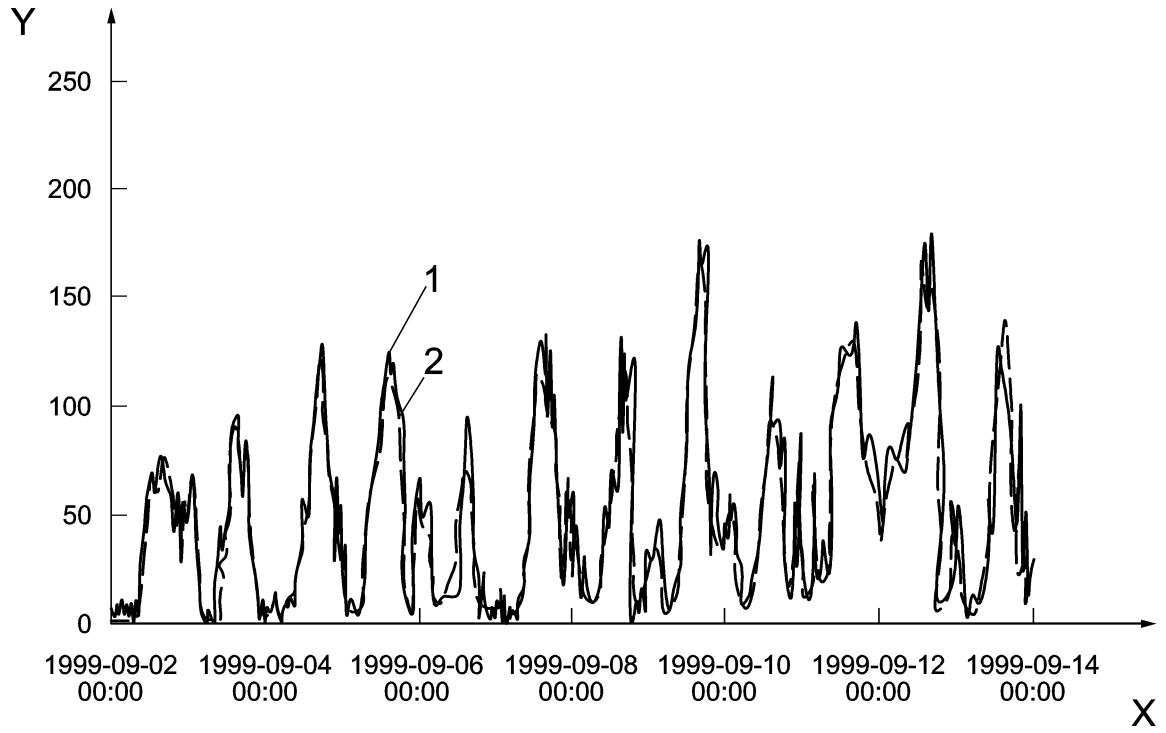

Key
1 UV-DOAS (continuous line)
2 Ozone analyser (dashed line)
X Date/time
Y Ozone concentration in µg/m^3

Figure F.1 — Comparison of ozone concentrations determined over a two-week period with an UV-DOAS system and a conventional ozone analyser

The good coincidence of these results, which is also attributable to the high quality of the calibration measurements, is clearly evident. A high validity of the measurements can therefore be assumed. This is important inasmuch as not all available UV-DOAS systems are suitability-tested ambient air measuring instruments.

Since the ozone concentration is also a function of the degree of insolation in the lower atmosphere, the measured ozone concentrations are compared with the recorded global radiation. This correlation is depicted in Figure F.2. The time delay between the maximum radiation level measured with the sun at its zenith and the maximum ozone concentration is clearly evident; it is attributable to the time constants in the chemical

reactions. Despite the fairly constant maximum insolation, the graph shows different maximum ozone levels. These variations are due, first of all, to different concentrations of precursor substances (e.g. NO and hydrocarbons) needed for the formation of ozone, as well as to changing meteorological parameters.

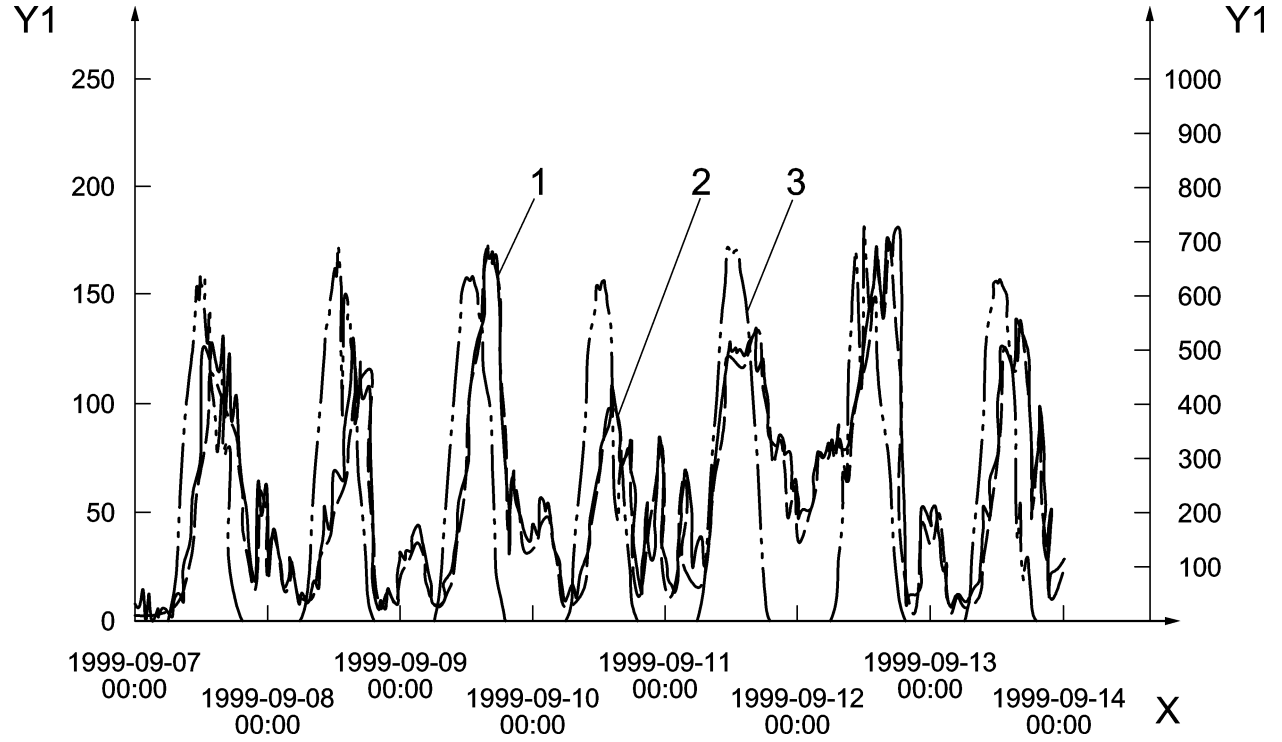

Key
1 UV-DOAS (thick continuous line)
2 Ozone analyser (thin continuous line)
3 Global radiation (dashed line)
X Date/time
Y Ozone concentration in µg/m^3

Figure F.2 — Ozone concentration and overall radiation

Figure F.3 shows the O_3 and NO_2 concentration curves to illustrate the photochemical processes.

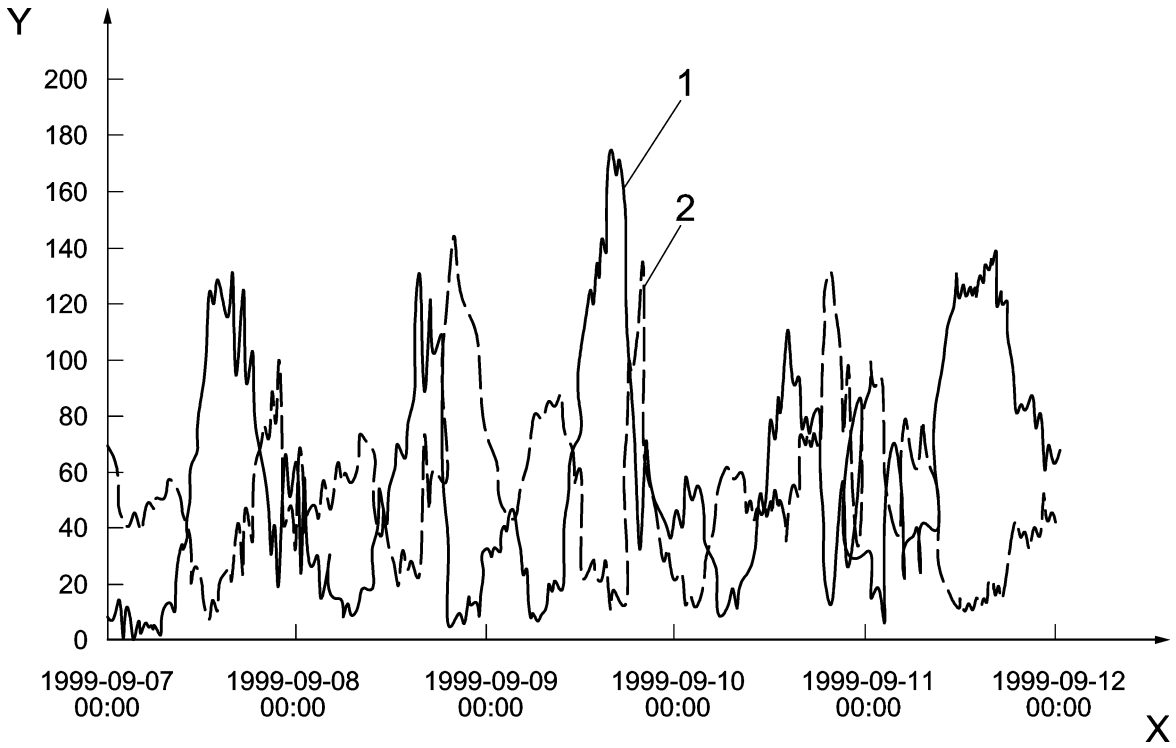

Key
1 Ozone concentration using UV-DOAS (continuous line)
2 NO_2 analyser (dashed line)
X Date/time
Y Concentration in µg/m^3

Figure F.3 — Comparison of measured O_3 and NO_2 concentrations

The correlation between the two constituents is clearly evident. Given the photochemical equilibrium laws, a drop in the ozone concentration is always accompanied by an increase in NO_2 levels and vice versa.

Figure F.4 shows a secondary ozone maximum as a further interesting effect.

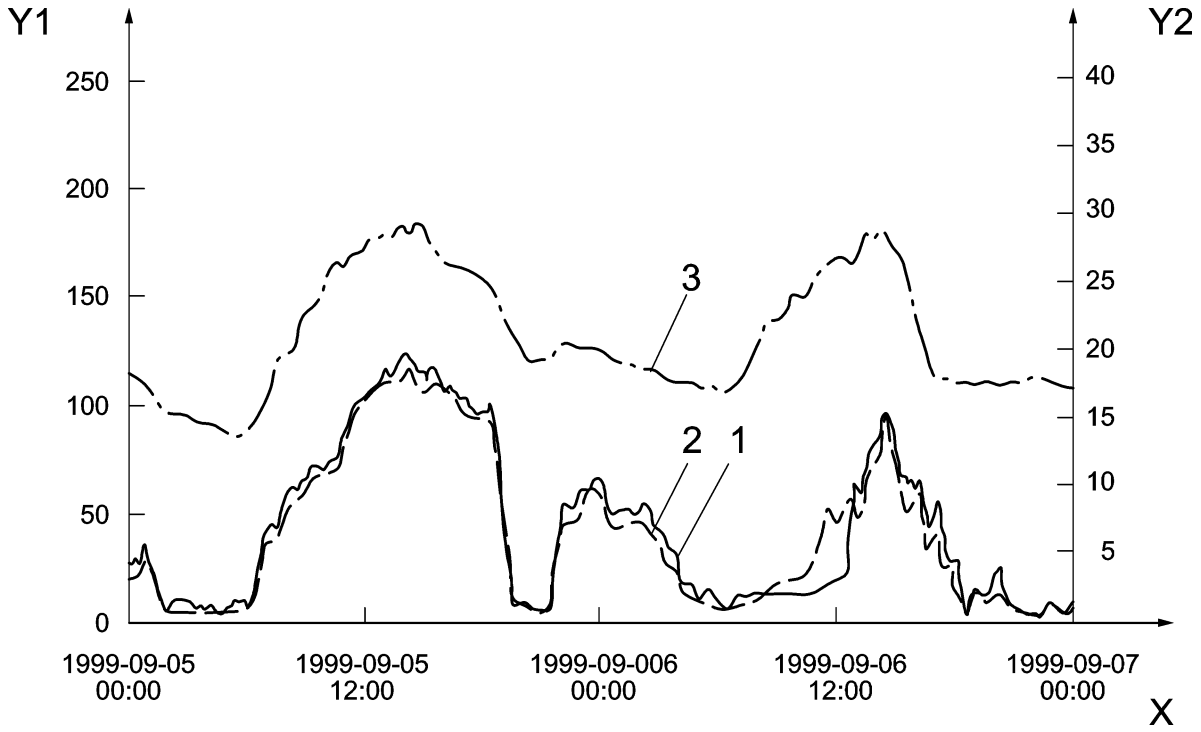

Key
1 UV-DOAS (continuous line)
2 Ozone analyser (dashed line)
3 Air temperature
X Date/time
Y1 Ozone concentration in µg/m^3
Y2 Air temperature in °C

Figure F.4 — One-day ozone concentration graph with occurrence of a secondary ozone peak

The occurrence of this second ozone peak during the night cannot be attributed to chemical ozone formation reactions given the lack of insolation. Instead, this peak appears to have meteorological causes. Figure F.4 also plots the temperature curve. A transient temperature increase of about 3 K taking place in parallel with this ozone peak can be observed. It suggests, in conjunction with the wind velocity data, a "mixing down" of ozone from higher (and warmer) "reservoir layers" into the ground level atmosphere.

F.2 Benzene measurement at filling stations

F.2.1 General

Filling stations are a widespread source of VOC emissions. Measurements at various filling stations were carried out to verify previously known data and the effectiveness of prescribed emission control measures (gas recovery systems) ([21], [22]). The survey relates to benzene.

F.2.2 Measuring method

An inverse propagation modelling method relying on length-averaged concentrations in the off-gas from the sources and concurrent meteorological measurements was used. The levels of benzene released from the source were measured in a non-contacting manner on one or more absorption paths crossing the entire off-air plume using differential optical absorption spectroscopy (DOAS). Another monitoring path had been set up to determine the background concentrations or additional sources (e.g. road traffic). The additional load due to filling station emissions was then calculated as the difference of the plume and background measurements.

To determine the emission rates, inverse modelling using micro-scale dispersion models (Lagrange model [23] with a wind field taken from the Euler model, MISKAM [24]) was employed to obtain length-averaged concentration values and meteorological data from which emission rates can be calculated.

F.2.3 Measuring campaigns and experimental set-up

In carrying out a measuring campaign, the representative nature of both the measuring location and the path lengths needs to be ensured [21]. Measuring campaigns of several days' duration were carried out at three filling stations (an example is illustrated in Figure F.5). The monitoring path length varied between 36 m and 200 m. The DOAS instruments, sourced from OPSIS AB [25], were equipped with 3 retro-reflectors, enough to configure three monitoring paths. The alignment with the monitoring path and the adjustments of the measuring system were made automatically so that the measuring sequence could be carried out on a continuous basis. Where several monitoring paths were installed, these were measured successively and always in the same order. The time allotted for benzene measurements on each path was 2 min to 3 min. The DOAS measuring system used had a detection limit of 3 $\mu g/m^3$ on a 500-m absorption path (low-resolution grating [25]).

Benzene measurements with the DOAS instrument using a low-resolution spectrometer grating call for an offset correction in view of the existing cross sensitivity to oxygen absorption processes. This requires careful measurements uninfluenced by the benzene source, conducted over a path whose length corresponds to the size of the plume from the emission source [24]. In the case of a filling station located in a rural area, background measurements could be carried out without modifying the measuring set-up since the wind kept turning over a measuring period of several days. In an urban environment the necessary corrections were effected with the aid of a second monitoring path.

The source levels of filling station emissions determined by the measuring method described above cover all potential sources in their entirety: emissions from vehicle fuel tanks and leaky fuel-carrying vehicle components, drip loss during pumping operations, emissions from the ventilation mast for the filling station's underground tanks, diverse other emissions due to leaks in the filling station's pipe system, and emissions released during transfer of fuel deliveries from road tanker trucks.

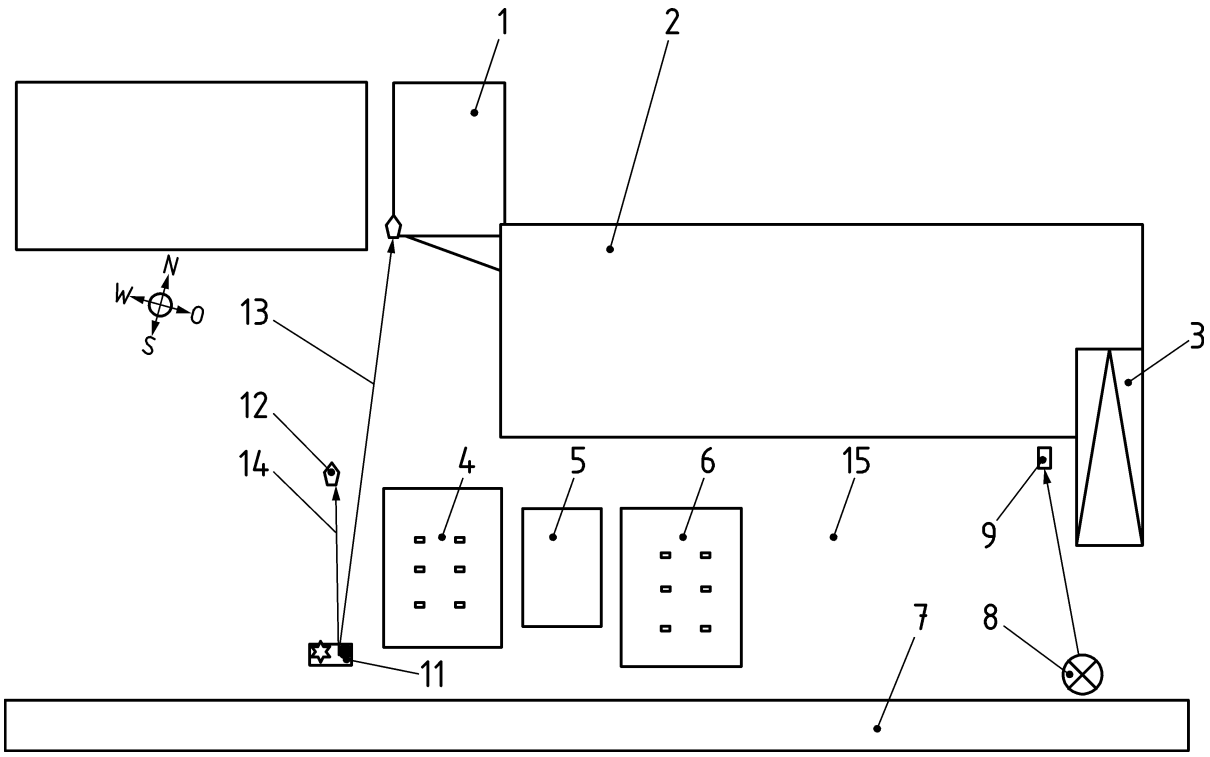

Key
1 Retro-reflector
2 Shopping centre
3 Ramp
4 Fuel dispensers
5 Shop
6 Fuel dispensers
7 Road
8 Radiation source
9 Receiver
11 Measurement vehicle
12 Retro-reflector
13 Optical path 1
14 Optical path 2
15 Car park

Figure F.5 — Arrangement of the measuring systems on an urban filling station to determine background and plume concentrations

F.2.4 Measuring results

The benzene concentrations in filling station off-air plumes were up by a maximum of 21 µg/m^3 and an average of 7 µg/m^3 from the background level.

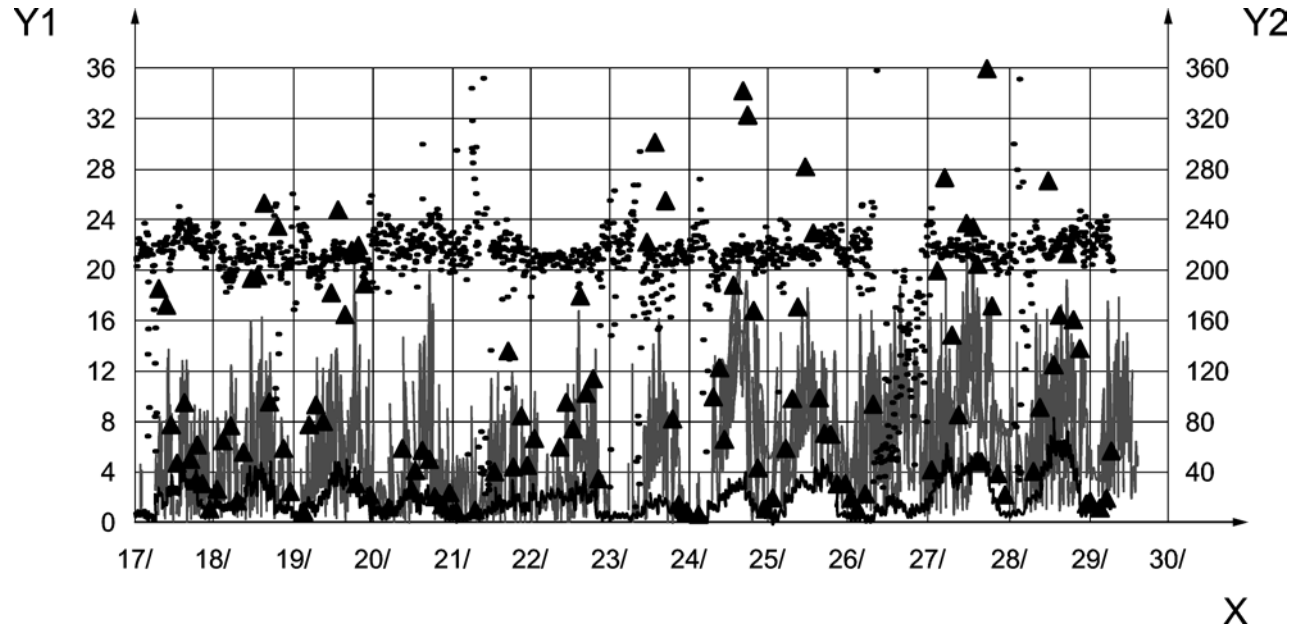

Wind velocity (in 7 m height) in m/s
Benzene mixing ratio in nmol/mol (optical path east (36 m))
Wind direction (in 7 m height) in degree
Calculated emission (2 h average) in µg/(m^2·s)

Key
X Time (day)
Y1 Benzene mixing ratio in nmol/mol / wind velocity in m/s
Y2 Wind direction in degrees / emissions in µg/(m^2·s)

Figure F.6 — Benzene mixing ratio on the eastern monitoring path, wind speed and direction and the emission rates

Figure F.6 shows the measuring and modelling results for the DOAS system installed to the east of the filling station as illustrated in Figure F.5 [26]. The measured concentrations peaked at 37 µg/m^3. There was a clear increase in benzene levels after the shut-down of the gas recirculation system on May 24 (from an average 17 µg/m^3 prior to May 24 to 22 µg/m^3 after that date). A turn in wind direction is clearly reflected in the data since the situation upwind and downwind of the filling station is reversed between monitoring paths (e.g. daytime levels of 24.5 µg/m^3 with west wind on May 25 and 10.5 µg/m^3 with east wind on May 26). The calculated emission rates reflect the measured concentrations as well as the wind direction and wind velocity.

The results of the measurement are presented in detail in Bibliographical Entry [21]. The key difference between these measurements and prior data lies in the very high diffuse emissions which could be determined directly with this method. In addition, the measurements showed that the gas recirculation systems are often not receiving enough maintenance, which translates into a low efficiency of this equipment.

F.3 Airport measurements

To determine the air quality at Düsseldorf airport and the impact of air traffic exhaust gases, two bistatic DOAS systems (manufacturer: OPSIS), each comprising two monitoring paths, have been installed there for a number of years. The systems are mounted at the ends of the runways, with monitoring paths (each having a length of several hundred metres) extending crosswise to the latter (see Figure F.7).

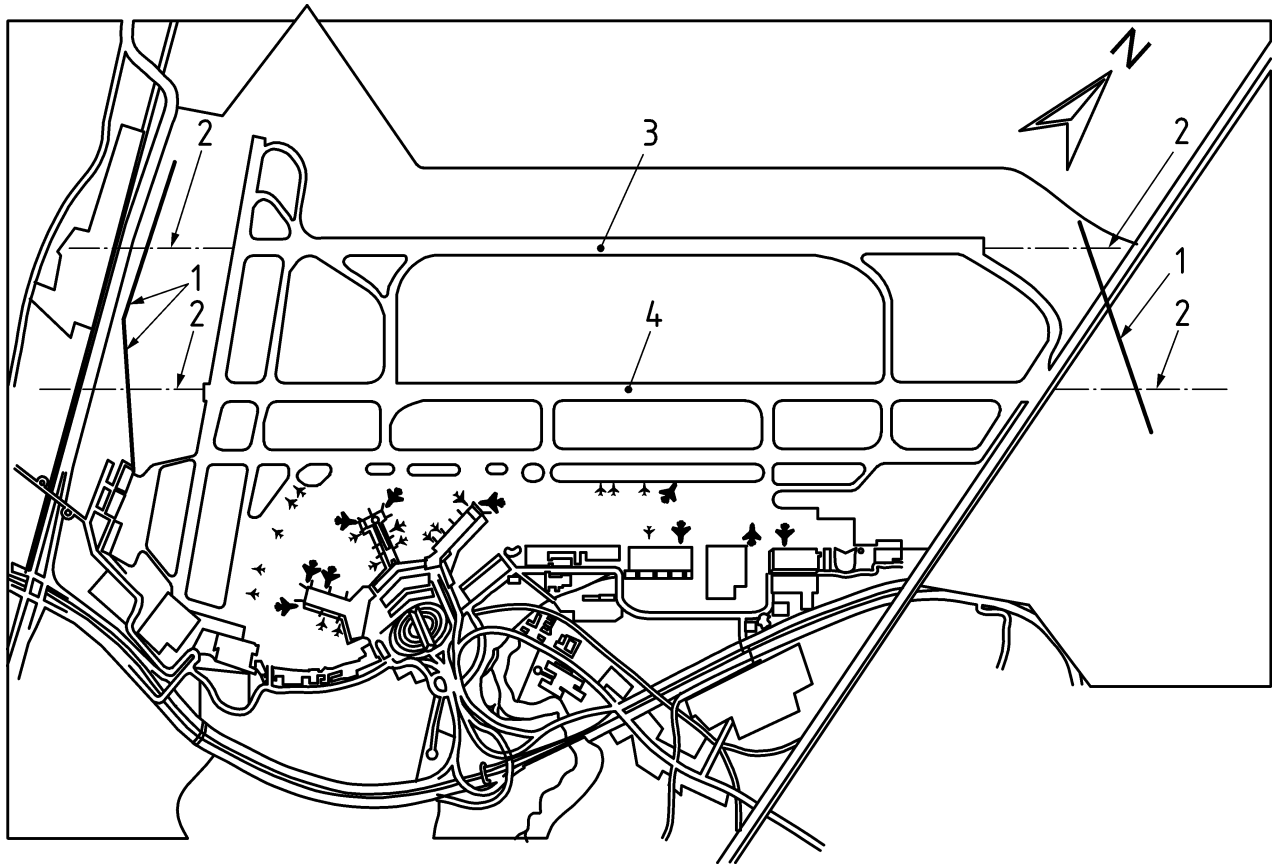

Key
1 DOAS 1 / DOAS 2
2 Monitoring path 1 / monitoring path 2
3 Northern runway
4 Southern runway

Figure F.7 — Layout of monitoring paths for the airport measurements

The system structure and monitoring path lengths are determined by component characteristics as well as by the layout of the facilities and applicable safety regulations.

Both DOAS systems measure trace gases, viz., nitrogen monoxide (NO), nitrogen dioxide (NO_2), ozone (O_3) and sulphur dioxide (SO_2). The monitoring paths are located at heights of 3 m to 5 m above ground. Both analysers are mounted in an air-conditioned container below the receivers.

Apart from permitting multiple-constituent measurements with the same equipment configuration, the DOAS system is an excellent tool for obtaining a representative description of the air quality situation on an airport with its predominantly inhomogeneous distribution of trace gases (specifically, exhaust gas fumes released by aircraft during take-off).

On an multi-year annual average, approx. 80 % of all aircraft movements (take-offs and landings) take place in a western direction; only about 20 % of these movements are eastbound. At present, the southern runway is used for virtually all take-offs (meaning that the plume extends mainly in the direction of DOAS 2 (east), monitoring path 1). Despite this variability of runways and directions, the annual average levels of nitrogen oxides (which are the main compounds release during take-off) show only small differences (Figure F.8). For NO_2 there exists no appreciable difference at all; in the case of nitrogen monoxide, the difference never exceeded 2 µg/m^3 throughout the year 2000 [27].

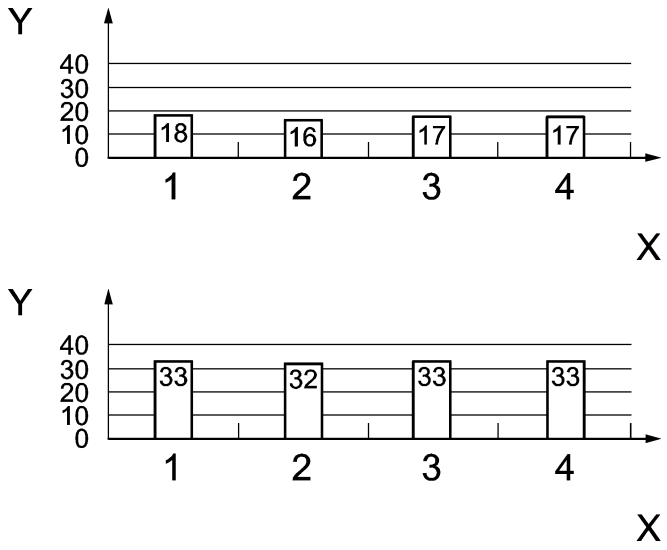

Key
1 DOAS west, monitoring path 1
2 DOAS west, monitoring path 2
3 DOAS east, monitoring path 1
4 DOAS east, monitoring path 2
X Measuring point
Y NO concentration in µg/m^3 (top)
Y NO_2 concentration in µg/m^3 (bottom)

Figure F.8 — Annual means for nitrogen monoxide and nitrogen dioxide

Only a wind-direction-related analysis of the measurements will reveal a slight influence of aircraft emissions for wind flows in the extended runway directions.

Such an analysis will demonstrate approx. 6 µg/m^3 higher NO_x concentrations along the affected monitoring paths for the year 2000. Both concentration roses (Figure F.9 and Figure F.10) show a concentration increase across all monitoring paths for periods of southerly wind flow. Air masses loaded with pollutants originating from the area of a major road intersection are transported toward the western DOAS system. The eastern measuring system is exposed to air masses from the IC train terminal, the freeway, and the airport's apron area in southerly winds.

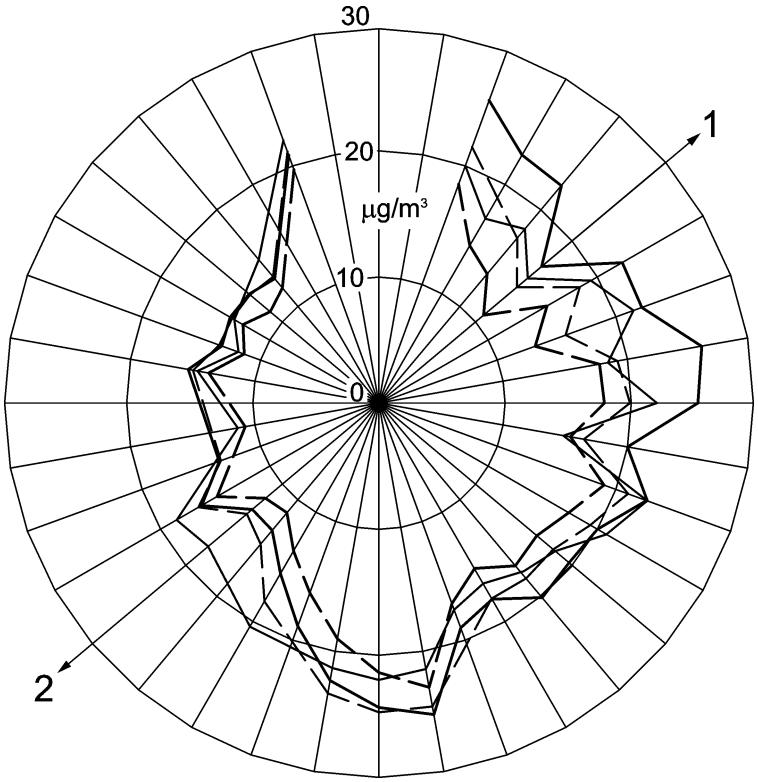

——— DOAS 1, monitoring path 1
——— DOAS 2, monitoring path 1
– – – DOAS 1, monitoring path 2
– – – DOAS 2, monitoring path 2

Key
1 Course 05
2 Course 23

Figure F.9 — Concentration rose NO

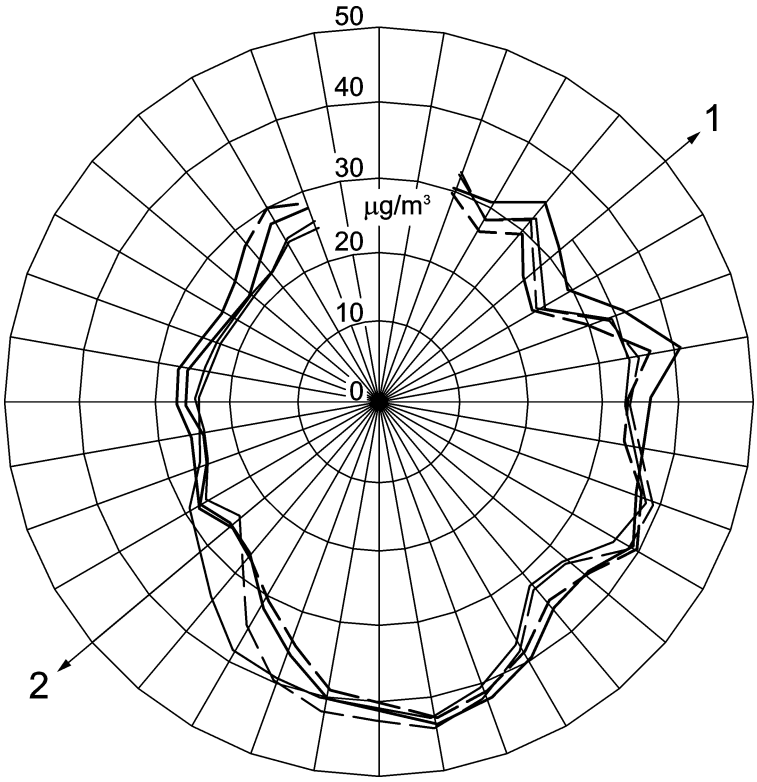

DOAS 1, monitoring path 1
DOAS 2, monitoring path 1
DOAS 1, monitoring path 2
DOAS 2, monitoring path 2

Key
1 Course 05
2 Course 23

Figure F.10 — Concentration rose NO_2

Measured against the general NO_x load caused mainly by car exhaust gases from the nearby main traffic arteries, aircraft take-off and landing movements account only for a small percentage of the ground level concentrations. Indeed, an impact of these movements can only be demonstrated through upwind/downwind measurements when the wind flow coincides directly with the extended runway directions.

F.4 Long-term NO_2 and NO_3 measurements

At the Kap Arkona measuring site located at the northern tip of the island of Rügen, DOAS measurements of O_3, NO_2 and NO_3 radicals were carried out from early April 1993 until early June 1994. The DOAS system employed is illustrated schematically in Figure F.11. The single radiation path (transmitter/receiver telescope - retro-reflector array) of the DOAS measuring system had a length of 3,515 km, i.e. the total radiation path length amounted to 7,03 km. During the measuring period, over 23 000 spectra from a continuous measuring period of more than 12 months were analysed [28].

There were two main wind directions (east and west) prevailing at this measuring site. Eastern winds, at more than 10 %, occurred with the highest relative frequency. A feature common to both wind directions was that the air packages coming from these directions have already travelled far over the Baltic Sea and have thus undergone a certain "ageing" process. Air from these directions has therefore not been in contact with major man-made contaminant sources over extended distances, so that reactive trace substances will have already disappeared from the air mass. Winds from eastern directions travel over the Baltic Sea water masses all the way to the measuring station.

Relative humidity levels were always above 40 %, although values between 95 % and 100 % still accounted for 10 % of the monitored time. Accordingly, the measurements were often impaired by mist and fog.

In the spring of 1993, pronounced daily fluctuations in the NO_2 concentration were discovered. These ranged from about 0.4 nmol/mol (detection limit) to peaks of 19 nmol/mol (Figure F.12), then dropped to levels between the detection limit and a maximum of 5 nmol/mol in the early summer. Throughout the rest of this summer, the NO_2 loads in this area averaged about 3 nmol/mol (with the exception of 10 nmol/mol peaks recorded on August 26, 1993). Elevated NO_2 levels were again observed for extended periods from mid-October until mid-February, in line with the duration of the winter heating period. The highest concentrations were recorded during two intervals in November 1993 (30 nmol/mol on November 18) and January 1994 (24 nmol/mol on January 23). Like their ozone counterparts, NO_2 concentrations in the spring of 1994 were again comparable to prior-year values.

Since NO_3 is destroyed by photolysis within a few seconds during the day, no measurements of this species were conducted during daylight hours. Instead, daytime was dedicated to measurements of the remaining wavelength bands.

In 206 out of a total of 291 nights in which measurements were possible, the measured NO_3 concentration exceeded the detection limit of < 1.5 pmol/mol. From Figure F.13 it is evident that the highest NO_3 levels of almost 100 pmol/mol were recorded in late April and early May 1993. Fairly high concentrations of nitrate radicals were also demonstrated on a few nights in early June.

On the other hand, the concentrations were mostly much lower throughout the summer, attaining levels between 6 pmol/mol and 20 pmol/mol. Nightly peaks between 40 pmol/mol and 50 pmol/mol were registered only in mid-July and late August. In the subsequent period, from mid-September until the end of winter, NO_3 concentrations were low or dropped entirely below the detection limit. In early spring 1994 the NO_3 concentration began to climb again. During this period, night values of 20 pmol/mol to 45 pmol/mol were measured. These data show that the conversion of nitrogen oxides into nitric acid (which, due to its high water solubility, is rapidly removed from the atmosphere by wet deposition) takes place not via OH radicals but via the non-photochemical reaction sequence NO_3 - N_2O_5 followed by N_2O_5 hydrolysis, particularly during the darker half of the year.

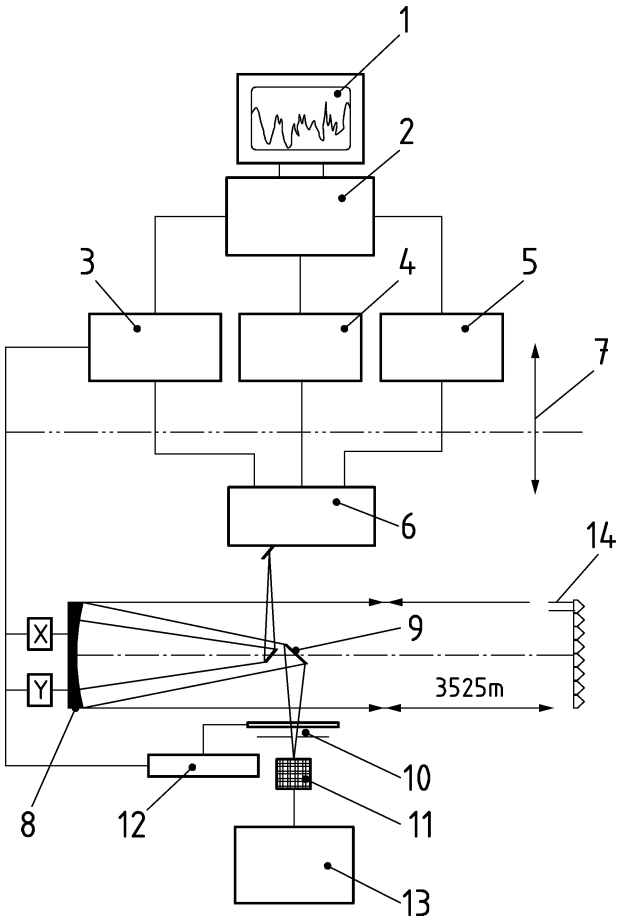

Key
1 Display
2 Computer
3 Stepper motor controller
4 Controller (ADC)
5 Temperature control
6 Spectrometer
7 Electronics/optics
8 Coaxial transceiver telescope
9 Tilted mirror
10 Aperture
11 Radiation source
12 Colour filter
13 Lamp supply
14 Retro-reflector system

Figure F.11 — Set-up of the DOAS measuring system

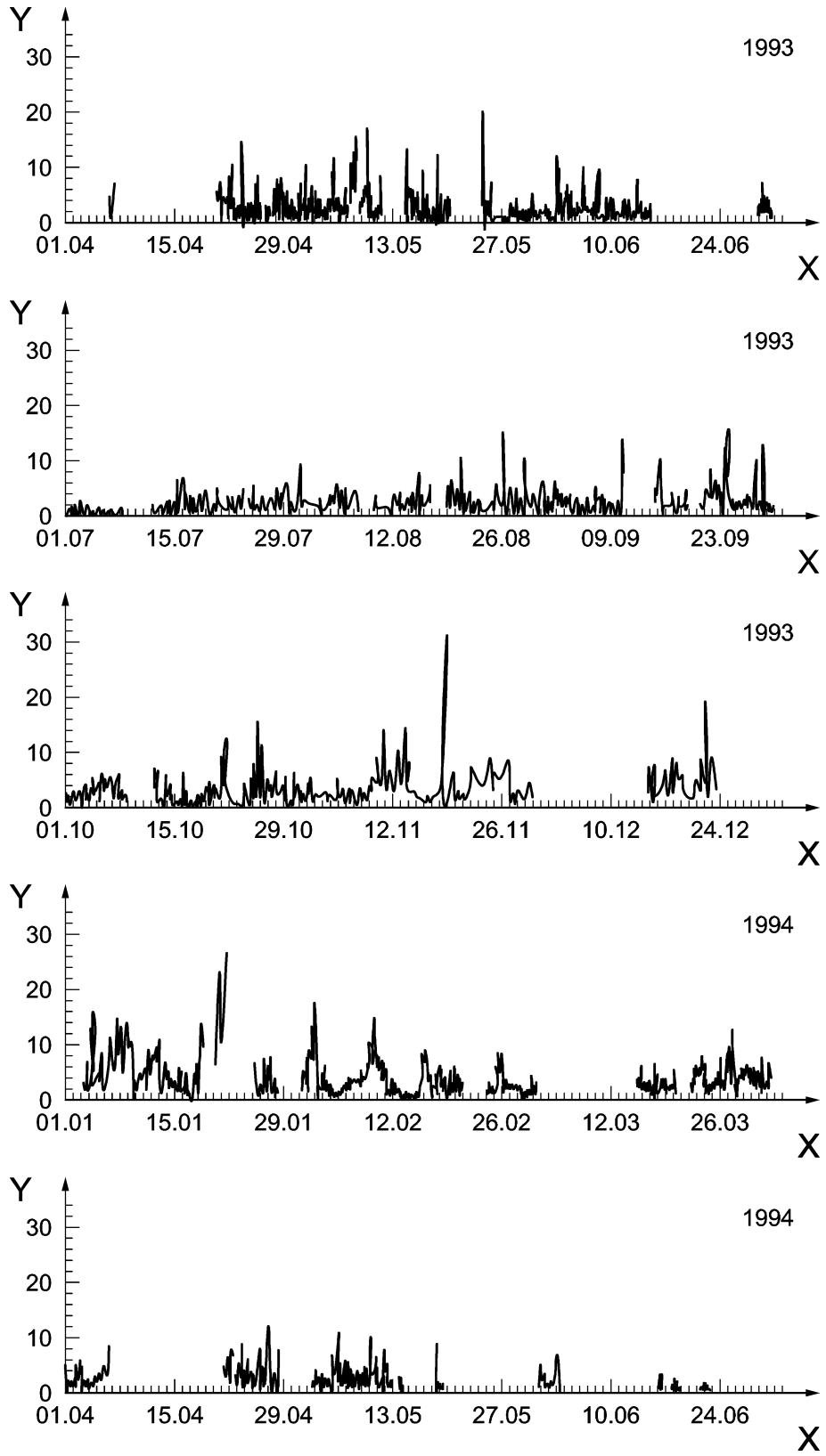

Key
X Time (date)
Y NO_2 mixing ratio in nmol/mol

Figure F.12 — Time series of the NO_2 measurements on Rügen

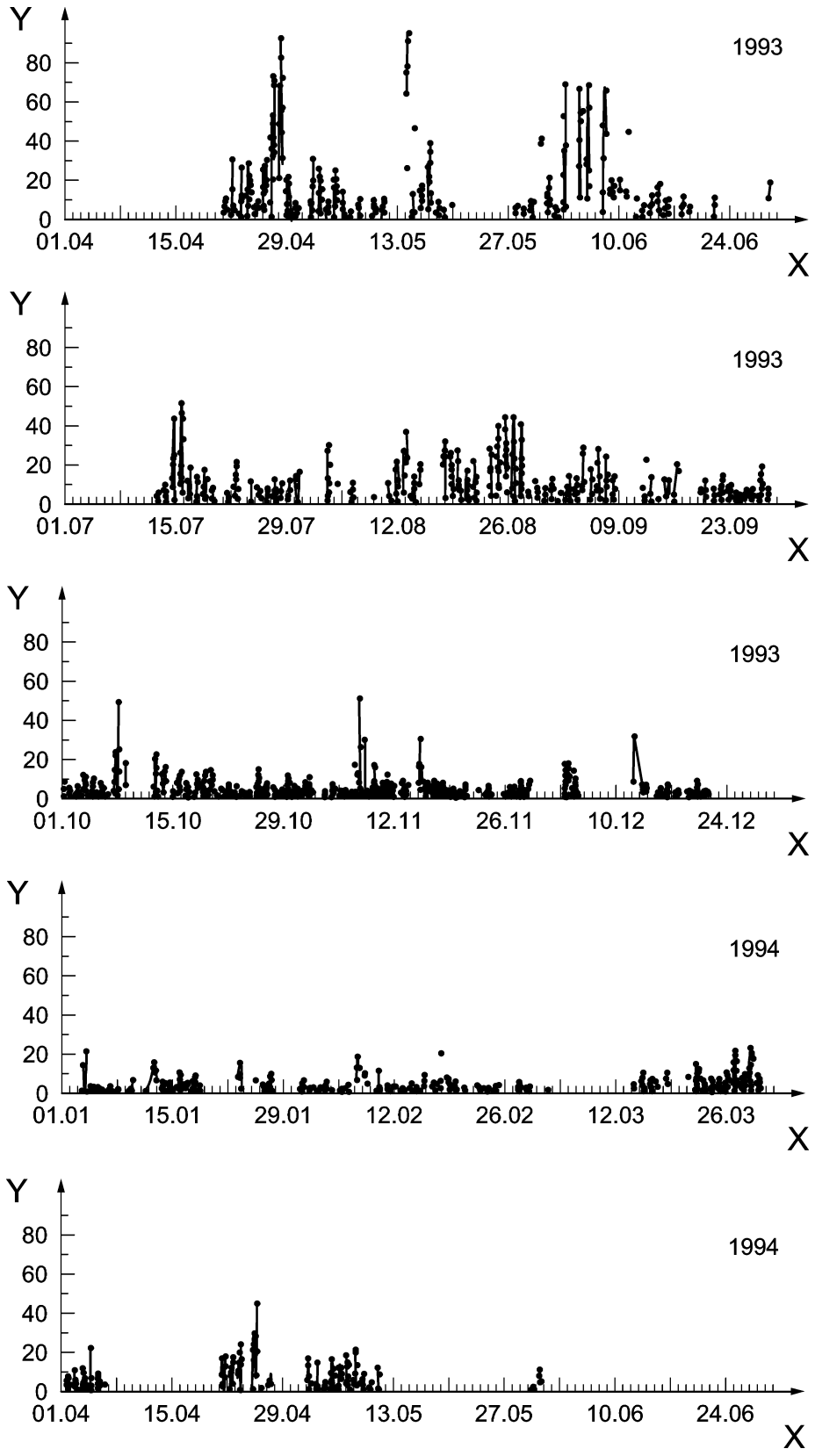

Key
X Time (date)
Y NO_3 mixing ratio in nmol/mol

Figure F.13 —Time series of the NO_3 measurements on Rügen

F.5 In-tunnel measurements based on a multiple reflection system

DOAS measurements were carried out in a road tunnel in the city of Wuppertal („Kiesbergtunnel“) [29]. This tunnel has a length of 1,1 km and connects the A46 motorway between Düsseldorf and Wuppertal with the downtown area of Wuppertal-Elberfeld. The tunnel consists of two independent tubes extending in a southwest-to-northeast direction. Throughout the measurements, the upper tube was shut down for maintenance work. The measurements were therefore conducted in the lower tube which had traffic passing through in both directions during this period. From its western mouth, the tunnel has a 3,25 % uphill gradient over a length of 130 m, followed by a gradient of about 1,0 % over the remaining length (900 m). It is assumed that the engines of the passing vehicles have reached their operating temperature by the time of entering the tunnel. Moreover, their exhaust gases can be assumed to have mixed very thoroughly over the tunnel cross-section due to the high turbulence produced by the two-way traffic. The DOAS system was equipped with a multiple reflection system (White System, see Figure F.14) having a base length of 15 m [30]. The field mirror had a diameter of 25 cm, the two reflectors measured 15 cm each. This gave the system a 1:100 aperture ratio; the radiation source (xenon lamp) and the spectrometer were adapted to the system's aperture ratio via a Newtonian optical block. With a total of 48 passages through the system (47 reflections) an overall optical absorption path with a length of 720 m was obtained. This multiple-reflection system was installed 3 m above road surface level.

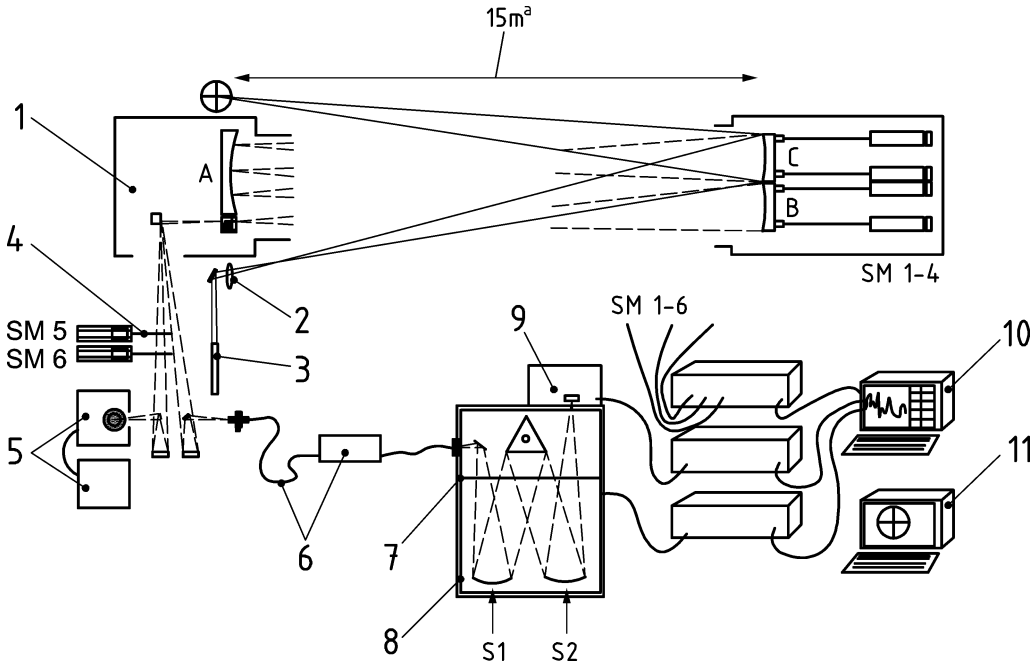

Key
1 Four quadrant detector
2 Lens
3 Laser
4 Aperture
5 Lamp housing with power pack
6 Quartz fibre with mode mixer
7 Aperture
8 Spectrograph
9 Detector with PDA
10 PC 1
11 PC 2
A, B, C Focal mirrors
S1, S2 Spherical mirrors
SM Stepper motor
[a] Base length

Figure F.14 — Set-up of the multiple reflection system used for the measurements in the Kiesbergtunnel, Wuppertal

The daily vehicle density curve and the concentration of monocyclic aromatic carbohydrates measured with the DOAS system are summarised in Figure F.15. For these measurements, the DOAS monitoring path having a total length of 720 m was folded to a basic length of 15 m using a multiple reflection system (White System).

Correlations between the traffic density and the toluene mixing ratio, as well as between further aromatic compounds and toluene, were established from the tunnel measurements and are shown in Figure F.16. The correlation between toluene and the traffic density is fairly low, since the absolute in-tunnel concentrations are modulated chiefly by the activation and de-activation of the tunnel ventilation system. On the other hand, the correlation between benzene, toluene and xylene isomers (BTX compounds) is very strong. This observation suggests that the monocyclic aromatics have a common source, viz., motor vehicle emissions.

The tunnel measurements of aromatic compounds were used in conjunction with wind speed and CO_2 data to determine the specific emissions of motor vehicles. The results are summarised in Table F.1

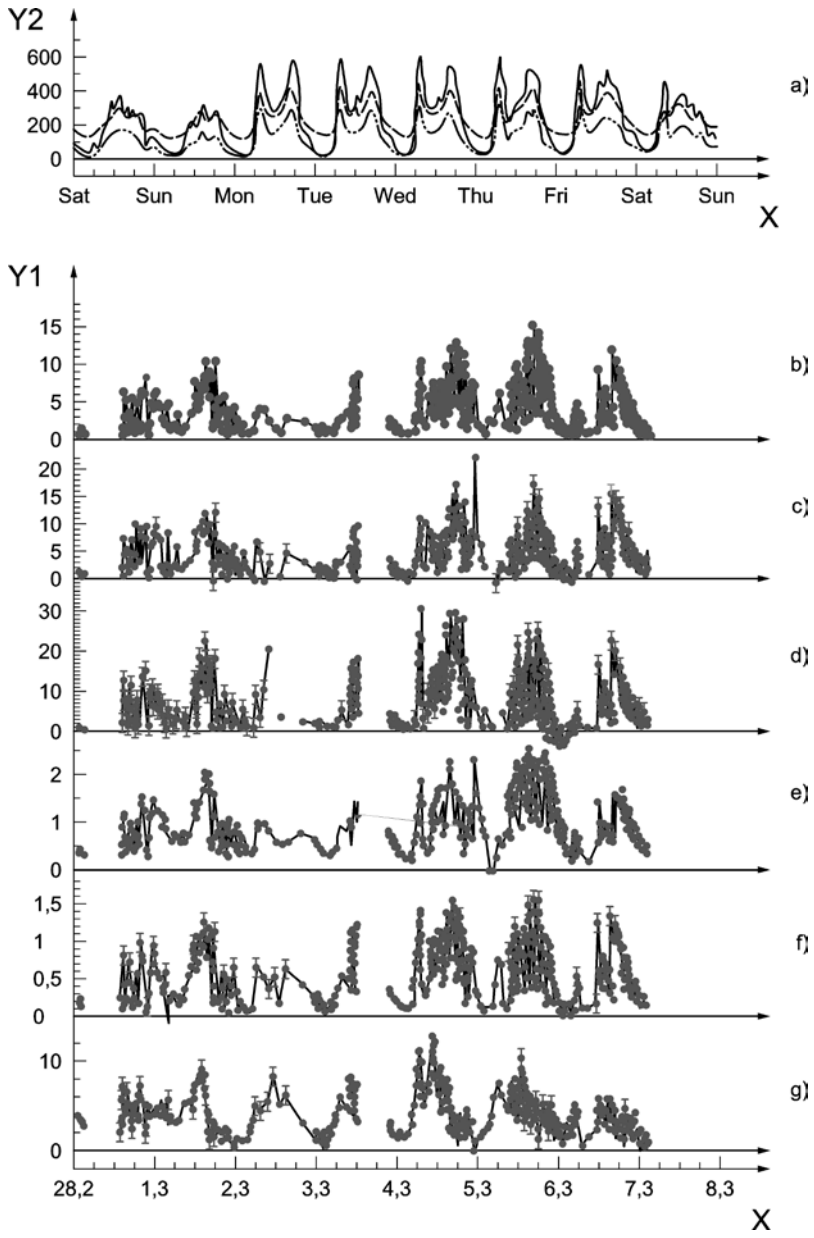

Total
Direction Düsseldorf
Direction Elberfeld

Key

X Time (day, date)
Y1 Mixing ratio in nmol/mol
Y2 Vehicles per 15 min
a Traffic density
b p-Xylene
c m-Xylene
d o-Xylene
e Phenol
f p-Cresol
g SO_2

Figure F.15 — Diurnal variations of vehicle densities in the Kiesbergtunnel and of the simultaneous measured levels of monocyclic aromatic hydrocarbons

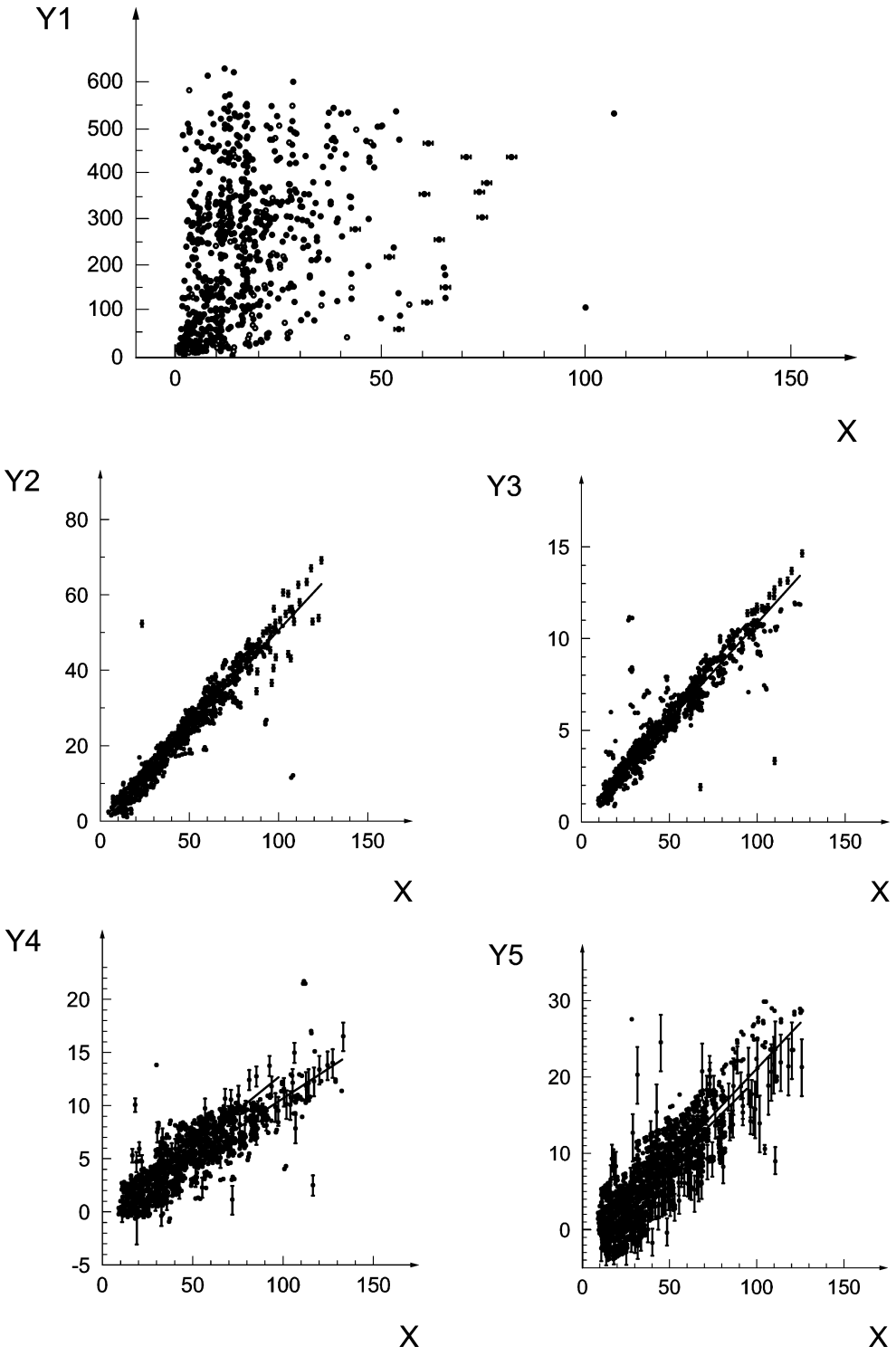

Key
X Toluene mixing ration in nmol/mol
Y1 Traffic density in vehicles per 15 min
Y2 Benzene mixing ratio in nmol/mol
Y3 p-Xylene mixing ratio in nmol/mol
Y4 m-Xylene mixing ratio in nmol/mol
Y5 o-Xylene mixing ratio in nmol/mol

Figure F.16 — Correlations between the traffic density and the toluene mixing ratio and correlations between several aromatic compounds and toluene

Table F.1 — Emission factors for monocyclic aromatic hydrocarbons determined from the DOAS measurements

Component	Molar mass in $g \cdot mol^{-1}$	Emission factors in $mg \cdot vehicle^{-1} \cdot km^{-1}$	
		1st campaign	2nd campaign
Toluene	92	35,6 ± 5,0	58,0 ± 6,5
Benzene	78	13,0 ± 2,2	25,4 ± 2,8
Ethylbenzene	106	6,9 ± 1,2	1,9 ± 0,2
Benzaldehyde	106	1,87 ± 0,25	1,08 ± 0,12
p-Xylene	106	5,8 ± 0,9	7,3 ± 0,8
m-Xylene	106	8,7 ± 1,4	9,2 ± 1,1
o-Xylene	106	12,8 ± 1,9	18,0 ± 2,0
Phenol	94	1,65 ± 0,24	1,48 ± 0,17
p-Cresol	108	0,70 ± 0,10	0,89 ± 0,15

F.6 Measurements close to an urban area

DOAS measurements were a key element of the "***BERLI****n* ***OZ****one Experiment*" (*BERLIOZ*) carried out from mid-July through mid-August 1998 in the Greater Berlin area (cf. [31], [32]). The overall objective of *BERLIOZ* was to analyse the chemical composition and to identify chemical processes in the Berlin exhaust air plume. The emphasis was to be placed on the chemistry of radicals. For this purpose a number of measuring stations were set up and operated in Berlin and its environs. To determine the radicals budget, the Pabstthum intensive observation site was installed about 50 km to the northeast of Berlin's downtown centre and about 35 km from its eastern city limit (Figure F.17). The main station (A) was located between a pinewood (pinus sylvestris) forest in the west (B) and a patch of level grassland in the east. A group of oak trees (quercus ilex) stood to the west of the measuring site (C). DOAS system 1 determined the average NO_3 mixing ratios over a radiation path (D) extending approximately in an east-west direction over the grassland patch. DOAS system 2 with its multiple reflection cell and all other instruments were installed near the station (A).

Apart from taking measurements of OH and NO_3 radicals, the station determined nitrous acid (HONO) as an important OH precursor. In addition to these two last-mentioned species, NO_2 and formaldehyde were surveyed with the aid of two DOAS systems.

— System 1 took measurements on a once-folded radiation path having a total length of 5,0 km. This radiation path (4) extended at an average height of 3,5 m above ground from the Pabstthum station (position 5 in Figure F.17) to a retro-reflector array located 2,5 km away and back from there to (5).

— System 2 used a radiation path folded by an open multiple-reflection system. The system's reflector distance was 15 m; the measuring radiation passed this distance 144 times altogether to obtain a total radiation path length of 2,16 km. The system was mounted on a platform, 8 m above ground, at the site of the Pabstthum station (position 5 in Figure F.17).

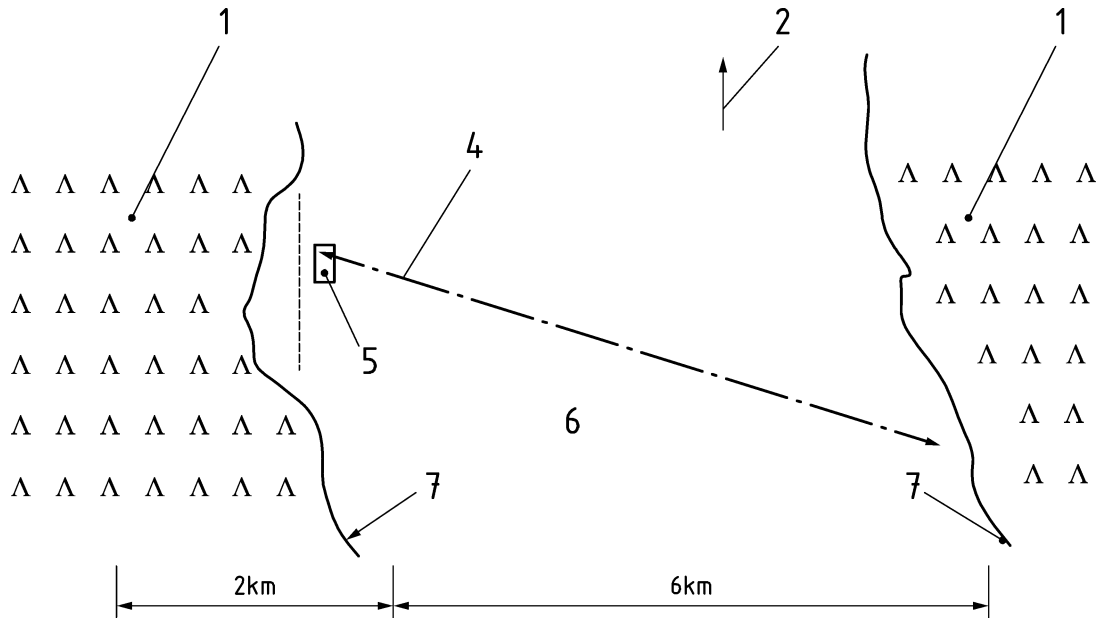

Key
1 Scots pine forest
2 Direction north
4 Radiation path
5 Station near Pabstthum
6 Meadow
7 Road

Figure F.17 — Layout sketch of the BERLIOZ measuring site

The diurnal variations in NO_2 and HONO [33] determined with DOAS system 2 (multiple-reflection system) are summarised in Figure F.18. The error bars (of the HONO data) show the 1σ error calculated according to [5]. The continuous line marks the 2σ measuring limit for HONO; negative concentrations lie within the statistical variation range of the measurement. The NO_2 mixing ratios vary between values below the detection limit (0,24 nmol/mol) and over 20 nmol/mol when wind in southerly directions brought air from Berlin's city area to the site (according to the trajectory analysis). On the whole, the HONO mixing ratios varied more or less concurrently with those of NO_2, at a HONO/NO_2 ratio of approx. 0,05. However, the system's limit of detection (approximately 0,11 nmol/mol HONO) was never exceeded during the day. The two species exhibit similar diurnal variations with nighttime peaks.

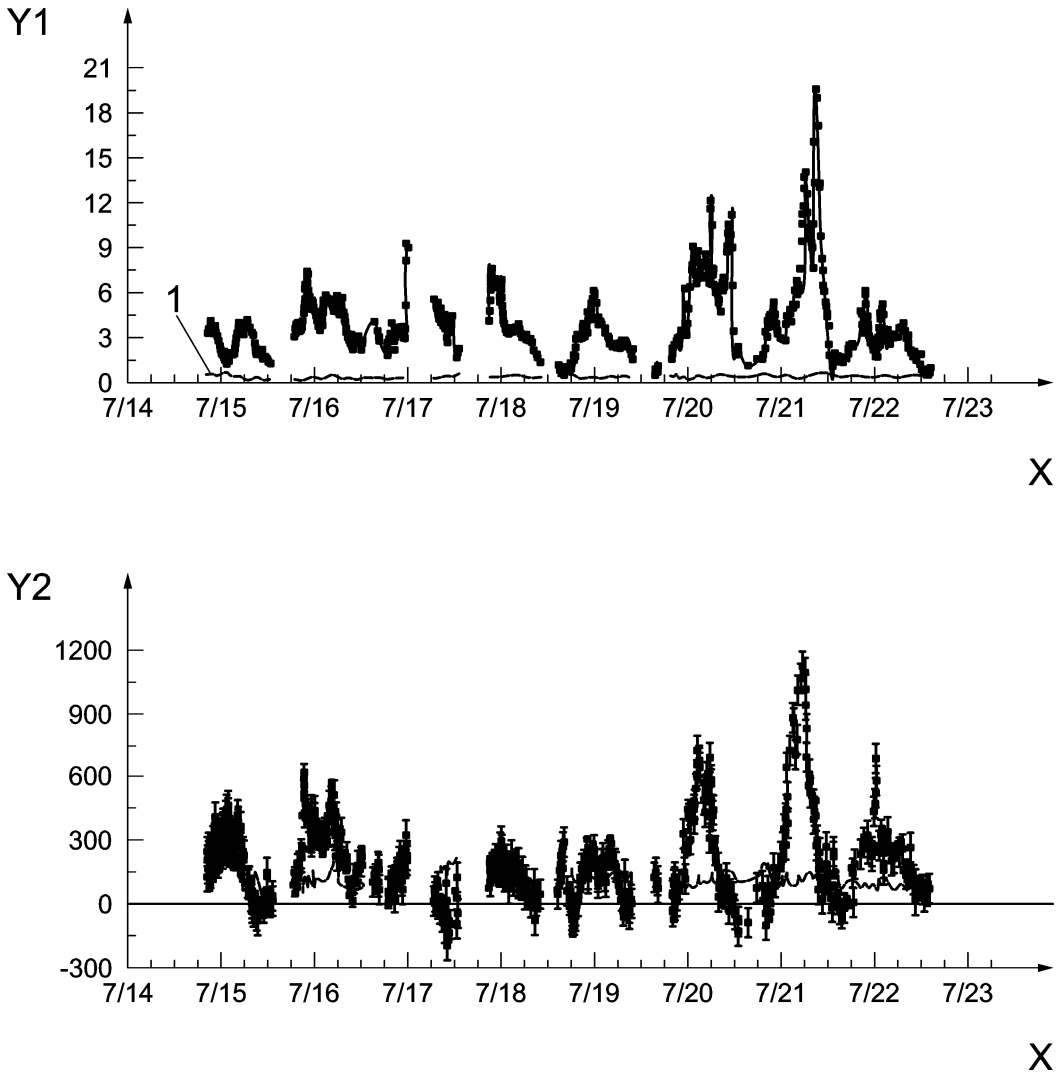

Key
X Time (date)
Y1 NO_2 mixing ratio in nmol/mol
Y2 HONO mixing ratio in pmol/mol

Figure F.18 — Time series of the HONO and NO_2 mixing ratios

The formaldehyde mixing ratios (Figure F.19) were determined by DOAS system 1 on radiation path 4 (see Figure F.17) and show rather high levels of up to about 8 nmol/mol. The general resemblance of these data to those of NO_2 (Figure F.18) suggests substances being transported from Berlin.

A comparison of measurements taken with the DOAS system 2 (multiple reflection system) and conventional techniques (gas phase chemiluminescence, photolysis converter) is represented in Figure F.20. The correlation between both measuring processes is good; the deviation of (36 $\pm$ 19) pmol/mol does not differ from zero in a statistically significant manner. The gradient of the regression line (DOAS versus chemiluminescence), at 1,006 $\pm$ 0,005, indicates consistent calibration of the instruments. The regression analysis yields a good correlation between the two data records, with a correlation coefficient R^2 = 0,98.

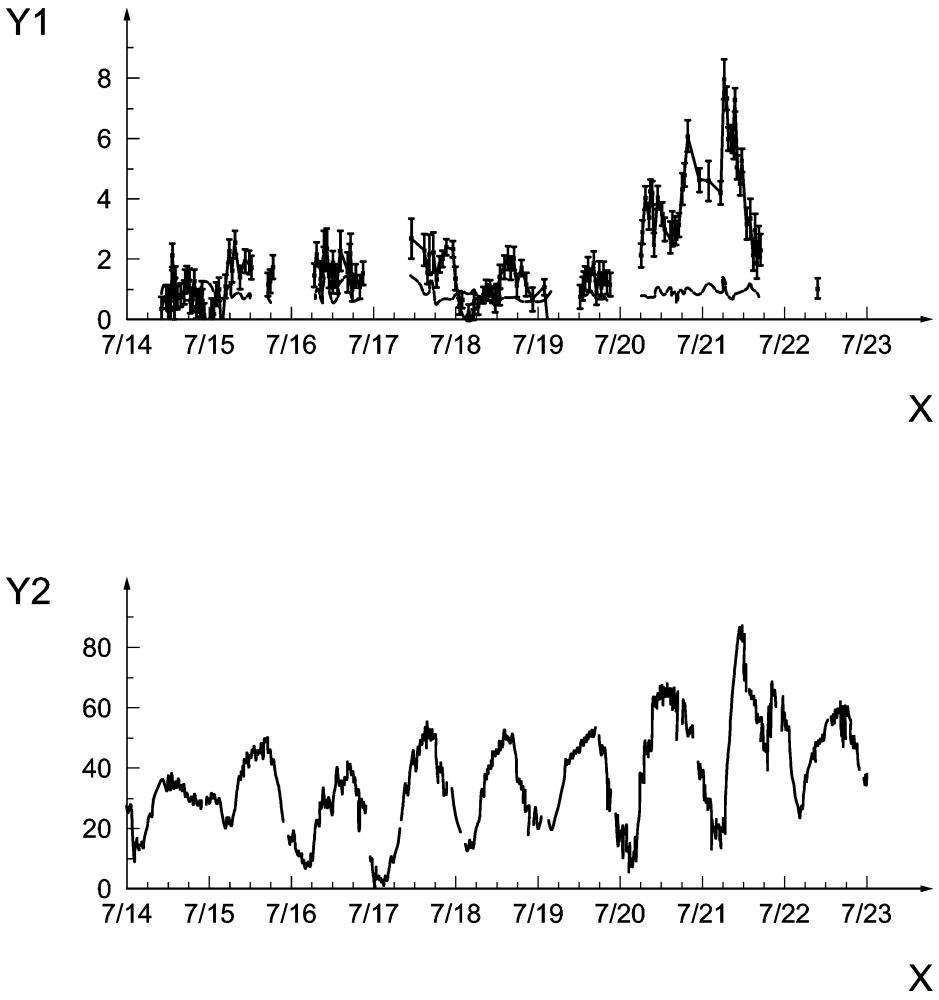

Key
X Time (date)
Y1 Ozone mixing ratio in nmol/mol
Y2 HCHO mixing ratio in nmol/mol

Figure F.19 — Time series of formaldehyde (HCHO) ozone mixing ratios (the continuous line marks the 2σ measuring limit for HCHO)

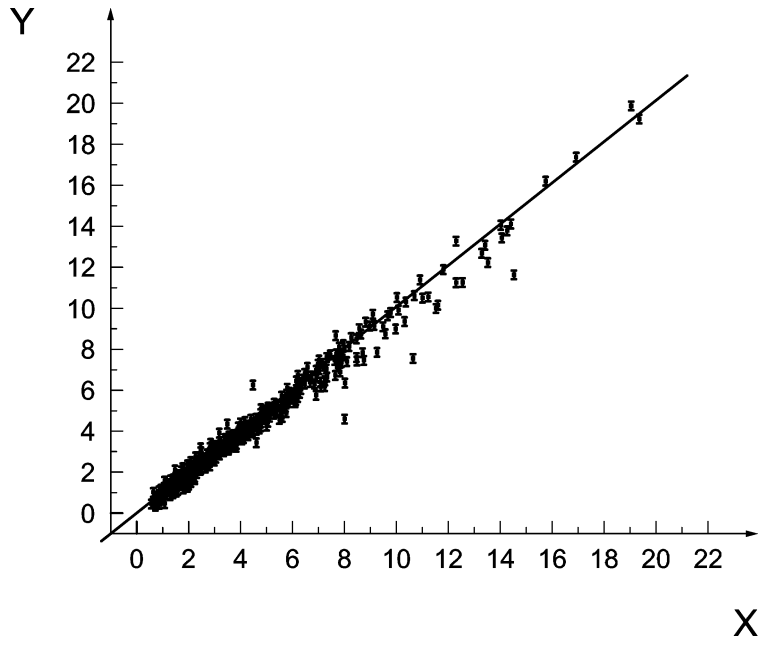

Key
X NO_2 mixing ratio in nmol/mol (chemiluminescence analyser with photolytic converter)
Y NO_2 mixing ratio in nmol/mol (White system)

Figure F.20 — Comparison of NO_2 mixing ratio measurements made by an in situ monitor (Eco Physics CLD 770 pmol/mol, Jülich) and a DOAS instrument (multiple-reflection system)

F.7 Study of the air pollution in a street canyon

In order to validate micro-scale model systems [34], continuous field measurements were carried out in an urban street canyon (Göttinger Strasse, Hannover) and 1 km x 1 km of surrounding area between early 2001 and late 2003 as part of the VALIUM [35] project. Airborne contaminants and meteorological parameters were measured in situ at a total of seven stations. Length-averaging optical measuring systems (two, sometimes 3 DOAS systems for parameters including NO_2) were installed on the ground and on the roof of a nearby building. In an effort to create validation approaches, a main objective was to benefit from the possibilities of remote surveying methods in order to overcome the limited representativeness of point measurements.

The model investigation site selected was Göttinger Strasse in Hannover, a busy four-lane arterial road built-up on both sides and located near the State Office of Ecology of Lower Saxony (NLÖ). The traffic load at this site comprises over 30 000 vehicles per day. This section of street canyon has been the subject of detailed measuring technology investigations for more than a decade [36]. Göttinger Strasse is oriented roughly in a north-south direction (see Figure F.21).

In the field experiments, measurements were carried out with bistatic and monostatic DOAS measuring systems sourced from OPSIS AB [25]. Since the alignment with the various monitoring paths and the adjustment of the measuring system are performed automatically, the measuring sequence was carried out continuously. Measuring times vary between 30 seconds and 2 minutes, depending on the constituent examined. The limit of detection, at an absorption path length of 500 m, amounts to the following values (low-resolution spectrometer grating) according to the manufacturer: 3 $\mu g/m^3$ for benzene, toluene and p-xylene (subject to a measuring uncertainty of approximately $\pm$ 30 %) and 1 $\mu g/m^3$ for NO_2, 1 $\mu g/m^3$ for SO_2, 3 $\mu g/m^3$ for O_3 and 2 $\mu g/m^3$ for NO (subject to a measuring uncertainty of $\pm$ 5 % to $\pm$ 10 %).

In addition to the in situ stations HRSW, HRV1, HRV2 and HRV3 (see Figure F.21), measurements of NO_2, O_3, SO_2, benzene and toluene were taken with a DOAS system (155 m monitoring path at street level, dotted line in Figure F.21) situated in Göttinger Strasse. The "background" load of the air contaminants NO, NO_2, SO_2, O_3 (and, intermittently, benzene and toluene) was continuously monitored by means of another DOAS system

and a set of retro-reflectors on the roof (20 m above ground) of a building adjoining Göttinger Strasse to the west (left dotted line in Figure F.21), as well as by the measuring station HRSW (33 m high building roof, camera site for Figure F.21). Other monitoring paths were set up temporarily in an effort to find the optimum configuration. During the intensive observation phases, another DOAS monitoring path for NO, NO_2 and SO_2 was set up on the western sidewalk under the DOAS monitoring paths on the roof above (126 path length, middle dotted line in Figure F.21). The aim was to establish a height gradient for the examined gases on the western side of the road using a length-averaging measuring technique. Figure F.21 also shows the SF_6 tracer line source with a length of 100 m in the middle of the road (continuous line), the sampling site using 5 l bags nearby tracer source (asterisks), and the monitoring paths for the FTIR spectrometry system used to measure CO in addition to SF_6.

Quality assurance comprised a comparison of the various measuring techniques [37] according to ISO 13752 [18] both with long-term measuring series and before or after each measuring campaign over a period of at least 36 hours (July 30 - August 1, 2002; October 26 - 28, 2002; April 8 - 10, 2003) at a background measuring station under conditions of a thoroughly mixed atmosphere. NLÖ measuring equipment served as reference instruments [38]. As a rule, the deviations of all comparative measurements lay within the measuring accuracy of the instruments employed.

The measurements clearly show the vertical-axis rotor effect in the canyon on the concentration distribution in the vertical direction and at street level. With cross-canyon wind directions, the ground-level flow direction in the canyon is opposed to the wind direction. As an example, Figure F.22 shows the NO_2 measuring result for westerly (or south-westerly, starting at about 8:30 p.m.) winds varying between 1 and 6.5 m/s in velocity above roof level (at HRSW). These data were gathered on April 11, 2003, under conditions of varying cloud cover. Figure F.22 shows the street-level NO_2 measurements at the top, NO_2 measurements on the western side of the road (on the sidewalk and on the roof) in the middle, and wind and radiation measurements at the bottom. With westerly wind, concentrations on the western sidewalk were higher than on the eastern sidewalk and the concentration decreased with height during the daytime. At night (starting at about 8:30 p.m.), with the wind direction reversed, these concentration differences are clearly less pronounced since the altered canyon flow promotes a homogeneous distribution of constituents. Moreover, concentrations rise starting at about 6:00 p.m. due to decreasing wind velocities.

The length-averaged contaminant measurements made by the DOAS and FTIR methods are particularly well suited for an examination of the canyon rotor since they involve less time variations and provide a higher spatial representativeness than point measurements. The individual in situ measuring points in the street canyon have a strictly local representativeness; this had already been found out for wind measuring locations by modelling techniques. These findings contribute to our understanding of high air contamination levels in cities.

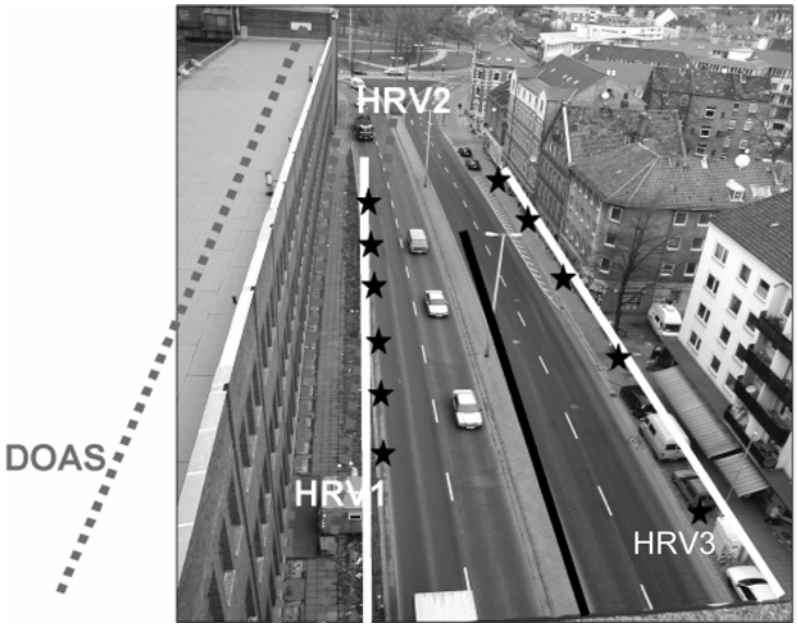

Key

★ Sampling sites
▭ FTIR monitoring path

Figure F.21 — Arrangement of measuring systems in the Göttinger Strasse street canyon in Hannover, viewed from the roof of the NLÖ administrative building (site of the HRSW in situ station) toward the north: in situ measuring stations (containers) HRV1 (western sidewalk - at left), HRV2 (Deisterplatz - at top) and HRV3 (eastern sidewalk - at right), DOAS monitoring paths (dotted lines), FTIR monitoring paths (light-coloured continuous lines), SF_6 line source (dark continuous line) and SF_6 bag sampling sites (asterisks). The HRSV in situ station is located 25 m to the south of HRV1 on the western sidewalk and is not visible in this image.

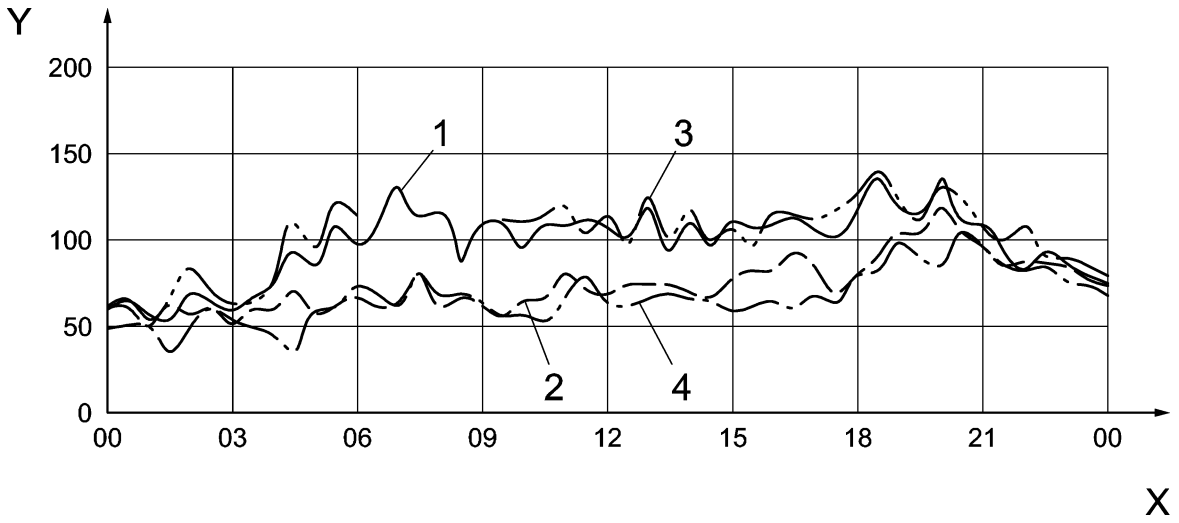

1 NO_2 (HRVS)
2 NO_2 (HRV3)
3 NO_2 (HRV1)
4 NO_2 (HRT4), DOAS street

a) DOAS and in situ NO_2 measurements of April 11, 2003, with data for the western (DOAS HRT4, HRV1, HRVS) and eastern sidewalk (HRV3) (horizontal variations)

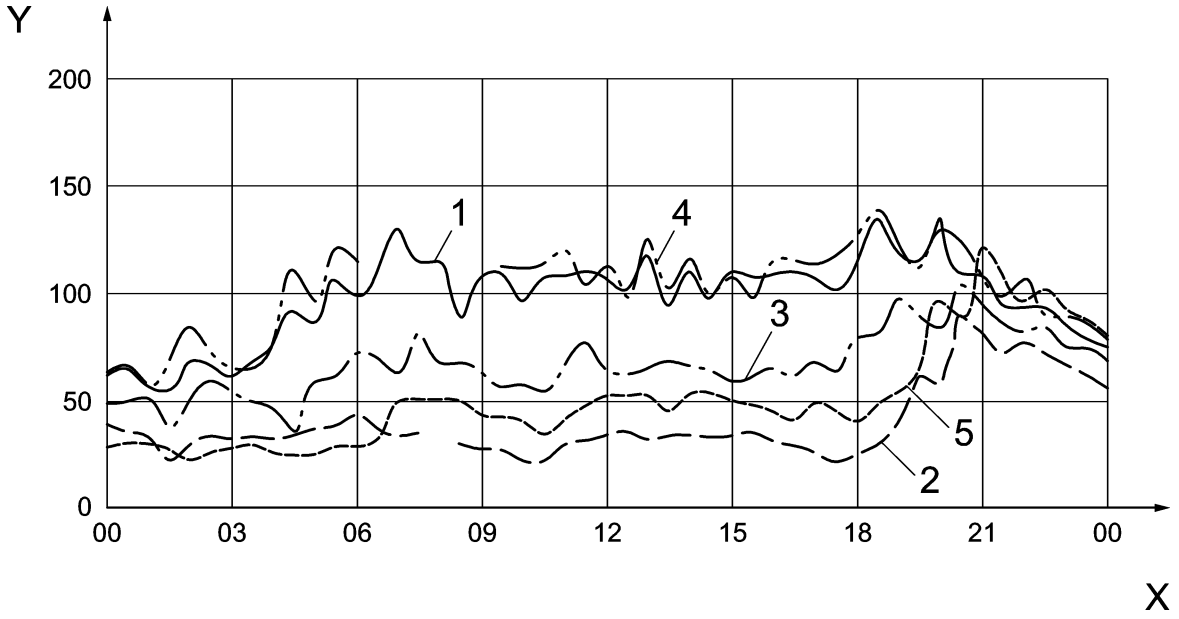

1 NO_2 (HRVS)
2 NO_2 (HRSW)
3 NO_2 (HRT4), DOAS street
4 NO_2 (HRV1)
5 NO_2 (average HRT2 – HRT3)

b) DOAS and in situ NO_2 measurements of April 11, 2003, taken at ground level (DOAS HRT4, HRV1, HRVS) and on the roof (DOAS HRT2-HRT3, HRSW) on the western side of the street (vertical variations)

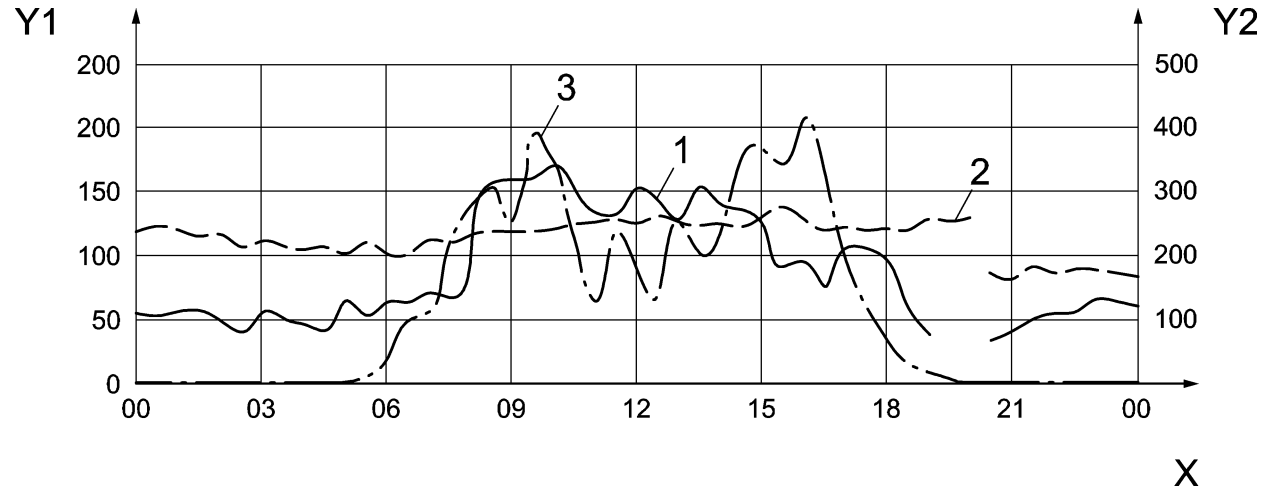

1 Wind velocity
2 Wind direction
3 Global radiation

c) DOAS and in situ NO_2 measurements of April 11, 2003; associated wind velocities, wind directions and global radiation intensities above roof level (at HRSW)

Key
X Time
Y Concentration in µg/m^3
Y1 Wind velocity in m/s
Y2 Wind direction in degrees / global radiation in W/m^2

Figure F.22 — DOAS and in situ NO_2 measurements

Annex G
(informative)

Example of sample form for a measurement record

G.1 Measurement objective

○ Measurement to determine the emissions
- ☐ from point source (for example stack outlet)
- ☐ from a line source (for example along a pipeline)
- ☐ from an area source (for example landfill)
- ☐ from a spatially distributed pollutant source (for example exhaust gas plume)

○ Measurement to determine the air pollution
- ☐ in a traffic-related monitoring path
- ☐ in an industrial monitoring path
- ☐ in an area-related monitoring path

○ Other:

_____
_____
_____
_____

G.2 Measuring site

1. Position

Radiation source:	**Measuring instrument:**
Address (if available): _____	Address (if available): _____
_____	_____
_____	_____
Coordinate system: _____	Coordinate system: _____
Easting: _____	Easting: _____
Northing: _____	Northing: _____
Height above sea level (in m): _____	Height above sea level (in m): _____
Height above ground (in m): _____	Height above ground (in m): _____
Distance from nearest emission source	Distance from nearest emission source
(in m): _____	(in m): _____

Length of the monitoring path (type and accuracy of distance measurement):

_____
_____

2. Description of surroundings

Position:

○ Plane ○ Basin ○ Valley

○ Slope ○ Hill ○ Mountain

○ Inner city ○ Suburb ○ Rural ○ Forest

District use:

○ Industry ○ Trade ○ Commerce ○ Housing

○ Recreation ○ Forestry ○ Agriculture

○ Other

Distance from relevant emission sources (in km):

Industry: _____ Commerce: _____ Housing: _____ Road traffic: _____

Other: _____

for measurements near traffic (roads closer than 100 m): _____

Type: _____ large and broad roads ○

narrow roads ○

”urban canyons“ ○

Traffic density:

very low ○ low ○ ○ medium ○ high

Number of vehicles/day: _____

3. Site plan

A site plan on a suitable scale (usually 1:1000) shall accompany this record. In addition to an exact representation of the environment, this plan shall include the following elements:

- positions of radiation source or reflector and instrument;
- monitoring path as their connection line;
- relevant emission sources;
- orography;
- obstacles to flow with heights;
- obstacles in the field of view of the instrument;
- prevailing wind direction.

G.3 Measurement conditions

1. Meteorological effects

Characterisation of the weather:

_____

Meteorological parameters measured:

○ Wind direction	○ Wind speed	○ Precipitation
○ Air temperature	○ Air humidity	○ Atmospheric pressure
○ Global radiation	○ Visibility	○ Other

2. Site-specific influences

○ high aerosol pollution

○ interference with the visual contact between radiation source and instrument varying with time

Characterisation of the background of the radiation source:

_____

_____

3. Instrument-specific parameters

Instrument type: _____

Lamp type: _____

Beam diameter: _____

Measurement of spectral range: _____

Spectral resolution: _____

Integration time for one measurement:

_____

Measured components evaluated: (check!!!)

○ NO_2	○ SO_2	○ NH_3	○ HF	○ HCl
○ HCN	○ CO	○ CO_2	○ O_3	○ NO
○ N_2O	○ $COCl_2$	○ AsH_3	○ SF_6	○ H_2O
○ Benzene	○ Toluene	○ p,m,o-Xylene	○ Ethylbenzene	
○ Methane	○ Ethane	○ Propane	○ Hexane	○ Cyclohexane
○ Ethene	○ Propene	○ Isobutene	○ 1,3 Butadiene	○ Ethyne
○ Formaldehyde	○ Acetone	○ Chloroform		

○ Other: _____

4. Particular eventualities

_____

G.4 Report of results

Example of a result table

End of the averaging period	**Averaging time** **s**	**Compound 1** **$mg \cdot m^{-3}$**				**Compound n** **$mg \cdot m^{-3}$**
dd.mm.yyyy hh:mm:ss						

(The meteorological components should also be recorded in the presentation of results.)

or reference to an existing file archiving system.

G.5 Details of the measuring institute

1. Address and telecommunications connections

_____

2. Name of the operator

_____

3. Signature

_____

Bibliography

[1] AVINO, P., and M. MANIGRASSO. Ten-year measurements of gaseous pollutants in urban air by an open-path analyzer. *Atmospheric Environment* 2008, **42**, 4138–4148

[2] PLATT, U. and J. STUTZ . Differential Optical Absorption Spectroscopy, Principles and Applications. 2008, Berlin: Springer

[3] PLATT, U. Differential optical absorption spectroscopy (DOAS). In: *Air Monitoring by Spectroscopic Techniques* (M.W. Sigrist, Ed.). Chemical Analysis Series, vol. 127, New York: Wiley, 1994

[4] TIETZE, U., and C. SCHENK. Halbleiter-Schaltungstechnik. Berlin: Springer, 2002

[5] STUTZ, J., and U. PLATT. Numerical analysis and error estimation of differential optical absorption spectroscopy measurements with least squares methods. *Appl. Optics.* 1996, **35**, 6041-6053

[6] STUTZ, J. Messung der Konzentration troposphärischer Spurenstoffe mittels Differentieller Optischer Absorptionsspektroskopie: Eine neue Generation von Geräten und Algorithmen. *PhD thesis*. Universität Heidelberg, 1996

[7] MERTEN, A., J. TSCHRITTER and U. Platt. New Design of DOAS-Long-path Telescopes based on Fiber optics. *Appl. Optics*, 2011, **50**, 783–754

[8] HITRAN, www.hitran.com

[9] WinDOAS 2.1 Software User Manual. www.oma.be/BIRA-IASB/Molecules/BrO/WinDOAS-SUM-210b.pdf

[10] HOLLAS, J.M. High Resolution Spectroscopy. Chichester: Wiley, 1998

[11] GREENBLATT, G.D., J.J. ORLANDO, J.B. BURKHOLDER, and A.R. RAVISHANKARA. Absorption measurements of oxygen between 330 and 1140 nm. *J. Geophys. Res.* 1990, **95**, 18577-18582

[12] RUTTEN, H.G.J., and M.A.M. van VENROOIJ. *Telescope Optics*. Richmond (Virginia): Willmann-Bell, 1999

[13] KORSCH, D. *Reflective Optics*. Boston: Academic Press, 1991

[14] STUTZ, J., and U. PLATT. Improving long-path differential optical absorption spectroscopy (DOAS) with a quartz-fiber mode-mixer. *Appl. Optics*. 1997, **36**(6), 1105-1115

[15] GRAINGER, J.F., and J. RING. Anomalous Fraunhofer line profiles. *Nature.* 1962, **193**, 762

[16] PÖHLER, D., S. SCHMITT, U. PLATT, S. LANDWEHR, J. TSCHRITTER, H. SIHLER, C. FISCHER, K. WEBER, A. VOGEL, and G. VAN HAREN. Multi component measurements with new LP-DOAS remote sensing instruments and their calibration with spectral data and analytic functions, in: *Neue Entwicklungen der Messung und Beurteilung der Luftqualität*, VDI-Bericht 2113, 2011.

[17] VDI 2449 Part 1 Measurement methods test criteria – Determination of performance characteristics for the measurement of gaseous pollutants (ambient air)

[18] ISO 13752, *Air quality — Assessment of the uncertainty of a measurement method under field conditions using a second method as reference*

[19] HAUSMANN, M., U. BRANDENBUEGER, T. BRAUERS, and H.-P. DORN. Simple Monte Carlo methods to estimate the spectra evaluation error in differential-optical-absorption spectroscopy. *Appl. Optics*. 1999, **38**(3), 462-475

[20] “Quantities, Units and Symbols in Physical Chemistry” International Union of Pure and Applied Chemistry (IUPAC), 1993, Blackwell Scientific Publications, ISBN 0-632-03583-8

[21] SCHÄFER, K., S. EMEIS, H. HOFFMANN, and C. JAHN. Emissions of gas stations and tankers determined by the inverse method. In: *Emissions of Air Pollutants – Measurements, Calculations and Uncertainties. Results from the EUROTRAC Subproject GENEMIS*. Rainer Friedrich, Stefan Reis (eds.), Berlin: Springer, 2004, 47-51

[22] Einundzwanzigste Verordnung zur Durchführung des Bundes-Immissionsschutzgesetzes (Verordnung zur Begrenzung der Kohlenwasserstoffemissionen bei der Betankung von Kraftfahrzeugen – 21. BImSchV) vom 7. Oktober 1992, BGBl. I, 1730, 1992

[23] VDI 3945 Part 3:2000, *Environmental meteorology – Atmospheric dispersion models – Particle model*, Berlin: Beuth

[24] STOCKHAUSE, M. Bestimmung von Emissionsraten diffuser Quellen mit Hilfe inverser Modellierung. Schriftenreihe des Fraunhofer-Instituts für Atmosphärische Umweltforschung. Aachen: Shaker-Verlag, 2000, Band 65

[25] Opsis, DOAS User Guide, Opsis AB, Furulund (Sweden), 1997

[26] ALTMANN, B.-R., K. OHLROGGE, K., J. WIND, K. SCHÄFER, H. HOFFMANN, I. DORMUTH, C. JAHN, S. EMEIS, P. SZALATA, J.-C. FRÖHLING, W. MARINKAS and H. SCHRÖDER. Emissionsmessungen an einer Tankstelle mit dem VACONOVENT-System. DGMK-Forschungsbericht 550-03, Deutsche Wissenschaftliche Gesellschaft für Erdöl, Erdgas und Kohle e.V. Hamburg, 2004

[27] Flughafen Düsseldorf International: Fluglärm und Luftqualität, Luftqualitätsmessbericht 2000

[28] HEINTZ F., H. FLENTJE, R. DUBOIS, and U. PLATT. Long-term observation of nitrate radicals at the TOR-Station Kap Arkona (Rügen). *J. Geophys. Res*. 1996, **101**, 22891-22910

[29] KURTENBACH, R., R. ACKERMANN, K.H. BECKER, A. GEYER, J.A.G. GOMES, J.C. LÖRZER, U. PLATT, and P. WIESEN. Verification of the contribution of vehicular traffic to the total NMVOC emissions in Germany and the importance of NO_3 chemistry in the city air. *J. Atmos. Chem*. 2002, **42**, 395-411

[30] ACKERMANN, R. Auswirkungen von Kraftfahrzeugemissionen in der urbanen Atmosphäre. *PhD thesis*. Universität Heidelberg, 2000

[31] VOLZ-THOMAS, A., H. GEISS, A. HOFZUMAHAUS, and K.H. BECKER. The fast photochemistry experiment in BERLIOZ (PHOEBE) – an introduction. *J. Geophys. Res*. 108 (D4), 2002. doi:10.1029/2001JD002029 2002.

[32] ALICKE, B. The Role of Nitrous Acid in the Boundary Layer, *PhD thesis*, Universität Heidelberg, 2000.

[33] ALICKE, B., A. GEYER, A. HOFZUMAHAUS, F. HOLLAND, S. KONRAD, H.W. PÄTZ, K. SCHÄFER, J. STUTZ, A. VOLZ-THOMAS, and U. PLATT. OH formation by HONO photolysis during the BERLIOZ experiment. *J. Geophys. Res*. 2003, **108**, 8247. doi:10.1029/2001JD000579

[34] TRUKENMÜLLER, A., D. GRAWE and K.H. SCHLÜNZEN. A model system for the assessment of ambient air quality conforming to EC directives. *Meteorol. Z*. 2004, **13**(5), 387-394

[35] Entwicklung und Validierung von Instrumenten zur Umsetzung der europäischen Luftqualitätspolitik (VALIUM), Projekt im Rahmen des Förderprogramms Atmosphärenforschung 2000 des BMBF, Förderkennzeichen 07ATF12.

[36] MÜLLER, W.J., B. HEITS, and M. SCHATZMANN. A Prototype Station for the Collection of Urban Meteorological Data. 8th International Conference on "Harmonisation within atmospheric dispersion modelling for regulatory purposes", 2002, Sofia, Bulgaria. Demetra Ltd. ISBN: 954-9526-12-7.

[37] SCHÄFER, K., S. EMEIS, H. HOFFMANN, C. JAHN, W. MÜLLER, B. HEITS, D. HAASE, W.D. DRUNKENMÖLLE, W. BÄCHLIN, H. SCHLÜNZEN, B. LEITL, F. PASCHEKE, and M. SCHATZMANN. Field measurements within a quarter of a city including a street canyon to produce a validation data set. *Int. J. Environment and Pollution*. 2005, **25**, 201-216.

[38] Van der MEULEN, A., D. van STRAALEN, B.G. van ELZAKKER, B. HEITS, E. HELMHOLZ, and H. RIENECKER. Field Comparison of Air Monitoring Networks. Nachhaltiges Niedersachsen, Niedersächsisches Landesamt für Ökologie, Hildesheim, 2003, **22**, ISSN 0949-8265.

This page deliberately left blank

British Standards Institution (BSI)

BSI is the national body responsible for preparing British Standards and other standards-related publications, information and services.

BSI is incorporated by Royal Charter. British Standards and other standardization products are published by BSI Standards Limited.

About us

We bring together business, industry, government, consumers, innovators and others to shape their combined experience and expertise into standards -based solutions.

The knowledge embodied in our standards has been carefully assembled in a dependable format and refined through our open consultation process. Organizations of all sizes and across all sectors choose standards to help them achieve their goals.

Information on standards

We can provide you with the knowledge that your organization needs to succeed. Find out more about British Standards by visiting our website at bsigroup.com/standards or contacting our Customer Services team or Knowledge Centre.

Buying standards

You can buy and download PDF versions of BSI publications, including British and adopted European and international standards, through our website at bsigroup.com/shop, where hard copies can also be purchased.

If you need international and foreign standards from other Standards Development Organizations, hard copies can be ordered from our Customer Services team.

Subscriptions

Our range of subscription services are designed to make using standards easier for you. For further information on our subscription products go to bsigroup.com/subscriptions.

With **British Standards Online (BSOL)** you'll have instant access to over 55,000 British and adopted European and international standards from your desktop. It's available 24/7 and is refreshed daily so you'll always be up to date.

You can keep in touch with standards developments and receive substantial discounts on the purchase price of standards, both in single copy and subscription format, by becoming a **BSI Subscribing Member**.

PLUS is an updating service exclusive to BSI Subscribing Members. You will automatically receive the latest hard copy of your standards when they're revised or replaced.

To find out more about becoming a BSI Subscribing Member and the benefits of membership, please visit bsigroup.com/shop.

With a **Multi-User Network Licence (MUNL)** you are able to host standards publications on your intranet. Licences can cover as few or as many users as you wish. With updates supplied as soon as they're available, you can be sure your documentation is current. For further information, email bsmusales@bsigroup.com.

BSI Group Headquarters

389 Chiswick High Road London W4 4AL UK

Revisions

Our British Standards and other publications are updated by amendment or revision.

We continually improve the quality of our products and services to benefit your business. If you find an inaccuracy or ambiguity within a British Standard or other BSI publication please inform the Knowledge Centre.

Copyright

Useful Contacts:

Customer Services
Tel: +44 845 086 9001
Email (orders): orders@bsigroup.com
Email (enquiries): cservices@bsigroup.com

Subscriptions
Tel: +44 845 086 9001
Email: subscriptions@bsigroup.com

Knowledge Centre
Tel: +44 20 8996 7004
Email: knowledgecentre@bsigroup.com

Copyright & Licensing
Tel: +44 20 8996 7070
Email: copyright@bsigroup.com

bsi.

...making excellence a habit.™